Louisiana State University
LSU Digital Commons

LSU Historical Dissertations and Theses | Graduate School

1980

Hydroisomerization of Pentane and Hexane Mixtures on Zeolite Catalysts.

James Jerome Spivey
Louisiana State University and Agricultural & Mechanical College

Follow this and additional works at: https://digitalcommons.lsu.edu/gradschool_disstheses

Recommended Citation
Spivey, James Jerome, "Hydroisomerization of Pentane and Hexane Mixtures on Zeolite Catalysts." (1980). *LSU Historical Dissertations and Theses*. 3537.
https://digitalcommons.lsu.edu/gradschool_disstheses/3537

This Dissertation is brought to you for free and open access by the Graduate School at LSU Digital Commons. It has been accepted for inclusion in LSU Historical Dissertations and Theses by an authorized administrator of LSU Digital Commons. For more information, please contact gradetd@lsu.edu.

INFORMATION TO USERS

This was produced from a copy of a document sent to us for microfilming. While the most advanced technological means to photograph and reproduce this document have been used, the quality is heavily dependent upon the quality of the material submitted.

The following explanation of techniques is provided to help you understand markings or notations which may appear on this reproduction.

1. The sign or "target" for pages apparently lacking from the document photographed is "Missing Page(s)". If it was possible to obtain the missing page(s) or section, they are spliced into the film along with adjacent pages. This may have necessitated cutting through an image and duplicating adjacent pages to assure you of complete continuity.

2. When an image on the film is obliterated with a round black mark it is an indication that the film inspector noticed either blurred copy because of movement during exposure, or duplicate copy. Unless we meant to delete copyrighted materials that should not have been filmed, you will find a good image of the page in the adjacent frame.

3. When a map, drawing or chart, etc., is part of the material being photographed the photographer has followed a definite method in "sectioning" the material. It is customary to begin filming at the upper left hand corner of a large sheet and to continue from left to right in equal sections with small overlaps. If necessary, sectioning is continued again—beginning below the first row and continuing on until complete.

4. For any illustrations that cannot be reproduced satisfactorily by xerography, photographic prints can be purchased at additional cost and tipped into your xerographic copy. Requests can be made to our Dissertations Customer Services Department.

5. Some pages in any document may have indistinct print. In all cases we have filmed the best available copy.

University
Microfilms
International

300 N. ZEEB ROAD, ANN ARBOR, MI 48106
18 BEDFORD ROW, LONDON WC1R 4EJ, ENGLAND

Reproduced with permission of the copyright owner. Further reproduction prohibited without permission.

8103649

SPIVEY, JAMES JEROME

HYDROISOMERIZATION OF PENTANE AND HEXANE MIXTURES ON ZEOLITE CATALYSTS

The Louisiana State University and Agricultural and Mechanical Col. PH.D. 1980

University Microfilms International 300 N. Zeeb Road, Ann Arbor, MI 48106

Reproduced with permission of the copyright owner. Further reproduction prohibited without permission.

PLEASE NOTE:

In all cases this material has been filmed in the best possible way from the available copy. Problems encountered with this document have been identified here with a check mark ✓.

1. Glossy photographs _____
2. Colored illustrations _____
3. Photographs with dark background _____
4. Illustrations are poor copy _____
5. Print shows through as there is text on both sides of page _____
6. Indistinct, broken or small print on several pages _____
7. Tightly bound copy with print lost in spine _____
8. Computer printout pages with indistinct print ✓
9. Page(s) _____ lacking when material received, and not available from school or author
10. Page(s) _____ seem to be missing in numbering only as text follows
11. Poor carbon copy _____
12. Not original copy, several pages with blurred type _____
13. Appendix pages are poor copy _____
14. Original copy with light type _____
15. Curling and wrinkled pages _____
16. Other _____

University Microfilms International

300 N. ZEEB RD., ANN ARBOR, MI 48106 (313) 761-4700

Reproduced with permission of the copyright owner. Further reproduction prohibited without permission.

Hydroisomerization of Pentane and Hexane Mixtures on Zeolite Catalysts

A Dissertation

Submitted to the Graduate Faculty of the
Louisiana State University and
Agricultural and Mechanical College
in partial fulfillment of the
requirements for the degree of

Doctor of Philosophy

in

The Department of Chemical Engineering

by
James Jerome Spivey
B.S., Chem. Eng., N.C. State University, 1972
M.S., Chem. Eng., N.C. State University, 1974
August, 1980

Reproduced with permission of the copyright owner. Further reproduction prohibited without permission.

ACKNOWLEDGMENTS

Special thanks and appreciation are due to Dr. Phillip Bryant for his understanding, encouragement, and personal attention during the course of this research. His guidance alone has made this research a rewarding experience. The author wishes to thank Mr. Alexis Voorhies, Jr. for his consideration and timely suggestions. Dr. Armando Corripio and Dr. Edward McLaughlin are acknowledged for their service on the author's committee and especially for their review of this paper.

Equipment and catalysts used in this research have been provided by Exxon Research and Development Laboratories and are gratefully acknowledged.

Appreciation is expressed to Mrs. Cindy Fuller for her patience and attention to detail in the typing of this dissertation.

The constant encouragement of my parents, Mr. and Mrs. Charles J. Spivey, to pursue this endeavor has been greatly appreciated.

Finally, special thanks are given to my wife, Jane. For her devotion and sacrifice during the years of this study the author is in debt.

Reproduced with permission of the copyright owner. Further reproduction prohibited without permission.

TABLE OF CONTENTS

Reproduced with permission of the copyright owner. Further reproduction prohibited without permission.

Reproduced with permission of the copyright owner. Further reproduction prohibited without permission.

LIST OF TABLES

Reproduced with permission of the copyright owner. Further reproduction prohibited without permission.

LIST OF FIGURES

Reproduced with permission of the copyright owner. Further reproduction prohibited without permission.

LIST OF FIGURES (Cont'd.)

Reproduced with permission of the copyright owner. Further reproduction prohibited without permission.

Abstract

Pure component and mixtures of pentane and hexane were hydroisomerized on Pd-H-mordenite and Pd-H-faujasite at 465°F, 100 to 300 psig, 6.2 to 6.6 w/hr/w, and 10/1 to 18/1 H_2/hydrocarbon mole ratio. The activity of both these catalysts was comparable to other developmental catalysts reported in the literature. Results showed that on the mordenite catalyst, the first order rate constant for n-C_5 decreased on dilution with n-C_6 while the n-C_6 rate constant increased on dilution with n-C_5. On the faujasite catalyst, the rate constant for both n-C_5 and n-C_6 decreased from the pure component values on dilution.

Models were proposed for the rate constants as functions of adsorption parameters and the partial pressures of the reactants and of hydrogen. These models were based on a Langmuir-Hinshelwood adsorption function. Statistical analysis of the various models indicated that on Pd-H-mordenite, n-C_6 is preferentially adsorbed. On Pd-H-faujasite, the analysis showed that neither n-C_5 nor n-C_6 predominates in adsorption and that the adsorption parameters for both reactants must be included in the model. The hydrogen adsorption parameter was negligible compared to both the pentane and hexane adsorption parameters on both catalysts.

Reproduced with permission of the copyright owner. Further reproduction prohibited without permission.

Introduction

Hydroisomerization of low molecular weight paraffins has become an increasingly important conversion process in recent years. This is due to the phase-down of antiknock concentrations in motor gasoline and the resulting need for higher octane, i.e., more branched hydrocarbon constituents. The research octane number (RON) of streams containing C_5 and C_6 mostly straight chain hydrocarbons can be boosted from about 70 to over 80 with the extent of improvement depending on the isomerization temperature and C_5/C_6 ratio (1).

Zeolite catalysts have been employed almost exclusively in new efforts in this area. Paraffin isomerization requires a stable catalyst with high activity to take advantage of the higher equilibrium conversions to branched products at lower temperatures (2). Zeolites have been shown to be highly active for this type of reaction and have additional advantages such as relative insensitivity to moisture, sulfur, nitrogen (3).

The earliest investigations into zeolite catalyst activity were acid-base type reactions such as cracking, isomerization, alkylation, and dehydration of alcohols. These reactions were also known to be catalyzed by amorphous aluminosilicates. Zeolites, being crystalline aluminosilicate compounds, were found to have special properties compared to amorphous catalysts. It was found that noble-metal free zeolites catalyze n-C_6 isomerization while the amorphous aluminosilicates do not (4). This is attributed to the unique adsorptive and acidic surface properties of zeolites. Modified zeolites have appeared in which ion exchange and deposition of a hydrogenating noble metal such as Pd are used to enhance specific reactions. Hydroisomerization of alkanes on

Reproduced with permission of the copyright owner. Further reproduction prohibited without permission.

such catalysts is generally considered to proceed through a mechanism in which dehydrogenation of the alkane at a metallic site is followed by skeletal rearrangement at an acidic zeolite site via a carbonium ion intermediate. The resulting isomer is hydrogenated at a metallic site to complete the reaction.

Problems currently being investigated in this field include the structure of the active centers (both metal and acid sites), intradiffusional inhibition due to intramolecular channels, and the nature of catalyst deactivation (3). Little has been reported in the literature on systematic studies of mixed n-C_5 and n-C_6 feeds although it is this type of feed that is typical of hydroisomerization feed stocks for octane enhancement. In fact, C_5 and C_6 hydrocarbons comprise 15-20% of the total motor gas pool (5). Any anomalies observed in hydroisomerization of such mixed feeds are important in the design of commercial systems and in the investigation of the mechanism and dynamics on a molecular level.

This study was designed to examine the kinetics of n-C_5/n-C_6 hydroisomerization of both mordenite and faujasite catalysts. The objectives were:

1. Using a simplified kinetic model, describe the effects of temperature and reactant partial pressures on the rate constant for both a mordenite and faujasite catalyst typical of developmental catalysts.
2. Explain any anomalies in terms of fundamental kinetic quantities such as adsorption parameters.
3. Compare the performance of the mordenite and faujasite catalysts in terms of the kinetic models developed.

Reproduced with permission of the copyright owner. Further reproduction prohibited without permission.

Literature Review

Zeolites are a special class of crystalline aluminosilicate compounds which have specific pore dimensions and pore structure. Their value in heterogeneous catalysis lies in the ability to tailor the pores to exclude certain reactants and thus obtain high selectivity; and in the special acidic and adsorptive properties of the zeolite surface which promote specific conversion reactions such as hydroisomerization.

In this section, the available literature on faujasite and mordenite zeolites will be examined as follows. First, the structure and physical properties for each catalyst will be described. Second, studies carried out involving specific reactions on these catalysts will be reviewed especially as they relate to the particular types of catalysts used in this study. Finally, studies which have compared the activities of mordenite and faujasite catalyst, particularly as differences in performance may be related to physical and chemical characteristics, will be reviewed.

Structure

There are more than 30 different crystalline zeolites occuring in nature. Over 100 additional zeolites have been manufactured synthetically in order to obtain enhanced chemical or sorptive properties. Whether synthetic or natural, all zeolites may be represented by the empirical formula (6):

$$M_{x/n}\ 0\ \left[(Al\ O_2)_x\ (Si\ O_2)_y\right]\ \cdot w\ H_2O$$

In this formula, M is the cation of valence n, w is the number of water molecules, and y/x has values of 1-5 depending on the structure.

Reproduced with permission of the copyright owner. Further reproduction prohibited without permission.

This structure consists of an infinitely extending three dimensional network of AlO_4 and SiO_4 tetrahedra linked to each other by sharing all of the oxygens.

In spite of the many varieties of natural and synthetic zeolites available, only few have practical importance at the present. Many zeolites, after dehydration, have very small channels which do not penetrate the particle and which are serious mass transfer blocks. In other cases, dehydration irreversibly disrupts the structure and the positions of the metal cations, causing the framework to collapse. To be of use, the structure must remain intact after dehydration. Breck (6) has summarized and classified the important synthetic and natural zeolite properties.

Faujasite

Faujasite is both a naturally occuring and synthesized zeolite. Type X and Y have been used to designate two synthetic faujasites which have received special attention. The empirical formulas for a typical oxide are given by Breck (6),

$Na_2O \cdot Al_2O_3 \cdot 2.5\ SiO_2 \cdot 6\ H_2O$ Type X.

$Na_2O \cdot Al_2O_3 \cdot 4.8\ SiO_2 \cdot 8.9\ H_2O$ Type Y.

The basic structure of the faujasite, both X and Y, is that of a truncated tetrahedron as shown in Figure 1 . Each vertex in the Figure represents a silicon or aluminum atom and each line represents a linking oxygen atom. Access to the inner pores is by way of four 12-sided windows with a diameter of $\sim 9\text{Å}$. The inner cavity has a diameter of $\sim 11\text{Å}$. The metal cation, such as Na^+, is located within the cavities as shown in Figure 2 . By decationization or ion exchange, it can be seen that the

Reproduced with permission of the copyright owner. Further reproduction prohibited without permission.

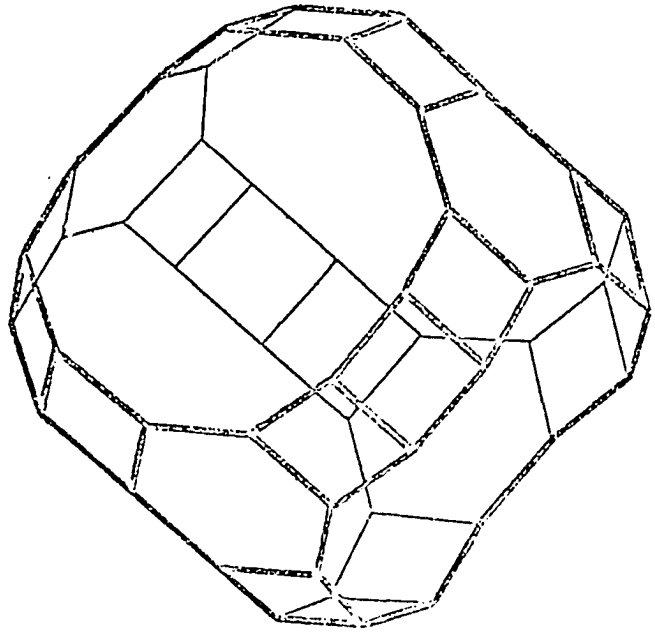

Figure 1. Structure of Type X or Type Y Zeolite.

Reproduced with permission of the copyright owner. Further reproduction prohibited without permission.

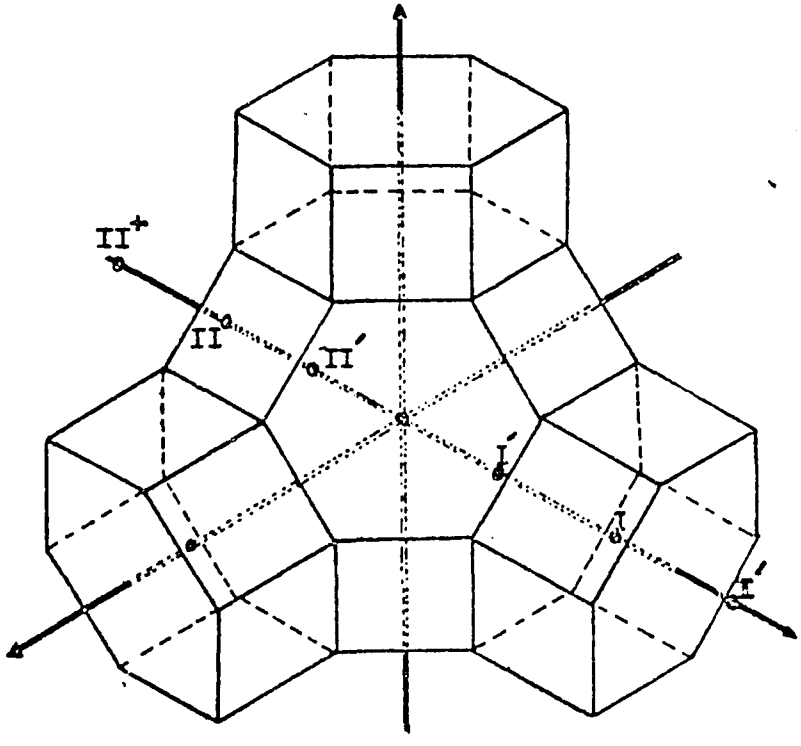

Figure 2. Three-Dimensional Structure of Sodalite Unit.

The truncated octahedron and three of the four hexagonal prisms are shown together with the cation sites along one of the four tetrahedral axes. The cation sites are: I at the center of a hexagonal prism, I' displaced from a shared hexagonal face into the sodalite cage, II' displaced from an unshared hexagonal face into the sodalite cage, II slightly displaced into the supercage, and II^+ displaced considerably into the supercage. From Smith (7).

Reproduced with permission of the copyright owner. Further reproduction prohibited without permission.

catalytic properties of a given structural X or Y faujasite can be altered. In addition, when it is recognized that the structural framework of the faujasite may be changed by such methods as steam leaching (8), it becomes apparent that a great deal of latitude exists in which to tailor the faujasite structure for a given reaction.

It has been found that the introduction of Group VIII transition metals into polyvalent or decationized faujasite yields catalysts very active for isomerization. It has been found that Pd-faujasite enables a 50-100°C lower temperature to be used when compared to conventional bifunctional catalysts (3). These metals provide a hydrogenation and a dehydrogenation function described earlier. A catalyst such as palladium-type Y-H-faujasite (Pd-H-Y) is called bifunctional, as it contains both metallic and acidic sites.

The method of preparation of such catalysts as Pd-Na-Y and the effect of catalyst pretreatment prior to use in reactions has been investigated extensively. This is due to the large effect that differences in preparation can have on structure and consequently on activity. For example, Minachev, et.al., found that the method of introduction of the metal can greatly effect activity. He found that Pt-Na-Y prepared by ion exchange has a greater activity than the same catalyst prepared by impregnation with chloroplatinic acid (3).

After ion exchange, the catalyst is typically activated under air or N_2 followed by reduction in H_2 to further enhance its activity, specifically the nature of the surface and the metallic sites. It is found that activity in n-C_5 isomerization falls off rapidly for catalysts reduced at >380°C (3). Another study investigated the effect of pretreatment of Pd-Ca-Y in air, N_2, and H_2 (9). Below 250°C the Pd was found

Reproduced with permission of the copyright owner. Further reproduction prohibited without permission.

not to be sufficiently reduced by H_2 and its dehydrogenation activity was low. However, when this catalyst was subsequently used in an isomerization reaction, the conversion increased during the course of the 1 hour run from 8 to 20%. This indicates that the metal was activated during the run. This same study investigated the effect of HCl treatment on the catalyst. The catalyst acidity increased with increasing HCl treatment, mainly as a result of increase in the medium to strong acidic sites.

Mordenite

Mordenite is unique among zeolites in that the structure consists of parallel elliptical channels which do not intersect. These channels have major and minor diameters of 6.95 and 5.81 Å respectively, as shown in Figure 3. Of primary interest is the fact that the effective pore dimensions of mordenite can be adjusted by ion exchange with a cation of suitable radius (10, 11, 12). Voorhies, et. al., found that acid leaching of mordenite produces on Al-deficient structure with decreased diffusional resistance (36). This procedure raises the SiO_2/Al_2O_3 ratio in mordenite by extracting aluminum atoms. It appears that the silica tetrahedra do not replace the alumina tetrahedra on extraction. As the aluminum is removed, the acidity decreases. However, since decreased diffusional resistance results, there exists an optimum SiO_2/Al_2O_3 ratio for a given reaction.

The preparation of H-mordenite has been studied by several investigators in order to find optimum activation conditions. Maile and Weisz found that treatment with O_2 or H_2 at 1000°F enhances the activity (13). Gray and Cobb found that maximum activity was produced by calcination at 510°C (14). These authors also studied the effect of the degree of ion exchange of Group VIII metals. They found that activity

Reproduced with permission of the copyright owner. Further reproduction prohibited without permission.

Figure 3

CROSS-SECTIONAL VIEW OF MORDENITE

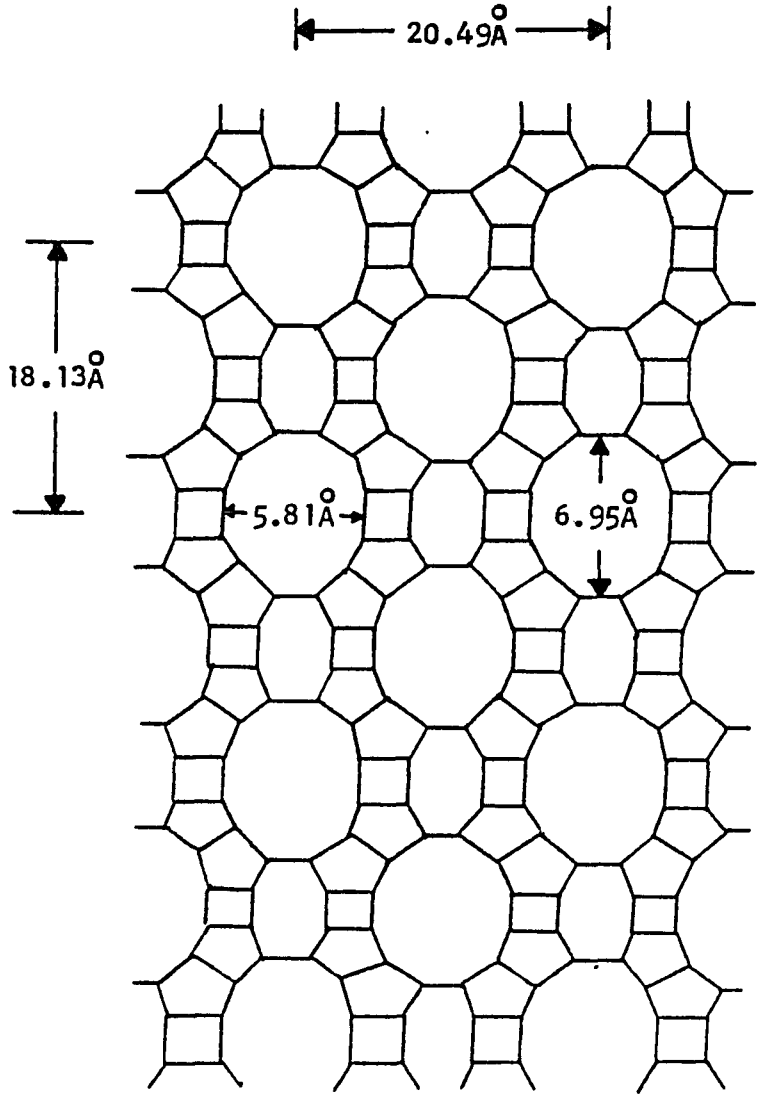

Reproduced with permission of the copyright owner. Further reproduction prohibited without permission.

increases rapidly above 80% exchange.

The nature of the metallic component of Pd-H-Mordenite was examined by Chick, et al. (2). They found that small metal crystallites uniformly distributed are best. In H-mordenite, .5 wt% Pd gives about one Pd atom per 180 Å of pore length. This level appeared to be optimum. Braun, et al., sintered a Pt-H-M catalyst which simultaneously increased the mean particle size of the metal and decreased the specific metal surface area (15). They found that the activity per unit surface area passed through a maximum at about 100 Å metal particle size. This supports the idea of a "structure sensitive" reaction being dependent on metal particle size.

Isomerization Reactions

Although the exact nature of the zeolite surface and the effects of crystallographic and physicochemical variables on reaction kinetics are somewhat unresolved, several aspects have been studied. It has been shown that both Lewis and Bronsted acid sites must be present and that optimum activity results when there are an equal number of these sites (16). Lewis acid sites are electron pair acceptors associated with the Al atoms of the faujasite. Bronsted acid sites are proton donors such as H atoms which are incorporated into the catalyst by ion exchange described in the next section. In addition, it has been found that increasing reduction temperature of decationized zeolite causes the Bronsted sites to go through a maximum while the Lewis sites beginto increase about 500°C (9). These independent results could explain why the activity of faujasite goes through a maximum with respect to reduction temperature. In addition, there is such a large degree of cooperation between the acidic and metallic sites that the activity

Reproduced with permission of the copyright owner. Further reproduction prohibited without permission.

reaches a point of diminishing returns after a certain metal concentration is reached (16). The performance of the catalyst is highly dependent on the ratio of acidic to metallic sites and on the efficiency of each (17). The metallic sites, by their hydrogenation function, serve to keep the acidic sites free of coke precursors (16).

Specific studies on catalysts similar to those used in this study will be reviewed next.

Faujasite

Faujasite catalysts in the monovalent cationic form have no activity in carbonium ion reactions (3). It is necessary to modify the faujasite by ion exchange with NH_4^+ or Ca^{+2}, for example. If NH_4 is used and the NH_3 is driven off by heating, the "hydrogen", H-, or decationized faujasite is left. This form is active for isomerization reactions.

For isomerization, the incorporation of .5 - 2.0 wt% Group VIII metals in the monovalent form of faujasite results in a catalyst active for hydrogenation but not for isomerization (3).

It is apparent then that a dual function faujasite catalyst, one with both metallic and acidic sites, would be active for isomerization in addition to having the stability offered by the metallic sites. The metallic sites not only aid in isomerization but are thought to hydrogenate coke precursors keeping the surface active longer.

Minachev has studied the contributions of the metallic and acidic sites on Pt-Ca-X and Pt-Ca-Y at 280 - 350°C, 30 atm (3). He examined the effect of Pt concentration while maintaining a constant acidic function. The isomerization rate of cyclohexane increased with Pt concentration

Reproduced with permission of the copyright owner. Further reproduction prohibited without permission.

until above .5 wt% Pt, the rate did not change with metal content. This implies that at above .5 wt%, this particular reaction is limited by rearrangement occuring on the acidic sites. Further evidence was obtained as follows. By isomorphic replacement of Al by Si atoms in .5 wt% Pd-X, i.e. changing Pd-X toward Pd-Y by increasing the Si O_2/Al_2O_3 ratio from 2.5 to 4.8, it was observed that the activity for n-C_6 isomerization increased substantially. Increasing SiO_2/Al_2O_3 ratio corresponded to increasing acidity. This result thus indicated that the acidic site isomerization of the intermediate olefin is rate limiting at these conditions. Comparing X and Y forms, it was found that if the two have the same crystal lattice and metal content, the hydrogenating activity was the same, as judged by the hydrogenation of C_2H_5. However, the hydrogenation activity was highly dependent on the metal chosen. Pt was more active than Pd. Both Pt and Pd were more active than Ni.

Topchieva, et al., have investigated the isomerization of n-C_6 on Ca-H-Y at 250-350°C, 30 kg/cm^2, and H_2/n-C_6 molar ratio of 3.5 (18). They found that the maximum yield of hexane isomers occurred at 330 -340°C, corresponding to 93% of equilibrium. At higher temperatures, cracking became significant while at lower temperatures the yield was lower due to slower reaction rate. As the yield increased, the monomethyl isomer concentration, 2- and 3- methyl pentane (2MP, 3MP), decreased while the dimethyl isomers, 2, 2 and 2, 3 dimethylbutane (2,2 DMB, 2,3 DMB) increased. This indicates that secondary isomerization from mono to dimethyl products on the acidic sites increases with conversion. Further increases in reaction temperature beyond 330-340°C caused the intermediates to crack, and then hydrogenate, rather than hydrogenate as C_6 isomers. The authors noted that as the total pressure was decreased at a fixed

Reproduced with permission of the copyright owner. Further reproduction prohibited without permission.

$H_2/n\text{-}C_6$ ratio, the cracking rate increased. This may be due to decreasing hydrogen partial pressure and hence surface hydrogen concentration which favored the further reaction (cracking) of the olefin intermediate. The authors also found that at 30 kg/cm^2, 220°C,and 1 hr^{-1} space velocity, no decrease in activity was found for a period of 2500 hr.

Yegiazarov, et al., looked at Pd-H-Y at 310°-390°C, 30 atm, and and $H_2/n\text{-}C_5$ of 3/1(19). Their catalyst had 18-20 wt% binders used as mechanical support for the catalyst. They found that HCl leaching of the catalyst increased $n\text{-}C_5$ isomerization activity up to 4.8 hours treatment time. They postulated that further leaching hindered the yield by retarding desorption of the olefin intermediate from strong acid sites that were created. This retarded desorption apparently led to increased cracking rates which the authors observed at severe leaching conditions. This paralleled the results of Topchieva discussed earlier (18).Yegiazarov also found that increasing the space velocity increased the product selectivity (isomerized versus cracked products) but reduced overall yield.

Garanin, et al., have studied $n\text{-}C_5$ isomerization on .5 wt% Pd-Ca-Y at 300°-360°C, 1 to 50 atm, 1 hr^{-1}, and 3.2/1 $H_2/n\text{-}C_5$ (20). They found a maximum $i\text{-}C_5$ yield at 360°C and 10-20 atm, corresponding to 90% of equilibrium yield or 57 mole % $i\text{-}C_5$. Above 360°C, hydrocracking began, although hydrocracked products were less than 2 mole %. At each reaction temperature the $i\text{-}C_5$ yield passed through a maximum at 5-15 atm total pressure and then decreased slowly. The author states that as the total pressure is changed, $P_{n\text{-}c_5}$, P_{H_2}, and the contact time all change. Additional experiments to determine the effect of these three factors separately showed that the isomerization rate, g-mole /g catalyst/hr, passed through a sharp maximum with respect to P_{H_2} at $\sim$ 3 atm at constant

Reproduced with permission of the copyright owner. Further reproduction prohibited without permission.

P_{C_5} while the rate asymptotically approached a limiting value with respect to P_{C_5} at $\sim$ 8 atm at constant P_{H_2}. Up to 6 atm, the rate was linear with P_{C_5}, indicating first order kinetics, with zero order kinetics above 6 atm. The authors stated that the initial low rate at low P_{H_2} is due to coke deposition on the catalyst surface. Above 3 atm, the hydrogen diluted the n-C_5 feed lowering its concentration and thus the overall rate. These results are consistent with the generally accepted mechanism of isomerization on a dual functional catalyst. This mechanism involves rapid dehydrogenation of the paraffin on the metallic site, rate-limiting isomerization on the acidic site followed by hydrogenation of the iso-olefin. Thus, the equilibrium olefin concentration and hence the overall rate depends on the initial partial pressures of the hydrogen and hydrocarbon. The authors show that their reaction rate is linear with P_{C_5}/P_{H_2} over the range .1 → .3, in agreement with the assumed mechanism and the rate law $r = k \frac{P_{C5}}{P_{C6}}$. It is also important to note that the authors found no variation in rate with catalyst particle size in the range of 1 → 4 mm which implies that gas to particle mass transfer is not rate-affecting.

An interesting study by Bolton and Lanewala questions the traditional concept of the olefin intermediate in hydrocarbon isomerization (4). Noting the close similarity in the initial products in the isomerization of n-C_6 and the hydrogenolysis of methylcyclopentane (MCP), they propose a cyclic intermediate in the isomerization reaction. Using a .5 wt% Pd-Y catalyst at 285°C, 500 psig, H_2/hydrocarbon ratio of 5-20/1, and 2-90 hr^{-1}, they found that cracking always accompanied isomerization of n-C_6, with typical cracked product concentration of .04 - 2.0%. By using each of the 5 hexane isomers as initial feed materials and carrying out

Reproduced with permission of the copyright owner. Further reproduction prohibited without permission.

the reactions at differential conversion levels, the authors studied the reaction paths of each intermediate in the conversion of n-C_6. They postulate the following reaction scheme based on their results:

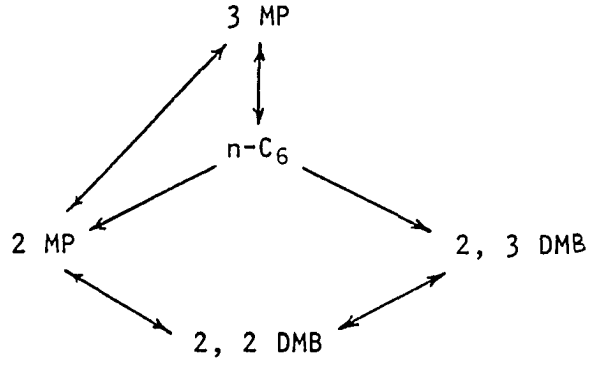

This scheme differs from the generally accepted bifunctional mechanism due to the direct formation of 2, 3 DMB from n-C_6, the formation of 2 MP from 2, 2 DMB and the absence of n-C_6 from the primary products of 2 MP. A simple molecular rearrangement of a carbonium ion intermediate does not explain these results. A cyclic reaction mechanism proposed by Barron, et al.,(21)involving an MCP intermediate is unsatisfactory since it does not allow for the direct formation of 2, 3 DMB from n-C_6. Since cracking accompanied each reaction, the mechanism must account for cracking as well as isomerization. Based on their results, the authors propose that isomerization and cracking proceed through a common surface transition state involving adjacently adsorbed hexane molecules. The thermodynamically favored six member ring is formed involving two hexane molecules. From this configuration, it is shown that the all experimental results can be accounted for, including cracking and isomerization reaction products. This is consistent with the results of Anderson (22) who found that hydrocracking and isomerization occurring on Pt and Pd films have the same activation energy. Bolton and Lanewala conclude by

Reproduced with permission of the copyright owner. Further reproduction prohibited without permission.

stating that further analysis of the hydrocracked products is needed to verify their proposal.

Weeks, et al., in studying the labeled n-C_5(3-C^{13}) reactions on .42 wt% Pd-H-Y at 325°C concluded that hydroisomerization occurs as a single reaction sequence rather than from repeated contact with the surface In the absence of H_2, it has been shown that isomerization proceeds both through intra and intermolecular rearrangement (24). However, hydroisomerization was found to be entirely intramolecular. In studies carried out to determine the effect of H_2 on the mechanism, it was found that hydroisomerization products differed substantially from simple isomerized products. The authors conclude that a random distribution of product resulting from isomerization may be explained by a cyclopentyl intermediate while one additional pathway occurs in hydroismerization, resulting in a more ordered product distribution.

Saito and Iwasaki studied n-C_5 hydroisomerization at 270-330°C, 1 to 50 atm on .05 - 1.0 wt% Pt-H-Y (8). They examined the effect of Pt content and reaction conditions. They found that below .3 wt% Pt, the rate was limited by dehydrogenation of n-C_5 or hydrogenation of iso-$C_5^=$ whereas above .3 wt%, rearrangement on the acidic site was limiting. They postulate that this rearrangement occurs on active Pt sites which are kinetically influenced by adjacent protonic acid sites. Further, they feel that hydrocracking, which accompanies the isomerization reaction, takes place on different active sites. They thus conclude that due to molecular influence, there is a varying degree of cooperation between the metallic and acidic components resulting in different types of active sites some of which seem to preferentially promote isomerization or cracking. Based on their results, they propose the following scheme for hydroisomeri-

Reproduced with permission of the copyright owner. Further reproduction prohibited without permission.

zation and hydrocracking of n-C_5

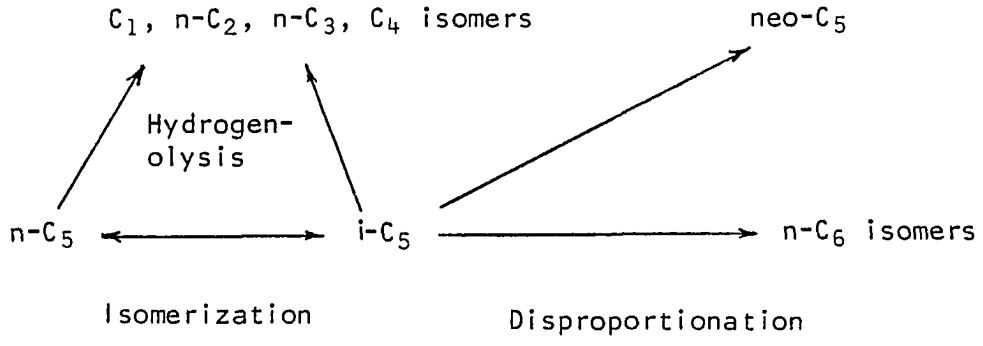

Mordenite

Mordenite has the highest SiO_2/Al_2O_3 ratio of any zeolite, 10/1, and it may be expected that a higher acid catalytic activity would result. Experiments have shown that mordenite is the most active catalyst discovered so far for isomerization of saturated hydrocarbons (3). In addition, mordenite will hydrogenate benzene at 250°C and 30 atm completely even without Group VIII metals (3). It will not dehydrogenate cyclohexane (25). The former study also showed that as the Na^+ ion concentration was decreased on decationization, the hydrogenation activity decreased, implying that the Na^+ may have some hydrogenation activity in mordenite(3). Group VIII metals are not necessary for paraffin isomerization on H-mordenite (H-M) and their presence has been reported to have no effect (3) or to only increase activity slightly (2).

Minachev, et al., have studied isomerization and hydrogenation activity of H-mordenite. They state that since the first step in isomerization on both bifunctional and metal zeolite catalysts is dehydrogenation as reported by others (26, 27), and since isomerization on H-M does not require a metal, another type of mechanism is indicated. They postulate that isomerization occurs without a dehydrogenation step.

Reproduced with permission of the copyright owner. Further reproduction prohibited without permission.

Specifically, for n-C_5 isomerization

$$n\text{-}C_5H_{12} + H\text{-}M \underset{k_{-1}}{\overset{k_1}{\rightleftarrows}} n\text{-}C_5H_{11}\text{-}M + H_2 \qquad (1)$$

$$n\text{-}C_5H_{11}\text{-}M \underset{k_{-2}}{\overset{k_2}{\rightleftarrows}} i\text{-}C_5H_{11}\text{-}M \qquad (2)$$

$$i\text{-}C_5H_{11}\text{-}M + H_2 \underset{k_{-3}}{\overset{k_3}{\rightleftarrows}} i\text{-}C_5H_{12} + H\text{-}M. \qquad (3)$$

If (2) is rate determing, the authors show that the rate is represented by

$$R\ \frac{\text{g-mole}}{\text{g-cat-hr}} = \frac{k_2 K_1 \left(\frac{P_{n\text{-}C_5}}{P_{H_2}} - \frac{k_2}{K_3} \frac{P_{i\text{-}C_5}}{P_{H_2}} \right)}{1 + K_1 \frac{P_{n\text{-}C_5}}{P_{H_2}} + \frac{1}{K_3} \frac{P_{i\text{-}C_5}}{P_{H_2}}}$$

where K_i is the equilibrium constant for reaction i. This rate expression implies that the dependence of the rate on $P_{H_2}/P_{n\text{-}C_5}$ takes the form of a Langmuir isotherm. Experimental results agreed with this model. They also studied the activity of other cationic forms of mordenite, namely Li, Na, Mg, Ca, Cd, and Al. They found that H-M had much higher activity, as measured by cyclohexane isomerization, than any other form. This may have been due to reduction of the effective pore diameter due to the size of the cations with respect to the H form.

Reproduced with permission of the copyright owner. Further reproduction prohibited without permission.

Chick, et al., investigated deactivation of 12.5/1 S_iO_2/Al_2O_3 H-M during n-C_6 isomerization at 250°C, and P_{H_2} of 1 atm (2), varying amounts of Pd from .106 → 1.47 wt%. Earlier qualitative results had shown that metal free H-M deactivates rapidly whereas high P_{H_2} or the addition of a noble metal stablizes the catalyst (28-33). Noble metal addition was also known to decrease cracking activity (32,34,35). The author's experimental results showed that on metal free H-M, the rate of cracking was initially high but decreased rapidly. Increasing the Pd content in stages to .7 wt% caused the cracking rate to decrease and the isomerization rate to increase. It was noted that above .1 wt% Pd, no olefins were formed although significant $C_3^=$ was present below .1 wt%. This reflects the hydrogenation activity of the Pd. The authors found that the deactivation behavior for both cracking and isomerization could be represented by $R = R_o \exp(-A_j t)$ where

R = reaction rate (for cracking, j=c; for isomerization, j=i)

R_o = initial reaction rate

t = time on stream

A_j = deactivation time constant

Thus, deactivation during both reactions could be compared using A_j.

A_c and A_i both decreased rapidly up to .5 - .6 wt% Pd and changed little thereafter with Pd content. The overall deactivation rate increased rapidly with cracking rate and the associated deposition of coke on the catalyst. The addition of Pd resulted in a sharp decrease in cracking rate and thus deactivation. Thus, cracking rate was directly related to deactivation rate. The authors stated that this was

Reproduced with permission of the copyright owner. Further reproduction prohibited without permission.

due to polymerization of olefinic products resulting in coke. This coke blocked the pores of the catalyst and inhibited activity. By contrast, the relatively slower deactivation observed in isomerization was attributed to slow poisoning of the active sites. The authors propose that since the isomerization rate increases with Pd content and the cracking rate decreases, isomerization proceeds independently but parallel to cracking. Cracking normally produces a small quantity of coke or coke precursors which are not hydrogenated at the Pd sites. By acting to reduce the cracking rate, the Pd sites thus stabilize the catalyst. The stability given by Pd is thus the result of a reduction of cracking rate rather than direct hydrogenation of coke or coke precursors or the establishment of more favorable olefin-paraffin carbonium ion ratios. Paraffin reaction is thought to begin with hydride abstraction at a Lewis acid site or protonation at strong acid sites, perhaps adjacent to Lewis acid sites. The authors postulate that suppression of cracking and deactivation by the addition of Pd may result from a reduction in the number or strength of these sites. Suppression of cracking may also result from a reduction in carbonium ion lifetime associated with a greater reactivity of hydrogen in the presence of Pd. This is not simply an occupation of the acidic sites by Pd since increased $H_2/n\text{-}C_5$ ratios led to reduced cracking rates and increased isomerization rates. While the authors do not rule out the generally accepted bifunctional mechanism, they suggest that deactivation is a direct result of cracking, i.e, the addition of Pd reduces the deactivation rate by reducing cracking rate rather than by hydrogenation of coke or coke precursors. Thus, Pd greatly influences the surface acid properties and may be used to alter the catalyst selectivity.

Reproduced with permission of the copyright owner. Further reproduction prohibited without permission.

The effect of surface acidity as influenced by SiO_2/Al_2O_3 ratio has been investigated. It has been shown by Beecher and Voorhies that acid extracted H-M with a SiO_2/Al_2O_3 of 64/1 has increased activity for cracking of cumene and hydrocracking of n-C_{10} and decalin (36). Weller and Bauer showed that n-C_6 cracking activity increased with SiO_2/Al_2O_3 up to 17.5/1 (66). However, Kranich has reported that at high ratios, the removal of aluminum resulted in a loss of cumene cracking activity (37). Voorhies, et al., investigated the effect of SiO_2/Al_2O_3 ratio on the properties of mordenite by studying the hydroisomerization of n-C_5 as well as physical and adsorption characteristics of the modified catalysts (38). They found that the unit cell of a 66/1 H-M was smaller than for a 12/1 catalyst. This may be expected due to the shorter Si-O bond length. Their results show that acidity is the dominant factor in determining n-C_5 hydroisomerization activity. The authors were able to correlate acidity, as measured by NH_3 adsorption, with isomerization activity. While the changes in pore structure associated with increased acidity had no effect on n-C_5 isomerization, it was proposed that the smaller pores may inhibit the reaction of a larger molecule. Related work by Voorhies and Beecher (36) on cyclohexane and n-C_5 hydroisomerization showed that the isomerization activity initially increased and then decreased with SiO_2/Al_2O_3 ratio. This maximum of activity may be related to a reduction in acid sites with a reduction in alumina content for acid extracted mordenites. Though no intraparticle diffusion limitations were noted on the standard 10.8/1 mordenite, the activation energy for cyclohexane decreased with increasing SiO_2/Al_2O_3 ratio. This may have been due to possible intrapore structural or chemical changes, noted earlier (37) on a similar catalyst, which caused mass transfer resistance. It has been noted that the

Reproduced with permission of the copyright owner. Further reproduction prohibited without permission.

interaction of surface acidity and pore accessibility may account for conflicting reports on the effect of alumina deficiency on catalytic activity (37). The authors were able to represent their rate constant with a Langmuir-Hinshelwood dual site adsorption model.

Lopez, et al., studied cracking and isomerization of n-C_6 on H-M and .6 wt% Pt-H-M at 250 and 400°C (39). At 400°C on H-M, no isomerization was observed and the selectivity was that which was predicted from the classical dual function theory with adsorption-desorption as the rate determining step. At 250°C on H-M, isomerization and cracking rates were approximately equal. No olefins were observed at 250°C while substantial olefins were present at 400°C. On Pt-H-M, isomerization and cracking occurred at both temperatures indicating that the rate controlling step was isomerization and β-scission of the intermediate carbonium ion. They propose the following reaction scheme for n-C_6 cracking and isomerization of n-C_6:

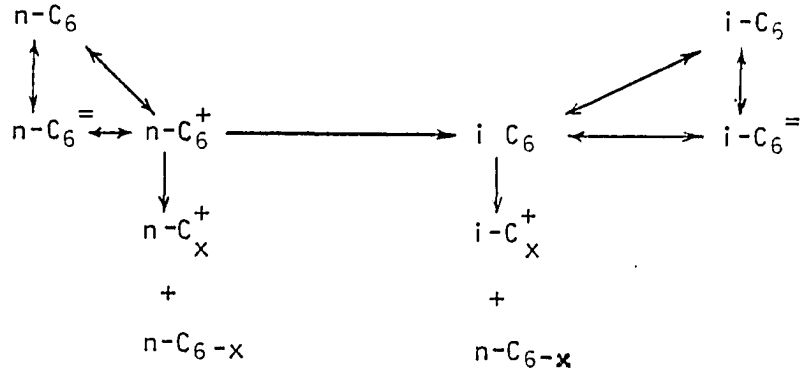

where $1 \leq x \leq 4$.

The authors conclude that the classical carbonium ion mechanism is consistent with results on both catalysts. At 400°C, the formation and desorption of carbonium ions is rate determining. Isomerization does not

Reproduced with permission of the copyright owner. Further reproduction prohibited without permission.

occur since it is slow relative to scission. Decreasing the temperature or adding Pt improves the adsorption and desorption rate of the intermediate and favors isomerization over cracking.

Comparison of Mordenite and Faujasite

Several studies comparing the activity and properties of mordenite and faujasite catalysts have been carried out. Gray and Cobb state that the active sites of mordenite are similar to their faujasite counterparts (40). Despite similarities, each has its own peculiarities. For example, steric effects are more pronounced on mordenite since it has a smaller pore size than type Y (25,41,42,43). Addition of a noble metal does not increase $n\text{-}C_5$ isomerization activity on H-M as it does on H-Y (25,33,35,43-45). Fetting and Schoeneberger examined the influence of structural parameters of H-M and Ca-Y on the activity and selectivity in $n\text{-}C_5$ and $n\text{-}C_6$ hydroisomerization (15). The H-M was found to have 7-8 Å primary and 10,000 Å secondary pore diameters while Ca-Y had 9 Å and 4000 Å diameters respectively. These properties were found to be unaltered after metal loading. The authors defined activity as the temperature dependence of the conversion and selectivity as the fraction of isomers of the total conversion. Various cations; Re, Ni, Ru, Rh, Pd, Pt, were selected to determine the effect of the metal type on activity and selectivity. Pd and Pt had the highest isomerization selectivity while Re had the highest activity. Ru, Rh, and Ni had high initial hydrogenating activity but also had high deactivation rates. Pt-H-M had a higher $n\text{-}C_6$ isomerization activity than Pd-H-M while this order of metal influence was reversed on Ca-Y. Ni-H-M was found to be active for cracking as was Ni-Ca-Y. However, on Ni-Ca-Y, the major product was CH_4 while on

Reproduced with permission of the copyright owner. Further reproduction prohibited without permission.

Ni-H-M, C_3 and C_4 isomers were the main products. This agrees with the results of Boudart (46), and may reflect the higher acidity of H-M associated with its higher SiO_2/Al_2O_3 ratio. In examing the effect of catalyst type at the same metal loading, Fetting and Schoeneberger found that Pt-H-M had an activity and selectivity at 523-583°K that Pt-Ca-Y did not exhibit until 613-693°K. This was true for both n-C_5 and n-C_6 isomerization

The authors suggested that this was due to a secondary pore resistance i.e., that associated with the spaces between zeolite crystals, on Pt-Ca-Y. The effectiveness factor was found to decrease with catalyst particle size resulting in a decrease in apparent activation energy from 97 to 67 kJ/g-mole. The authors found that Pt-H-M had a higher activity at low temperatures than did Pt-Ca-Y.

Reproduced with permission of the copyright owner. Further reproduction prohibited without permission.

Experimental Procedure

The equipment described is located in the Petroleum Processing Laboratory of the Chemical Engineering Department of Louisiana State University in Baton Rouge. The equipment was obtained primarily through donation of apparatus or funds by Exxon Research and Development Labs in Baton Rouge. The .5% Pd-H-M catalyst used in this study, batch LJJ-289, as well as the .5% Pd-H-Y, a physical mixture of two identically prepared batches HJE-243 and HJE-244, were provided by Exxon Labs.

A schematic flow diagram of the equipment is shown in Figure 4 . With the exception of the hydrocarbon feed pumps, gas cylinders, and control panelboard, the equipment was located in a walk-in hood with a 3000 CFM exhaust fan and sliding safety glass window. The gas cylinders, containing high purity electrolytic hydrogen, were located remotely from the laboratory.

The hydrogen was fed through a $Pd-Al_2O_3$ catalyst bed maintained at $350^{\circ}F$ by thermostatic control to convert any O_2 in the stream to H_2O. The water was subsequently removed in beds containing 3A molecular sieves and indicating Drierite desiccant.

Hydrogen flow was regulated by a Foxboro flow control valve coupled with an indicating flow controller located on the panel. A Foxboro DP cell equipped with a .006-in. integral orifice was used to measure the H_2 flow and provide an input signal to the flow controller. A Matheson pressure regulator assured a relatively constant hydrogen supply pressure immediately upstream of the control valve. A Mity-Mite back pressure regulator provided a constant pressure downstream of the orifice.

Reproduced with permission of the copyright owner. Further reproduction prohibited without permission.

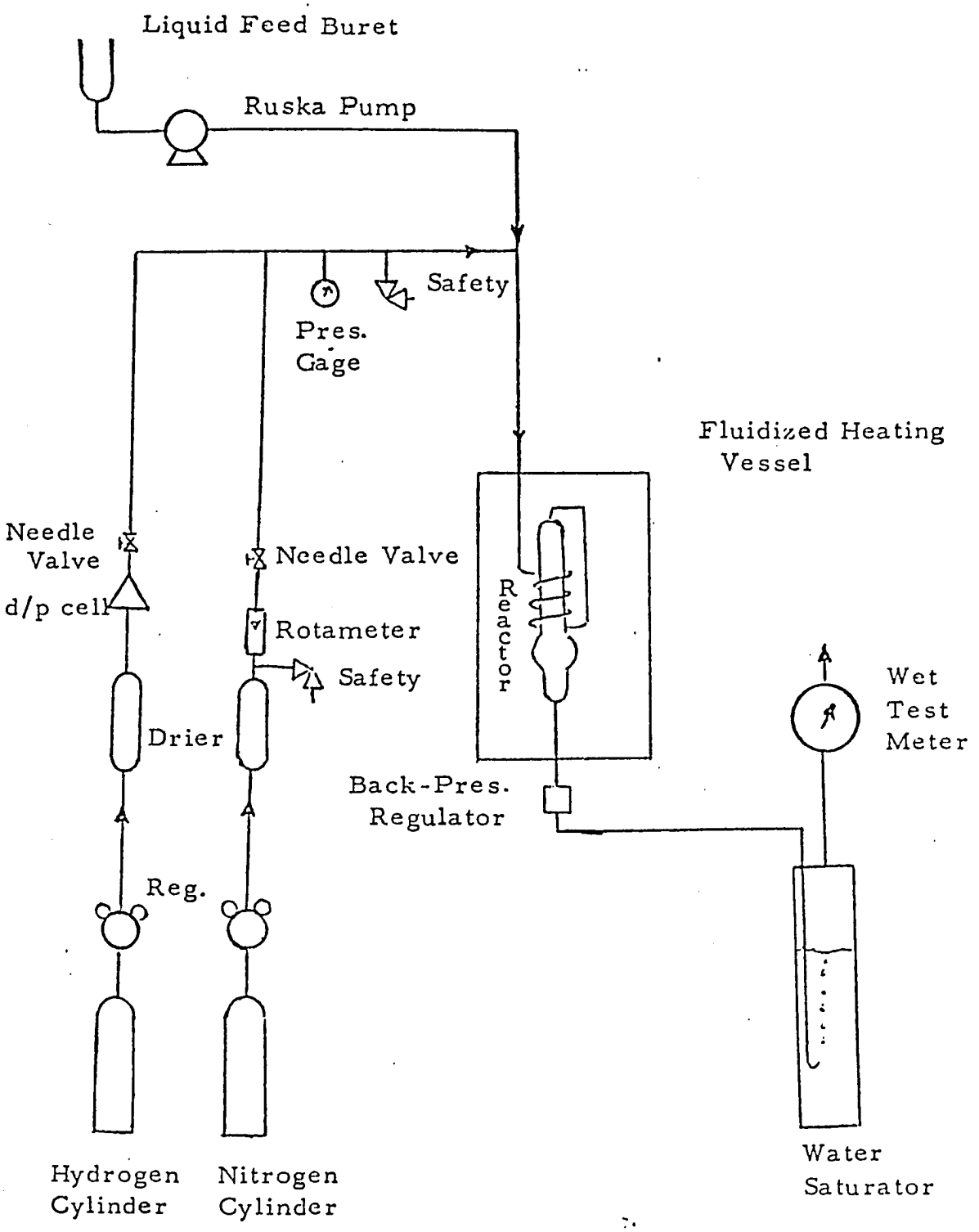

Figure 4. Simplified Flow Plan.

Reproduced with permission of the copyright owner. Further reproduction prohibited without permission.

Three hydrocarbon feed pumps were used to feed n-C_5, n-C_6, and mixtures to the reactor. The n-C_5 and n-C_6 were Phillips reagent grade (99^+ mole % minimum) materials. Gas chromatographic analysis confirmed their purity. The feed pumps were positive displacement Ruska pumps, each having a 250 cc capacity. The feed rate could be varied from 2 to 240 cc/hr by changing gears in the drive system. The motors for these pumps were explosion proof.

The reactor was a fixed bed tublar type. Figure 5 shows a detailed cross section of the reactor with catalyst in place. The reactor is made of ½-in. sch 80 Inconel pipe with a 40 cc capacity. The catalyst was physically mixed with inert mullite to avoid hot spots in the catalyst bed by enhancing heat transfer. The volume of the catalyst plus mullite charges was 10 cc. This charge was located between glass wool plugs which filled the remaining reactor volume. A single iron constantan thermocouple located in the middle of the catalyst charge was used to monitor the reaction temperature. The reactor was sealed using a replaceable steel O-ring held in place by a temperature compensating coupling.

An air-fluidized sand bath, heated by six 500 watt strip heaters surrounding the submerged reactor was used to control the reaction temperature. The air fluidizing rate was controlled by a rotameter. Three of the strip heaters were controlled manually by a Variac rheostat while the remaining three were controlled automatically by a Eurotherm temperature controller. Both the Variac and Eurotherm controls were located on the panel. The sandbath temperature was monitored by an iron-constantan thermocouple, which provided input to the Eurotherm controller,

Reproduced with permission of the copyright owner. Further reproduction prohibited without permission.

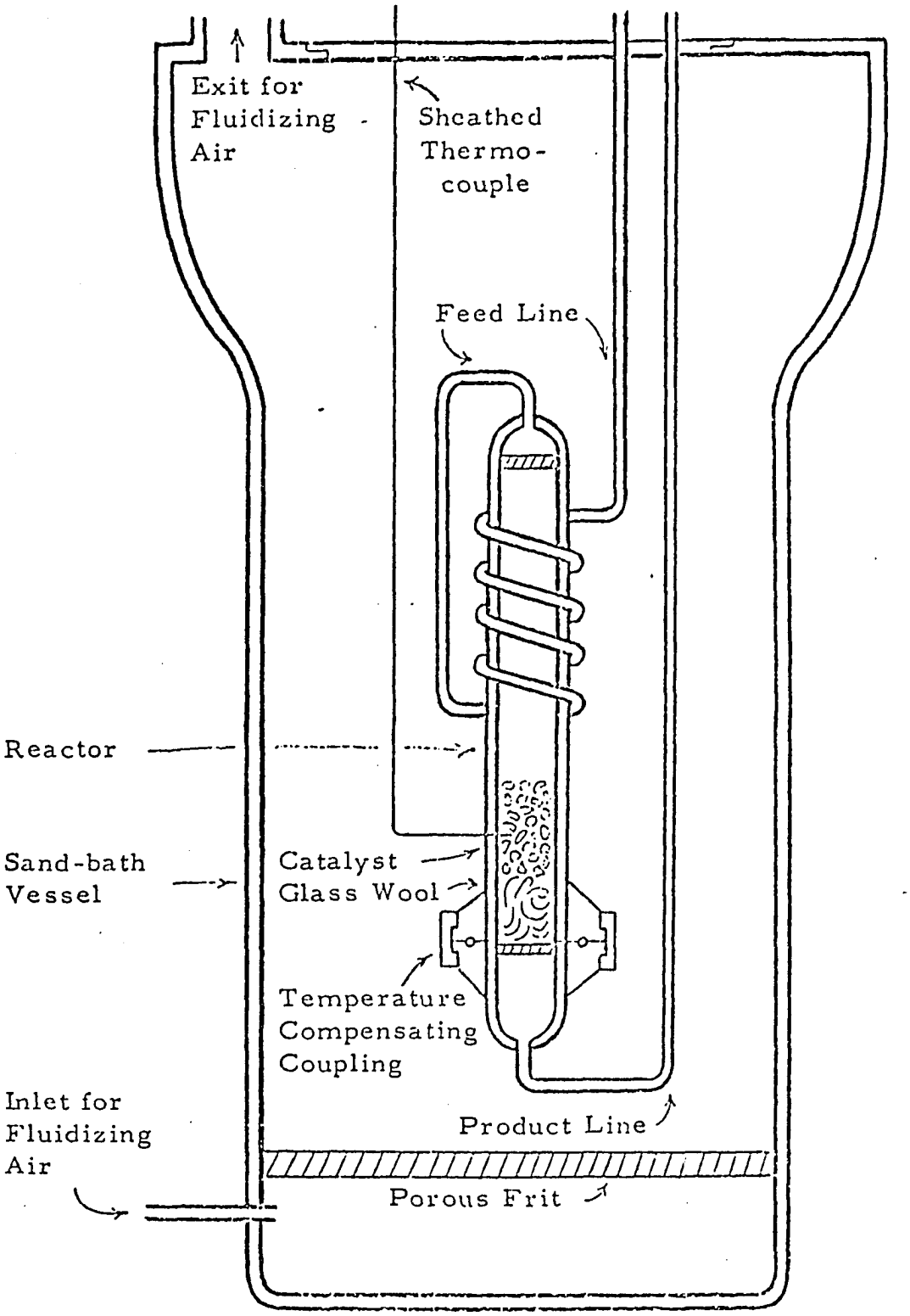

Figure 5. Reactor System in the Sand Bath Vessel.

Reproduced with permission of the copyright owner. Further reproduction prohibited without permission.

located in a top-entering thermowell. The reactor, sandbath, and other routinely monitored temperatures were displayed on a Doric digital temperature indicator located on the panel. A West Guardsman temperature safety device located on the panel shut off hydrogen and hydrocarbon flows and sandbath heat in the event of an unsafe reactor temperature.

The hydrocarbon liquid feed was mixed with the hydrogen, fully vaporized, and brought to the reactor temperature by passing through a coiled length of tubing submersed in the sandbath. The reactor pressure was set and controlled by a Mity-Mite back pressure regulator downstream of the reactor. Pressure gauges 0-1000 psig, were located at the reactor inlet and exit to monitor reactor pressure. Mercoid pressure switches for shutting off hydrogen and hydrocarbon feeds as well as sandbath heat in the event of excessively low/high air supply pressure or low/high reactor pressure were located in the hood. The reactor was also protected by a 1000 psig pressure relief valve.

Since the dew point of the reactor effluent gas was well below ambient temperature, the product gas was measured and sampled as follows. The effluent was passed through a counterflow fixed bed Rashig ring water saturator and then through a .05 ft^3/rev. wet test meter. The gas was then vented through the exhaust fan to the atmosphere. The gas was sampled for GC analysis through a septum located between the reactor outlet and the water saturator. Glass syringes used to extract samples were Teflon sealed and gas tight. The reactor effluent gas was analyzed on a dual column Perkin-Elmer model 990 gas chromatograph equipped with hot wire detectors. The column was 10 foot by 1/4-inch aluminum tubing packed with 20% Ucon HB-280X on 60/80 Chromasorb W. Integration

Reproduced with permission of the copyright owner. Further reproduction prohibited without permission.

of the peaks was carried out on a Varian CDS III integrator and recorded on a Varian 9176 recorder. Proportionality constants relating peak areas to mole fractions were obtained from a previous study (33) and confirmed in this study. These factors are shown in \Appendix 1.

Catalyst Preparation

The catalyst used in this study was prepared for use in the isomerization studies as follows:

1. About 100 cc of the catalyst was placed in a quartz glass open container which was then placed in a 2-inch O.D. glass tube. This glass tube lay inside a horizontal electric oven with both ends extending past the ends of the furnace.
2. An iron-constantan thermocouple was inserted through one end of the glass tube and rested in the catalyst charge to measure its temperature.
3. Air flow over the catalyst was begun as soon as heating started. The air served to remove moisture from the calcining catalyst. The air was treated to remove any traces of hydrocarbons by passing it through a copper oxide catalyst bed at 1000°F. The air was then dried by passing through 13 X molecular sieves and indicating Drierite before entering the oven. The air flow rate was controlled by a rotameter.
4. The temperature of the oven was programmed as follows:
   a. Increase from ambient to 350°F at a maximum rate of 100°F/hr.

Reproduced with permission of the copyright owner. Further reproduction prohibited without permission.

b. Maintain at 350°F for 16 hours.

c. Increase from 350°F to 1000°F at a maximum rate of 125°F/hr.

d. Maintain at 1000°F for 3 hours.

e. Cool to 350°F as rapidly as practical.

5. The temperature was monitored by a Doric digital temperature indicator. The hot calcined catalyst was placed in a desiccator to cool to ambient temperature. The catalyst was stored in the dessicator until needed.

6. Inert mullite used to dilute the catalyst charges was calcined in an open ceramic dish in a muffle furnace at 1000°F for 24 hours. The calcined mullite was cooled to 350°F at ambient conditions and stored in a desiccator for later use.

Catalyst Loading

The catalyst was weighed with a Mettler analytical balance and mixed with sufficient mullite to make 10 cc volume. The reactor was charged with a section of glass wool and then the catalyst mixture was placed in the reactor. A second section of glass wool was inserted behind the catalyst charge. The reactor was sealed using a temperature compensating coupling and a steel O-ring coated with copper based anti-seize compound. The reactor was pressure tested with hydrogen at a pressure at least 50% higher than the run pressure. It was then de-pressurized, placed in the sandbath, and connected to the feed and product lines. The reactor was then checked at the run pressure for any leaks in the connecting lines. The sandbath was then heated rapidly to 465°F

Reproduced with permission of the copyright owner. Further reproduction prohibited without permission.

with hydrogen flowing through the reactor. This activation of the catalyst was carried out for 1/2 hour to reduce the noble metal impregnated in the catalyst.

Run Procedure

The runs were carried out as follows:

1. The hydrogen flow rate was set on the automatic flow controller.
2. After about 15 minutes for equilibration, the flow rate was measured on the wet test meter and recorded.
3. Pure pentane was fed to the reactor using a positive displacement pump. Mixtures of pentane and hexane were fed from a second pump. These mixtures were prepared using volumetric flasks and pipettes. Pure hexane was fed from a third pump.
4. The runs were made in the following order; pure pentane, mixtures, pure hexane, then a repeat pure pentane run to determine if there had been any catalyst deactivation. None was found in any run on either catalyst.
5. For each run, a material balance was made after 3/4 to 1 hour on feed. This was done by noting the hydrocarbon feed rate, reactor effluent flow rate, and reactor effluent composition. The material balance procedure is outlined in Appendix 1 .
6. Gas samples were taken after the 3/4 to 1 hour equilibration period and analyzed on the gas chromatograph.
7. After obtaining the material balance and samples, the hydrocarbon feed was stopped. The hydrogen flow rate was

Reproduced with permission of the copyright owner. Further reproduction prohibited without permission.

allowed to return to the set conditions and re-checked.

Run Data

Data necessary for the material balance and rate constant calculation is shown below:

1. Barometric pressure was measured using a mercury barometer. The room temperature was measured using a thermometer.
2. Elapsed time for a .05 ft^3 revolution of the wet test meter along with the wet test meter water temperature were measured at the beginning, during, and end of each run.
3. For the material balance, the wet test meter reading and temperature and the displaced volume of the Ruska positive displacement pumps were taken both at the beginning and end of each run.
4. For each reactor effluent sample, the reactor, sandbath, and wet test meter temperatures along with the reactor pressure and time for a .05 ft^3 revolution were taken. The corresponding time on feed was also noted.
5. For each gas sample, the concentrations were calculated automatically and recorded.

Reproduced with permission of the copyright owner. Further reproduction prohibited without permission.

Kinetic Model

It is of primary interest in this study to develop a kinetic model for both catalysts. Such models can be used not only to compare the two catalysts but to predict performance as a function of feed concentrations and reaction conditions.

There are basically two types of kinetic models. A theoretical model may be derived directly from a postulated mechanism. By assuming certain steps to be rate controlling, various forms of the rate expression may be obtained and checked experimentally. In order to formulate a theoretical model, a complete reaction mechanism must be postulated. Once verified, a theoretical model may be used to extrapolate to conditions beyond experimental data. In addition, valuable insight into a given reaction can often lead to more general applications of the findings in related reaction studies. However, there are limits to the use of theoretical models. Complete mechanisms are known with certainty for few reactions. Also, there are often so many parameters to be found that they cannot be determined with acceptable accuracy. Empirical models are those which use experimental data together with simplified forms of the theoretical model to extract a rate expression. Such models are valuable in that they are soundly based on experimental data. However, extrapolation beyond the range of the data is generally not valid.

In this study, theoretical models will be developed to determine the form of the rate expression. Certain groups of parameters will be lumped and simplifying assumptions made in order to make statistical analysis of the data tractable and

Reproduced with permission of the copyright owner. Further reproduction prohibited without permission.

determination of the lumped parameters valid.

In this section, the theoretical basis of the kinetic model for the hydroisomerization of n-C_5 and n-C_6 will be developed. Simplifying assumptions will be made to arrive at a final model. Methods of statistical analysis of the data will be discussed.

Heterogeneous reactions have been described by Langmuir-Hinshelwood equations and are presented by Hougen and Watson (47). The phenomena of solid-gas reactions may be described by the following steps:

1. Mass transfer of reactants from the bulk gas phase to the exterior surface of the catalyst bed.
2. Diffusion of the reactants from the catalyst surface through the pores.
3. Adsorption of reactants on active catalyst sites.
4. Surface reaction on the active sites.
5. Diffusion of products to the exterior surface of the catalyst.
6. Mass transfer of the products to the bulk gas phase.

Any of these six steps could conceivably be rate determining. It is necessary to examine the effects of internal and external mass transport to determine their effect on the observed reaction rate. In addition, it is necessary to examine several other phenomena which are vital in the formulation of the kinetic model: the degree of isothermality along the catalyst bed, the fugacity coefficients of the reactants and products, and the nature of the flow in the reaction zone.

Reproduced with permission of the copyright owner. Further reproduction prohibited without permission.

Internal Mass Transport

Since essentially all the reaction on the catalyst takes place within the catalyst particle, the reactants must diffuse into the particle and products must diffuse out. This mass transport occurs as the result of a concentration gradient between the bulk fluid phase and the interior of the catalyst. A gradient must exist for diffusion to occur. If the diffusion rate for the reactant and product species is very high compared to the surface reaction rate, then whenever even a small gradient occurs in the catalyst particle, diffusion of that species is rapid and the concentration within the catalyst is essentially constant. This is the case when surface reaction is rate controlling. If the diffusion rate is slow compared to the reaction rate, diffusion is rate controlling. Since the concentration at the interior catalyst surface is lower when diffusion is rate controlling, for first and higher order reactions a diffusion controlled rate will be lower than a surface controlled rate.

The catalyst effectiveness factor, E, is defined as the ratio of the actual overall reaction rate to the rate that would be observed if the reactant concentration in the entire catalyst were the same as the concentration at the catalyst surface. This effectiveness factor can be shown to be a function of a group of catalyst and kinetic parameters known as the Thiele modulus, h_s. For spherical particles, in which the simple reaction A→B is proceeding, as shown by Petersen (48),

$$h_s = R\sqrt{\frac{\rho_p S_g k_o}{D_e}} \qquad (1)$$

Reproduced with permission of the copyright owner. Further reproduction prohibited without permission.

where ρ_p = catalyst density, g/cc

R = catalyst particle radius, cm

S_g = specific surface area, cm^2/g

k_o = surface reaction rate constant, cm/sec

D_e = effective diffusivity of reactant, cm^2/sec

In order to investigate the effective diffusivity coefficient, the controlling diffusion regime must be defined. Diffusion within the catalyst pore usually occurs by either Fickian or Knudsen diffusion. Fickian diffusion is the predominant mechanism accounting for mass transfer in the catalyst when the pore diameter is much larger than the mean free path of the diffusing gas. In other words, Fickian diffusion is important when a given gas molecule collides with other gas molecules much more often than with the pore wall. Fickian diffusivities are of the order of 10^{-2} cm^2/sec. When the diameter of the pore is of the same order as the mean free path, collisions with the wall become important and Knudsen diffusion predominates. Knudsen diffusivities are of the order of $10^{-3} \rightarrow 10^{-4}$ cm^2/sec. When the diameter of the diffusing molecule approaches the pore diameter, a third form of diffusion may occur, configurational diffusion (49). In this regime, the size and shape of the diffusing molecules and the pores affect diffusion. Diffusivities in this regime are of the order of 10^{-5} cm^2/sec.

Spry and Sawyer (50) studied the configurational diffusion effects of large asphaltene molecules with molecule diameters, MD, of 25 to 100 Å in hydrotreating catalysts with pore diameters, PD, from 25 to over 1000 Å. They found that the molecular diffusivity could be multiplied by a correction factor accounting for the ratio MD/PD to yield a configurational diffusivity as follows,

Reproduced with permission of the copyright owner. Further reproduction prohibited without permission.

$$D_C = D_m \left(1 - \frac{MD}{PD}\right)^4 \qquad (2)$$

where D_C = configurational diffusivity

D_m = molecular or bulk diffusivity.

The results of Spry and Sawyer show that configurational diffusion becomes important when MD/PD is more than 0.1. Since the pores of the mordenite and faujalite catalysts used in this study are of the order of 6-10Å and the molecular diameters of n-C^5 and n-C^6 are ~5Å, significant configurational diffusion resistance may be expected. To study this phenomenon, catalysts of various sized pores could be used at the same reaction conditions. Such catalysts have not been available. Thus, the effects of this diffusion were included in the overall rate expression. This procedure has been followed by others such as Voorhies and Hopper (63) and Braun, et al., (15).

To determine the effect of internal diffusion resistance, both molecular and Knudsen, a Thiele modulus can be calculated and correlated, as shown by Petersen (48), with the effectiveness factor. An effectiveness factor of 1.0 corresponds to insignificant diffusion resistance.

First, the diffusion regime in which the catalyst operates under conditions of this study, must be determined. Petersen states that the mean free path, λ, must be compared to the pore diameter, D. For $D/\lambda \ll 1$, molecular diffusion predominates. When $D/\lambda \to 1$, Knudsen diffusion becomes important. The transition between these two regimes is called the slip region. A "slip" diffusivity, D_s, can be calculated from the Knudsen and molecular diffusivities, D_k and D_m, respectively, as will be shown below.

From the kinetic theory of gases, it can be shown that the mean free path is given by

Reproduced with permission of the copyright owner. Further reproduction prohibited without permission.

$$\lambda = \frac{kT}{\sqrt{2}\,\pi\,\sigma^2\,P} \qquad (3)$$

where k = Boltzman's constant, cm^2-atm/°K

T = absolute temperature, °K

σ = molecular diameter, cm

P = absolute pressure, atm

The molecular diameters of the reacting species, n-C_5 and n-C_6, may be calculated from viscosity data as shown by Reid and Sherwood (64). This value represents the effective diameter of a molecule which corresponds to the hard sphere assumption upon which equation (3) is based. Reid and Sherwood list Lennard-Jones molecular radii for n-C_5 and n-C_6. Using these values, the mean free paths may be calculated at 465°F and 300 psig to be,

$$\lambda_{C_5} = 23.0\ \text{Å}$$

$$\lambda_{C_6} = 22.1\ \text{Å}$$

Since the pore diameters for the mordenite and faujasite catalysts used in this study are of the order of 8 Å, then by Petersen's criterion

$$\frac{D}{\lambda_{C_5}} = \frac{D}{\lambda_{C_6}} = .36$$

Thus, the diffusivities must be calculated based on the formula given by Bosanquet (51) for the slip region,

$$\frac{1}{D_s} = \frac{1}{D_m} + \frac{1}{D_k} \qquad (4)$$

Reproduced with permission of the copyright owner. Further reproduction prohibited without permission.

To calculate this effective diffusivity in the slip region, both the molecular and Knudsen diffusivities, D_m and D_k, must be calculated. Using the equation of Wilke and Lee (52), it can be shown that at 465°F, 300 psig,

$D_m = .061\ cm^2/sec$ $n\text{-}C_5$

$D_m = .056\ cm^2/sec$ $n\text{-}C_6$

and from Peterson (48)

$D_k = 2.04 \times 10^{-3}\ cm^2/sec$ $n\text{-}C_5$

$= 1.86 \times 10^{-3}\ cm^2/sec$ $n\text{-}C_6$

and it can be seen that

$D_s = 1.97 \times 10^{-3}$ $n\text{-}C_5$

$= 1.80 \times 10^{-3}\ cm^2/sec$ $n\text{-}C_6$

An alternate method of determing the true effective diffusivity is given by Petersen. He states that D_m must be multiplied by a geometric factor accounting for the tortuous paths of the true catalyst particle. Petersen summarizes several theoretical approaches to the problem of determining an accurate geometric factor, including electrical analogies. He states however that such methods fail in describing materials of relatively low porosity, such as a zeolite catalyst. In this case, experimental results are best. In general, the true effective diffusivity, D_e, may be related to the geometric factor as shown

$$\frac{D_e}{D_m} = \frac{\varepsilon\sigma}{\tau} = f_1(\text{geometry}) \qquad (5)$$

Reproduced with permission of the copyright owner. Further reproduction prohibited without permission.

Similarly

$$\frac{D_e}{D_k} = \frac{\varepsilon\sigma}{\tau} = f_2(\text{geometry}) \qquad (6)$$

where ε = porosity of the catalyst

σ = constriction factor

τ = totuosity factor

While there are wide ranges of results, in the worst cases, Petersen shows that D_e/D_m is approximately .04. In this case,

$D_e = 2.44 \times 10^{-3}$ cm^2/sec . n-C_5

$= 2.24 \times 10^{-3}$ cm^2/sec n-C_6

Since these values approximate those calculated from Bosanquet's equation, it can be said that there is additional evidence for accepting the slip region values.

From equation (2), using the Lennard-Jones radii for n-C_5 and n-C_6 and the appropriate pore diameters for mordenite and faujasite, it can be shown that on the mordenite, $D_c|_{C_5} = 4.6 \times 10^{-5}$cm^2/sec and $D_c|_{C_6} = 2.9 \times 10^{-5}$ cm^2/sec while on the faujasite $D_c|_{C_5} = 9.7 \times 10^{-4}$ cm^2/sec and $D_c|_{C_6} = 7.9 \times 10^{-4}$ cm /sec. Using these values, it can be shown from equation (1) that on the mordenite $h_s|_{C_5} = 3.3$ and $h_s|_{C_6} = 8.3$ while on the faujasite $h_s|_{C_5} = .72$ and $h_s|_{C_6} = 1.6$. From Petersen (48), the effectiveness factors corresponding to these values of the Thiele modulus, h_s, are

	E	
	Mordenite	Faujasite
n-C_5	.30	.90
n-C_6	.12	.55

Reproduced with permission of the copyright owner. Further reproduction prohibited without permission.

Thus, configurational diffusion effects result in significant diffusion resistance. In order to study the effect of configurational diffusion, catalysts with varying pore sizes would be needed. Such catalysts have not been available and configurational diffusion resistance was not examined. The first order rate constant in this study includes configurational diffusion effects. As stated earlier, this is the procedure used by other investigators (15, 63).

To observe experimentally in this study the extent of internal mass transfer effects, the particle size of the catalyst could be decreased to decrease the resistance. If the rate constant increased with decreased particle size, internal mass transfer is important and must be accounted for. Bryant (33) and Hopper (53) observed no variation in the first order rate constant for n-C_5 isomerization on Pd-H-mordenite over a ten-fold change in catalyst particle size, 0.1 to 1.0 mm diameter. Since the catalyst particle size and reaction conditions in this study corresponded closely to those used by Bryant and Hopper, resistance was assumed to have an insignificant effect on the first order rate constant as defined by equations (26) and (27) and calculated from equation (15).

Flow Patterns

Another phenomenon that must be investigated is the bulk flow pattern of the reactants and products over the catalyst bed. Plug flow is desired since this results in higher conversions. Any significant backmixing would lower conversions and complicate modelling of the reaction. Bryant(33) studied the flow patterns in a reactor nearly identical to that used in this study. He related the extend of axial dispersion to the Peclet number. The Peclet number, Pe, is the ratio of the bulk stream flow to the random motion of eddies. A Peclet number of

Reproduced with permission of the copyright owner. Further reproduction prohibited without permission.

zero corresponds to complete backmixing while ∞ corresponds to plug flow. Bryant found that for Pe > 50 and conversions from 20% to 70% the effects of backmixing are negligible.

A Peclet number for typical conditions used in this study is calculated as follows. The particle Reynolds number, Re_p, is found using the following relation:

$$Re_p = \frac{d_p W}{\mu A} = 2.49 \qquad (7)$$

where d_p = diameter of the catalyst particle, cm

μ = viscosity of the fluid, gm/cm-sec.

A = cross sectional area, cm^2

w = mass flow rate, g/sec

Levenspiel and Bischoff have correlated a mixing intensity, M, with Re_p (54). In this study

$$M = \frac{\varepsilon L}{Pe\ d_p} = .83$$

from which a Pe of 63.2 is calculated. Since this is well above the value of 50 below which backmixing first becomes significant, plug flow is assumed in this study.

External Mass Transport

External mass transfer refers to the convective and diffusive processes by which reactant is transferred from the bulk gas phase to the catalyst surface and products from the surface back to the bulk phase. This process may be modelled as mass transfer through a thin gas film in laminar flow at the catalyst surface. The higher the gas flow rate across the catalyst particle, the thinner the laminar layer becomes and the

Reproduced with permission of the copyright owner. Further reproduction prohibited without permission.

higher the mass transfer rate. If external mass transfer were rate controlling, it would be expected that varying the gas velocity would affect the conversion.

Pure component studies have been carried out on Pd-H-mordenite at conditions nearly identical to those used in this study. Bryant (33) found no variation in the rate constant for n-C_5 isomerization at 550°F and 450 psig while varying the gas velocity by a factor of four. Luzarraga (55) showed no variation in rate constant over an eight-fold change in gas velocity. On Pd-H-faujasite, Hatcher (56) showed no change in rate constant for n-hexane hydrocracking over a factor of 3 change in gas velocity. It may be concluded that previous studies imply that there is no significant external mass transfer resistance in the catalysts and under the conditions of this study.

Temperature Gradient in the Reactor

In studying the isomerization of pentane and hexane mixtures, the model for the reaction is based either on an isothermal or non-isothermal assumption. If the heat of reaction and the reaction rate were large, there would be significant temperature gradients along the tubular reactor used in this study. If such gradients existed, the reaction rate would vary along the reactor and the model would have to account for this effect.

In this study, a thermocouple measuring the temperature at the end of the catalyst bed was monitored routinely during each run. If there had been significant heat of reaction effects, this thermocouple would have registered a temperature significantly different from the sand bath in which the reactor was located. A maximum temperature difference from the sand bath of 3°F was observed with the normal temperature difference

Reproduced with permission of the copyright owner. Further reproduction prohibited without permission.

within ± 1°F. Since this was well within experimental error, it was concluded that the isothermal model for the catalyst bed was adequate.

Reactant Fugacities

To formulate the model, the fugacity coefficients of each of the reactants in the reactor must be calculated. In order to calculate the fugacity coefficients of the components of the reaction, an equation of state must be selected. Since the Redlich-Kwong equation has been shown to be valid at conditions such as those involved in this study, it was used.

At constant temperature, it can be shown that (57),

$$\ln \hat{\phi}_i = \int_V^\infty \left[\left(\frac{\partial nZ}{\partial n_i} \right)_{T, nV, n_j} - 1 \right] \frac{dV}{V} - \ln Z \qquad (8)$$

where $\hat{\phi}_i$ = fugacity coefficient of component i in the mixture

V = molar volume of the mixture, cc/g-mole

Z = compressibility of the mixture

T = temperature, °R

n_j = moles of component $j \neq i$, g-moles

n = mole of mixture, g-moles

the Redlich-Kwong equation of state is given by

$$Z = \frac{1}{1 - b/V} - \frac{a}{RT^{3/2}\, V(1 + b/V)} \qquad (9)$$

Where a and b are constants dependent on P and T but independent of composition.

Carrying out the indicated integration of equation (8) gives the result

$$\ln \hat{\phi}_i = \frac{b_i}{b} (Z-1) - \ln(Z-Zh) + \frac{a}{bRT^{3/2}} \left[\frac{b_i}{b} - \frac{2}{a} \sum_k y_k a_{ik} \right] \ln(1+h) \qquad (10)$$

Reproduced with permission of the copyright owner. Further reproduction prohibited without permission.

where $h = \frac{b}{v}$.

In order to use the above equation, certain interaction and mixture properties must be calculated as outlined by Prausnitz (58). The presence of hydrogen has a significant effect on this calculation, which is not detailed here. The results, calculated at 465°F, 300 psig, and 10/1 H_2/HC ratio, are

$$\hat{\phi}H_2 = 1.00888$$

$$\hat{\phi}C_5 = 1.00566$$

$$\hat{\phi}C_6 = 1.00953$$

Thus, the deviation from ideality at typical reaction conditions is <1%. The mixture will be assumed to be ideal in formulating the model.

Cracking

In studying hydroisomerization of n-C_5 and n-C_6, the extent of hydrocracking must be examined. If the extent of hydrocracking were large, it would have to be accounted for in the kinetic model. The products of hydrocracking of n-C_5 and n-C_6 would be C_1, C_2, and C_3 which are detectable even in small quantities ($\geq$.5 mole%) in the analysis of the reacting gas.

In the range of conditions used in this study, no hydrocracking was observed. Investigators using similar conditions and catalysts have not

Kinetic Model

The general Langmuir-Hinshelwood model describing reactions of gases on solid catalysts is given by:

Reproduced with permission of the copyright owner. Further reproduction prohibited without permission.

$$\text{rate} = \frac{[\text{kinetic term}]\ [\text{potential term}]}{[\text{adsorption term}]} \qquad (11)$$

The kinetic term includes both the true surface reaction rate constant, as well as constants characterizing the surface of the catalyst and in some cases adsorption constants. These constants may be lumped together to describe the dependence of the kinetic term on temperature as

$$k = A_o \exp\ (-E_{app}/RT) \qquad (12)$$

where E_{app} = apparent activation energy, kcal/g-mole

R = ideal gas constant, kcal/g-mole °K

A_o = pre exponential term, cc/g/sec

T = absolute temperature, °K.

The potential term for a first order elementary reaction $A \rightleftarrows B$ has the form

$$K_A P_A - \frac{K_B P_B}{K} \qquad (13)$$

where K_i = adsorption constant of species i, atm^{-1}

P_i = partial pressure of species i, atm

K = reaction equilibrium constant, dimensionless.

The adsorption term has the form

$$(1 + K_A P_A + K_B P_B)^n$$

where n = number of active catalyst sites involved in the reaction.

The exponent n usually has a value of 1 or 2. The exact form of the adsorption term may change depending on the rate-limiting step for a given reaction. Although this term is somewhat temperature

Reproduced with permission of the copyright owner. Further reproduction prohibited without permission.

dependent, the exponetial temperature dependence of the kinetic term makes the variation of the adsorption term with temperature relatively insignificant. However, the ratio $k' = \frac{\text{kinetic term}}{\text{adsorption term}}$ will vary depending on the nature of the catalyst, surface kinetics and the rate-determining step. Strickland (60) has developed the various forms that k' can take depending on the rate controlling step for a catalyst with acidic and metallic sites for the reaction $A \rightleftarrows B$. These will be examined in discussing the statistical analysis of the data later in this chapter.

The overall rate constant expression must be developed to relate experimental results to the kinetic parameters of importance. The material balance equation for an integral reactor in plug flow is given by

$$r = \frac{dN_B}{dW} = k(C_A - C_B/K) \qquad (14)$$

where r = reaction rate, g-mole/gm/sec

N_B = flow rate of product B, g-mole/sec

W = weight of catalyst, gm

k = first order rate constant, cc/gm/sec

$C_{A,B}$ = concentrations of A, B, g-mole/cc

K = thermodynamic equilibrium constant, dimensionless.

The rate constant above, k, is a lumped term including both the adsorption term and the effectiveness factor.

Assuming first order kinetics, pure A as feed, and fugacity coefficients of unity for all hydrocarbon species, the first order rate constant may be calculated from experimental data as shown by Livesay (65) to be,

Reproduced with permission of the copyright owner. Further reproduction prohibited without permission.

$$k = \frac{Y^*_B}{\rho_B t_H} \ln\left(1 - \frac{Y_B}{Y^*_B}\right) \qquad (15)$$

which is the integrated form of equation (14) assuming no B in the feed gas, where Y^*_B = equilibrium mole fraction of isomerized products for $A \rightleftarrows B$

t_H = catalyst volume/total volumetric flow rate or superficial holding time, sec.

Y_B = experimental mole fraction of isomers

ρ_B = bulk density of the catalyst, gm/cc.

The experiments are carried out to determine Y_B from analysis of the reactor effluent gas. Knowing t_H from the volumetric flow rates of reactants and products, ρ_B from measurement, and Y^*_B from literature data, it is possible to calculate k for a given set of conditions. In the case of n-C_5 and n-C_6 mixtures as feed, t_H accounts for both hydrocarbon feed rates and equation (15)is used to calculate the individual rate constants. For mixtures, the rate constant for n-C_5 or n-C_6 isomerization is found by

$$Y_B = \frac{\Sigma \text{ isomer concentrations}}{\Sigma(\text{isomers + normal}) \text{ concentrations}} .$$

Y_B was determined from analysis of the reactor effluent gas. Knowing t_H from the volumetric flow rates of reactants and products, ρ_B from measurement, and Y^*_B from literature data, it was possible to calculate k for a given set of conditions. In the case of n-C_5 and n-C_6 mixtures as feed, t_H accounts for both hydrocarbon feed rates and equation (15) is used to calculate the individual rate constants. For mixtures, the isomer concentration for n-C_5 or n-C_6 isomerization

Reproduced with permission of the copyright owner. Further reproduction prohibited without permission.

was calculated by

$$Y_B = \frac{\Sigma \text{ isomer concentrations}}{\Sigma(\text{isomers + normal}) \text{ concentrations}}$$

as calculated from the reactor gas effluent. Appendices 1, 2, and 3 give details of this calculation.

Now, assuming that Langmuir adsorption isotherms may be applied to the simple first order reversible model for hydroisomerization (47), the first order rate constant may be expressed as

$$k = \frac{k_o \prod_i K_i}{(1 - \sum_i K_i P_i)^n} \qquad i = n\text{-}C_5,\ n\text{-}C_6,\ H_2 \qquad (16)$$

where n = number of catalyst sites involved in the reaction, usually 1 or 2

k_o = true surface reaction rate constant

K_i = equilibrium adsorption constants for component i

P_i = partial pressure of component i, psia

k = first order rate constant, cc/gm/sec

Since k_o and K_i are functions of temperature only, then for a given isothermal set of runs, they may be considered constant. In the statistical analysis of the rate constant, we will then assume the following general form

$$k = \frac{\bar{k}}{[1 + \Sigma K_i P_i]^n} \qquad (17)$$

From this general form, the dependence of k on pressure, temperature, H_2/HC ratio, space velocity, and a mixed hydrocarbon feed will be examined. By defining the relationship between k and these variables, important properties of the catalyst and the reaction kinetics can be determined.

Reproduced with permission of the copyright owner. Further reproduction prohibited without permission.

Effect of Pressure

If the adsorption constants for the hydrocarbon species are approximately equal, it can be shown that

$$k^{-1/n} = \bar{k}^{-1/n} \left[1 + P_{tot} \frac{(\tilde{R}K_{H_2} + K_{HC})}{(1 + \tilde{R})} \right] \qquad (18)$$

where $\tilde{R}$ = H_2/HC ratio

K_{H_2} = hydrogen adsorption constant

K_{HC} = hydrocarbon adsorption constant

By plotting $k^{-1/n}$ against P_{tot} at constant $\tilde{R}$, a straight line should be obtained with a positive intercept corresponding to $\bar{k}^{-1/n}$. In order to determine the value of n, different values of n are assumed and the above plot is made. For a given n, if a negative intercept is obtained, that value of n may be rejected since $\bar{k} > 0$. Note that if the hydrocarbon adsorption constants are not equal, the same plot could be made for a given series of pure component, say n-C_5, runs to determine the value of n for C_5 isomerization.

Effect of Temperature

We assume that the temperature dependence of k_o may be represented by

$$k_o = A\, e^{-E'/RT} \qquad (19)$$

where E' = true surface reaction activation energy.

The variation of the adsorption constants with temperature is given below where ΔH_i is the heat of adsorption of species i,

$$K_i = K_{oi} \exp\left[\frac{\Delta H}{R} i \left(\frac{1}{T} - \frac{1}{T_o}\right)\right] \qquad i = C_5,\ C_6,\ H_2 \qquad (20)$$

Reproduced with permission of the copyright owner. Further reproduction prohibited without permission.

The simplified rate constant defined by equation (16) includes the temperature effects of the surface reaction as well as adsorption. If (19) and (20) are substituted into (16) and the derivative of ln k is taken with respect to 1/T, it can be shown that

$$E_{app} = E' + \sum_{i=1}^{m} \Delta H_i + nR \frac{d}{d(\frac{1}{T})} [\ln (1 + \sum_{i=1}^{n} K_i P_i)] \qquad (21)$$

where E_{app} = apparent activation energy.

E_{app} is the value that would be obtained when a typical Arrhenius plot of ln k vs. 1/T is made. It includes both the true activation energy, E', and the adsorption effects. Its value will thus depend on the nature of the catalyst surface and the particular adsorbates. It may be anticipated that E_{app} will vary substantially from catalyst to catalyst. Levenspiel (61) has shown that if diffusion is rate-limiting, then

$$E_{app} = \frac{E' + E_d}{2}$$

where E_d = activation energy for diffusion. Since E_d is typically 1 ÷ 4 kcal/g-mole and E' is of the order of 30 ÷ 60 kcal/g-mole, then

$$E_{app} \simeq \frac{E'}{2}$$

for reactions influenced by strong pore resistance.

Effect of Space Velocity

From equation (15) it can be seen that since t_H is the ratio of the catalyst volume to the total volumetric flow rate, V_T, then $t_H = \frac{W}{\rho_G V_T M_G}$, where ρ_G is the molar gas density and M_G is the gas molecular weight. But $V_T = \frac{RT}{P_{tot}} (N_{RO} + N_{H_2}) = \frac{N_{RO}}{\rho_G} (1 + R)$. Substituting it

Reproduced with permission of the copyright owner. Further reproduction prohibited without permission.

can be seen that

$$\ln\left(1 - \frac{Y_B}{Y_B^*}\right) = k \left[\frac{\rho_G}{Y_B^* \ (1+\tilde{R})} \ \frac{W_c}{N_{RO}}\right] \tag{22}$$

But $\frac{N_{RO}}{W_c}$ = weight hourly space velocity, τ_w.

Thus

$$\ln\left(1 - \frac{Y_B}{Y_B^*}\right) = k \frac{\rho_G}{Y_B^* \ (1+\tilde{R})} \ \frac{1}{\tau_w} \tag{23}$$

If the assumption that the hydroisomerization of n-C_5 and n-C_6 may be represented by a first order reversible reaction is valid, a plot of $\ln(1 - Y_B/Y_B^*$ versus $1/\tau_w$ should be a straight line with an intercept of 1.0 at any given temperature.

Effect of H_2/HC Ratio

From equation (18) it can be seen that at a given temperature and pressure, k will vary with $\tilde{R}$ as

$$k = \bar{k}^{-1/n} + \bar{k}^{-1/n} P_{tot} \frac{[\tilde{R} K_H + K_{HC}]}{1 + \tilde{R}} \tag{24}$$

From this relationship, the relative values of the hydrocarbon and hydrogen adsorption constants may be determined as follows.

1. If $K_{HC} >> K_{H_2}$, a plot of $k^{-1/n}$ vs. $1/\tilde{R}+1$ should give a straight line with a negative abscissa intercept.

Reproduced with permission of the copyright owner. Further reproduction prohibited without permission.

2. If $K_{H_2} >> K_{HC}$, a plot of $k^{-1/n}$ vs. $\tilde{R}/(\tilde{R}+1)$ should give a straight line with a negative abscissa intercept.

3. If $K_{H_2} \simeq K_{HC}$, k will not vary with $\tilde{R}$.

Effect of a n-C_5/n-C_6 Mixture as Feed

From equation (17) it can be seen that if a mixture of hydrocarbons is used as feed, the adsorption term must include the $K_i P_i$ product for both hydrocarbons. If the two reactants have different adsorption constants, it can be seen that k for the more strongly adsorbed species will increase on dilution with a more weakly adsorbed species. This can be reasoned as follows. For a C_5/C_6 feed;

$$k_i = \frac{\bar{k}}{(1 + K_{C_5} P_{C_5} + K_{C_6} P_{C_6} + K_{H_2} P_{H_2})^n} \qquad i = C_5, C_6 \tag{25}$$

If $K_{C_6} >> K_{C_5}$, as P_{C_5} is increased, P_{C_6} must decrease since all runs are made at a given H_2/HC ratio. Since K_{C_5} is small, the product $K_{C_5} P_{C_5}$ is also small and negligible to $K_{C_6} P_{C_6}$. However, $K_{C_6} P_{C_6}$ is getting smaller on dilution and thus k_{C_6} must increase.

It should be noted that the psuedo first order rate constants are calculated for the reactions

$$\text{n-}C_5 \xrightarrow{k_{C_5}} \text{i-}C_5 \tag{26}$$

$$\text{n-}C_6 \xrightarrow{k_{C_6}} \text{isomers of } C_6 \tag{27}$$

using a model in which the rate constants are constant for a given P_{tot}, T, and $\tilde{R}$, i.e., for a given run.

Reproduced with permission of the copyright owner. Further reproduction prohibited without permission.

Now, having established the experimental variation of k with the important independent variables used in this study, it is necessary to examine the statistical methods to be used in analysis of the data.

Statistical Analysis of k

The simplified rate constant may be subjected to statistical analysis to determine the rate controlling step and to some extent the nature of the surface kinetics. This is accomplished by analysis of the parameters of various postulated models of k to decide not only the best model but the relationships among the parameters of a given model. By postulating various forms of $k(P_i)$ from different mechanisms and different rate limiting steps, it is possible to determine:

1. The apparent rate controlling step
2. The relative magnitude of the adsorption constants of the feed components
3. The number of sites involved in the surface reaction.

It is important to recognize that the information obtained by analyzing the rate constant as it varies with temperature, pressure, space velocity, and H_2/HC ratio is independent of the information obtained through statistical work. For example, the fact that a plot of $k^{-\frac{1}{2}}$ vs. P_{tot} indicates a dual site mechanism is independent of the fact that

$$k = \frac{\bar{k}}{[1 + \Sigma K_i P_i]^2} \qquad (28)$$

may give the best fit of the data, although equation (28) indicates a dual site mechanism also. However, it would be expected that results from statistical analysis and from other analysis would not be contradictory,

Reproduced with permission of the copyright owner. Further reproduction prohibited without permission.

but complementary. If both types of analysis indicate, for example, that dehydrogenation was the rate controlling step for hydroisomerization of n-C_5 on the mordenite catalyst, this must be considered strong evidence that such is the case.

Strickland (60) has derived the various forms of the rate expression for the reaction A $\rightleftarrows$ B on a dual function catalyst such as those used in this study. Basically, they may be summarized as shown below:

Rate Controlling Step	Single Site Mechanism	Dual Site Mechanism
Isomerization	$k = \frac{\bar{k}_1}{P_{H_2}(1 + \Sigma K_i P_i)}$	$= \frac{\bar{k}_1'}{P_{H_2}(1 + \Sigma K_i P_i)^2}$
Dehydrogenation		$= \frac{\bar{k}_2'}{(1 + \Sigma K_i P_i)^2}$

Within each of these basic forms, there are numerous variations depending on the relative magnitude of the adsorption constants. For example, if there is reason to believe from previous analysis that $K_{H_2} << K_{C_5}, K_{C_6}$, then it may be possible to delete the hydrogen adsorption constant.

It can be seen that if a series of mixtures of two hydrocarbons is fed to the reactor and k for each species is calculated, it is possible to determine, through a non-linear least squares algorithm, quantitatively how well a given model represents the functional dependence of k_{C_5} and k_{C_6} on the partial pressure of each reaction. In such an analysis, the independent variables are the P_i's, the dependent variables are the k's, and parameters to be determined are the adsorption constants and the numerators, k_i''s.

Reproduced with permission of the copyright owner. Further reproduction prohibited without permission.

Daniel and Wood (62) have developed a non-linear least squares routine which can be used to test each model. Each model to be tested is of the form, for an m parameter model,

$$k = k(P_i, B_j) \qquad i = C_5, C_6, H_2 \qquad j = 1, \ldots, m$$

From the program (62), the following information is obtained for each model.

1. For each parameter; σ, t-value, 95% confidence limits, and the numerical value are given. This allows each parameter to be evaluated individually. For a given model, the confidence limits on each parameter are one measure of the validity of the model. The confidence limits are boundaries which, at a given confidence level, include the true value of the parameter. These limits represent a region in which the null hypothesis may be rejected at this given confidence level. The null hypothesis states that the variable in question, in this case a given parameter B_i, is drawn from a population of mean zero and a standard deviation corresponding to that calculated for a given parameter. This is called the null population. The standard deviation is calculated for each parameter as described by Daniel and Wood. For example, 90% confidence limits on B_i define two points symmetric to the mean at which there is a 10% chance that the value of B_i was drawn from the null population. For a two parameter model, a plot of B_1 vs. B_2 would be an ellipsoid. Various confidence regions would then define concentric ellipsoids. The larger the confidence probability, the larger the

Reproduced with permission of the copyright owner. Further reproduction prohibited without permission.

ellipsoids. For a three parameter model, the confidence region defines a response surface shaped as a hyperelipsoid, i.e., a roughly egg-shaped surface. The t-value for a given parameter defines, for the degrees of freedom corresponding to a given model, the probability that the value calculated for that parameter was not drawn from the null population. For example, for a t-value of 2.0 and 18 degrees of freedom, the probability that the null hypothesis can be rejected is .970 . σ is the standard deviation for the given parameter corresponding.

2. The cross correlation matrix for the parameters is given. This matrix assigns a value from -1.00 to 1.00 to each set of parameters to describe the interdependence of those parameters. For example, a value of .98 to describe the relationship of B_1 to B_2 would indicate that B_1 and B_2 are "highly correlated" and one may be deleted from the model without significant effect on the fit of the experimental data being analyzed. This matrix is a valuable tool in distinguishing between say a 4 and 5 parameter model of basically the same functional form.
3. The residual root mean square (RRMS), residual sum of square (RSS), and residual mean square (RMS) are given. RSS is simply the sum of the squares of the residuals between the model and the data. It gives the total "variation" between the best fit the model can give and the actual data. When RSS is divided by the residual degrees of freedom, RMS is obtained. Then RRMS = $(RMS)^{1/2}$. RRMS is a measure of the average experimental error.

Reproduced with permission of the copyright owner. Further reproduction prohibited without permission.

4. A plot of the cumulative frequency of residuals, both positive and negative, is given. If the model results in a normal distribution of residuals this plot should be a straight line with a positive slope passing through the point (0, .5). This indicates that no statistical bias is present in the experimental errors.
5. A plot of residual values as a function of the fitted values of k is given. This plot enables one to visualize the distribution of the residuals around zero and determine if there are any particularly suspect data points. If, for example, one suspect point accounted for a large part of the error of a given model, this point would be quite far from the others on this plot. Also, the trend of the residuals with fitted k's allows one to determine if the model is biased toward small or large values of k in determination of the parameters. For example, if all the large residuals were found at large values of k, this may indicate that the model is biased toward low values of k.

Variations of each of the models shown previously was used with the program described above to determine the statistically best one. For example, if the model derived from the assumption of dehydrogenation as the rate controlling step, a dual site mechanism, and $K_{H_2} << K_{c_5}, K_{c_6}$ was found to be clearly superior to any other, then this would constitute strong evidence in favor of such a model. Of course, it is possible to check these assumptions by the methods described earlier. Within each model there are several variations to be considered. For example, the relative values of the adsorption constants

Reproduced with permission of the copyright owner. Further reproduction prohibited without permission.

may make it possible to delete K_{H_2} from a model.

If the parameters represent true equilibrium adsorption constants, whose values do not change on dilution with another hydrocarbon, then B_1, B_2, and B_3 should be the same for both k_{c_5} and k_{c_6}. Only the numerator, which contains the true surface reaction rate constant, should be different for k_{c_5} and k_{c_6}. It is possible to "couple" the data for k_{c_5} and k_{c_6} in order to force the parameters corresponding to the adsorption constants, here B_1 and B_2, to be equal for k_{c_5} and k_{c_6}. However, as noted previously, there is not always a relationship between equilibrium adsorption constants and those obtained on reacting systems (60). Thus, such coupling may not be valid. It is possible to determine from statistical analysis of various models whether or not coupling is valid. For example, if a coupled model resulted in a smaller residual root mean square than the corresponding models for the individual k_{c_5} and k_{c_6}, then it could be said that coupling is valid. Mechanistically, this would imply that the adsorption parameter for each of the two reacting species, n-C_5 and n-C_6, were independent of dilution by the other. If the coupled model resulted in a higher RRMS than the individual models, it implies some interaction between the adsorption of C_5 and C_6.

Due to experimental error, it may not be possible to select one specific model as clearly superior to all others. However, it is anticipated that several general forms may be eliminated from consideration. Coupled with an analysis of the data as described previously, insight into the mechanism of the reaction and the interaction of n-C_5 and n-C_6 and their isomers on the catalyst surface may be obtained. In addition, the differences, if any, in Pd-H-faujasite and Pd-H-mordenite catalysis may be examined from a mechanistic view point.

Reproduced with permission of the copyright owner. Further reproduction prohibited without permission.

Mordenite Experimental Results

In order to establish baseline activity data for each catalyst, pure component runs were made using both n-C_5 and n-C_6. Table 1 shows the first order rate constants for pure n-C_5 hydroisomerization at 500°F, 350 psig over Pd-H-Mordenite and Table 2 shows similar results at 500°F, 450 psig. It can be seen that the mordenite catalyst used in this study had an activity for C_5 isomerization comparable to those used previously with 14/1 SiO_2/Al_2O_3 ratios at 10/1 H_2/hydrocarbon. Note that the studies of Wallace (1) at 20/1 H_2/HC ratios on a similar catalyst resulted in lower rate constants. This is consistent with previous findings of Bryant (33). Tables 1 and 2 also show that a 14/1 SiO_2/Al_2O_3 ratio resulted in a more active catalyst than a 10/1 ratio. This was due to decreased pore diffusion resistance resulting from larger pores resulting from the removal of Al atoms.

Since each study shown in Tables 1 and 2 was done on the same type catalyst but ones which were made in different batches, some scatter in the rate constants was to be expected. Activity is strongly dependent on the preparation procedures and batch to batch variation is inevitable. In addition, small temperature variations of $\pm$ 2-3°F which were typical in previous studies added to scatter of the data.

It may be concluded, then, that the catalyst used in this study was of a comparable activity to those used in the past.

In order to check the assumption of a first order reversible reaction, a plot of $\ln(1-Y_B/Y_B^*)$ versus $(w/hr/w)^{-1}$ for n-C_6 is shown in Figure 6. As shown previously, such a plot should be linear with an intercept of 1, if the reaction can be represented by a first order model. It can be seen that this assumption was valid. Previous studies

Reproduced with permission of the copyright owner. Further reproduction prohibited without permission.

TABLE 1

n-Pentane Hydroisomerization Over a Pd-H-Mordenite Catalyst
500°F, 350 psig

Investigator	H_2/HC	SiO_2/Al_2O_3	k_{1ST}
This study	10/1	14/1	.148
Livesay	10/1	14/1	.1935
Livesay	10/1	14/1	.1899
Livesay	10/1	14/1	.1606
Livesay	10/1	14/1	.1542
Livesay	10/1	14/1	.1971
Livesay	10/1	14/1	.1600
Livesay	10/1	14/1	.1541
Wallace	20/1	14/1	.10373
Wallace	20/1	14/1	.09541
Wallace	20/1	14/1	.18318
Wallace	20/1	14/1	.08551
Wallace	20/1	14/1	.07913
Bryant	3.5/1	10/1	.047

Reproduced with permission of the copyright owner. Further reproduction prohibited without permission.

TABLE 2

n-Pentane Hydroisomerization Over a Pd-H-Mordenite Catalyst
500°F, 450 psig

Investigator	H_2/HC	SiO_2/Al_2O_3	k_{1ST}
This study	10/1	14/1	.1061
Livesay	10/1	14/1	.1012
Livesay	10/1	14/1	.1236
Livesay	10/1	14/1	.0976
Livesay	10/1	14/1	.1218
Livesay	10/1	14/1	.1147
Livesay	10/1	14/1	.1119
Livesay	10/1	14/1	.1081
Livesay	10/1	14/1	.1087
Livesay	10/1	14/1	.0958
Wallace	20/1	14/1	.04821
Wallace	20/1	14/1	.04871
Wallace	20/1	14/1	.04477
Wallace	20/1	14/1	.06059
Wallace	20/1	14/1	.06506
Wallace	20/1	14/1	.04857
Wallace	20/1	14/1	.04966
Wallace	20/1	14/1	.05659
Wallace	20/1	14/1	.05212
Habibe	6/1	10/1	.0139
Habibe	6/1	10/1	.0107
Bryant	3.5/1	10/1	.034
Bryant	3.5/1	10/1	.026
Hopper	3.2/1	26/1	.0057

Reproduced with permission of the copyright owner. Further reproduction prohibited without permission.

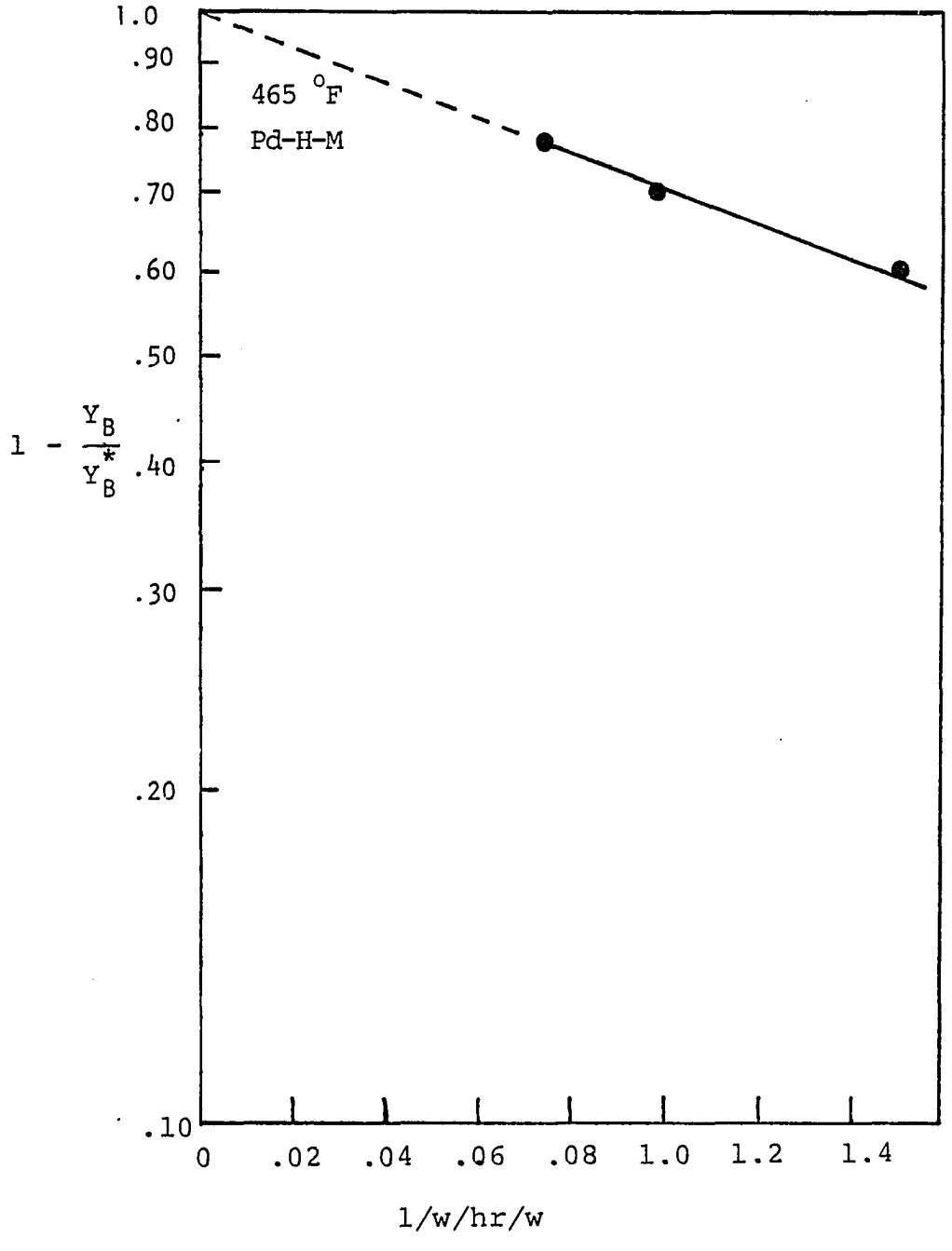

Figure 6. Test for first order reversible reaction, $n\text{-}C_6$.

Reproduced with permission of the copyright owner. Further reproduction prohibited without permission.

have shown that similar results were obtained on this catalyst for n-C_5 hydroisomerization (65).

Now, having established the relative activity of this catalyst and the validity of first order reversible kinetics, the assumption of a dual site mechanism must be checked. As discussed earlier, a plot of $k^{-1/n}$ versus P_{tot} should give a straight line with a positive intercept. This intercept corresponds to the true surface reaction rate constant. Figures 7 and 8 show plots of the C_5 and C_6 rate constants versus total pressure at 450° and 465°F. In both cases, only the plot of $k^{-1/2}$ gave a positive intercept. This confirmed the assumption of a dual site mechanism for both C_5 and C_6 hydroisomerization.

Figure 9 shows the effect of temperature on k_{C_6} and k_{C_5}. As expected, the Arrhenius relationship was observed. As noted previously, the apparent activation energy calculated from such a plot is given by

$$E_{app} = E' + \sum_{i=1}^{m} \Delta H_i + nR \frac{d}{d(\frac{1}{T})} \ln(1 + \sum_{i=1}^{m} K_i P_i).$$

As the nature of the catalyst surface changes, the surface adsorption energy, ΔH, will change. Thus, some variation from catalyst to catalyst may be expected even if the true surface reaction activation energy, E', were the same. Previous studies on a mordenite of this type found E_{app} to be between 30 and 50 $\frac{kcal}{g\text{-mole}}$ for n-C_5 hydroisomerization (59). From Figure 9, it can be shown that $(E_{app})_{n\text{-}C_5}$ is 55 $\frac{kcal}{g\text{-mole}}$ and $(E_{app})_{n\text{-}C_6}$ is 53 $\frac{kcal}{g\text{-mole}}$. These values were comparable to those

Reproduced with permission of the copyright owner. Further reproduction prohibited without permission.

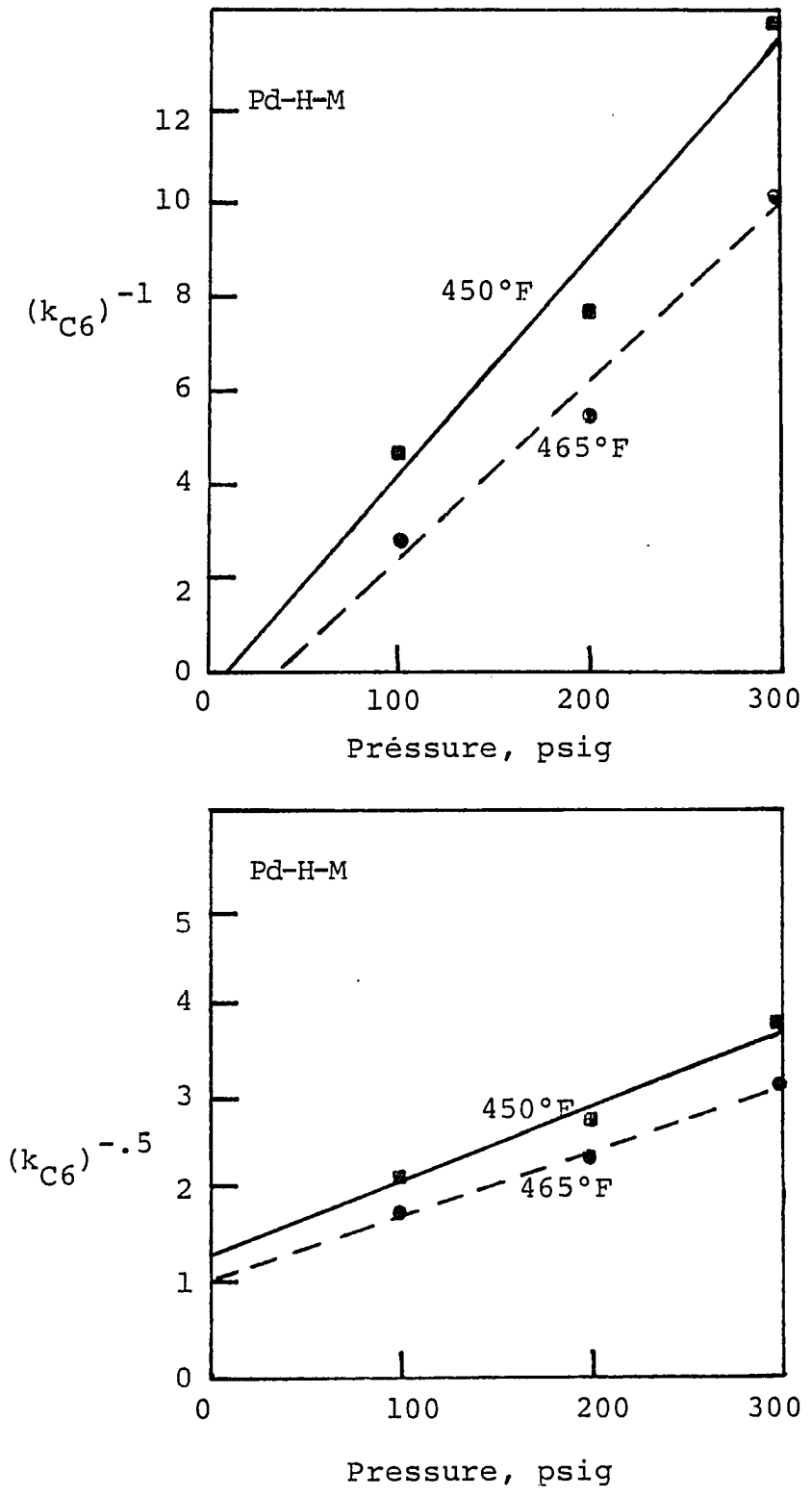

Figure 7. Test for a dual site mechanism, n-C_5.

Reproduced with permission of the copyright owner. Further reproduction prohibited without permission.

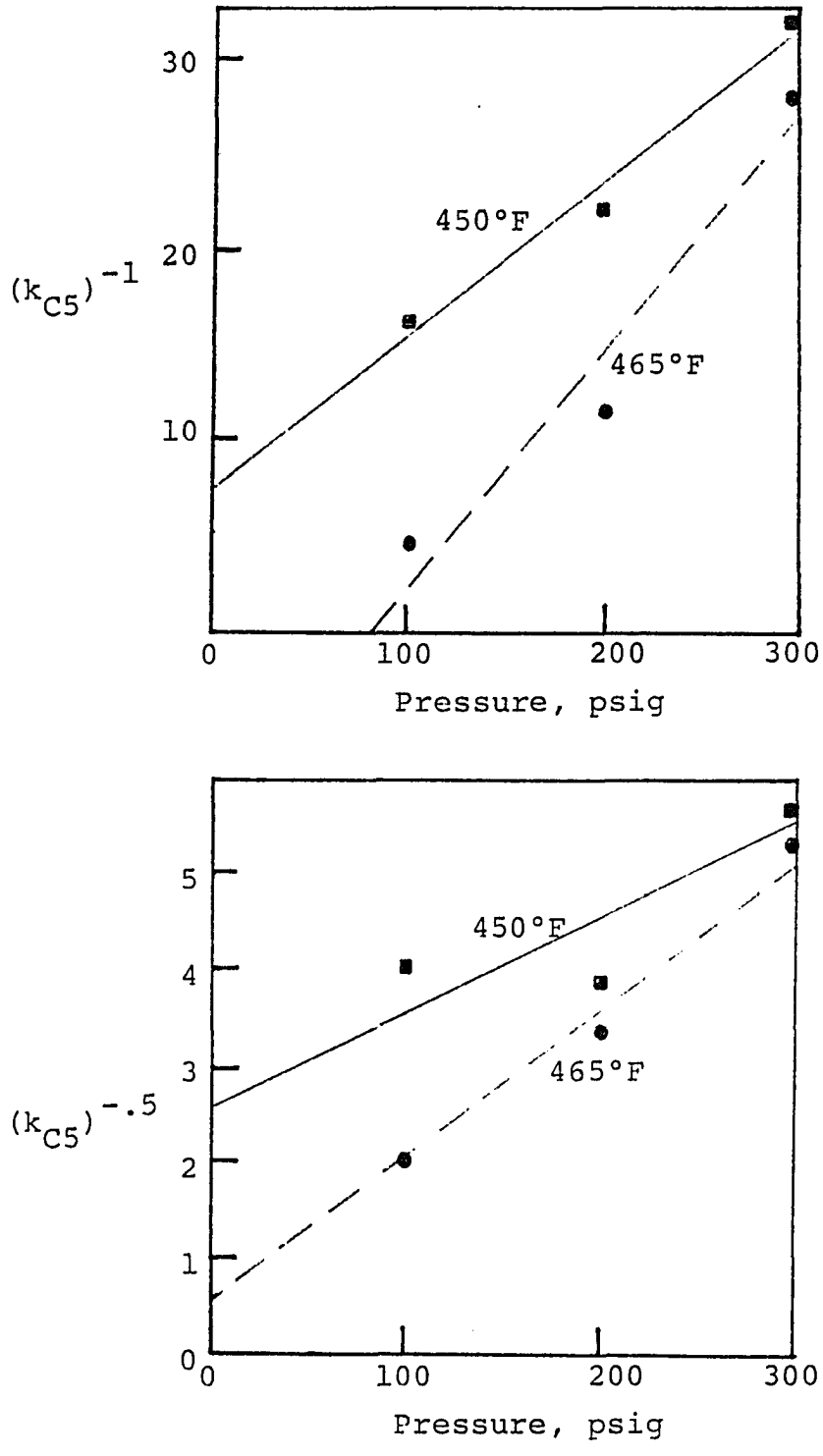

Figure 8. Test for a dual site mechanism, n-C_6.

Reproduced with permission of the copyright owner. Further reproduction prohibited without permission.

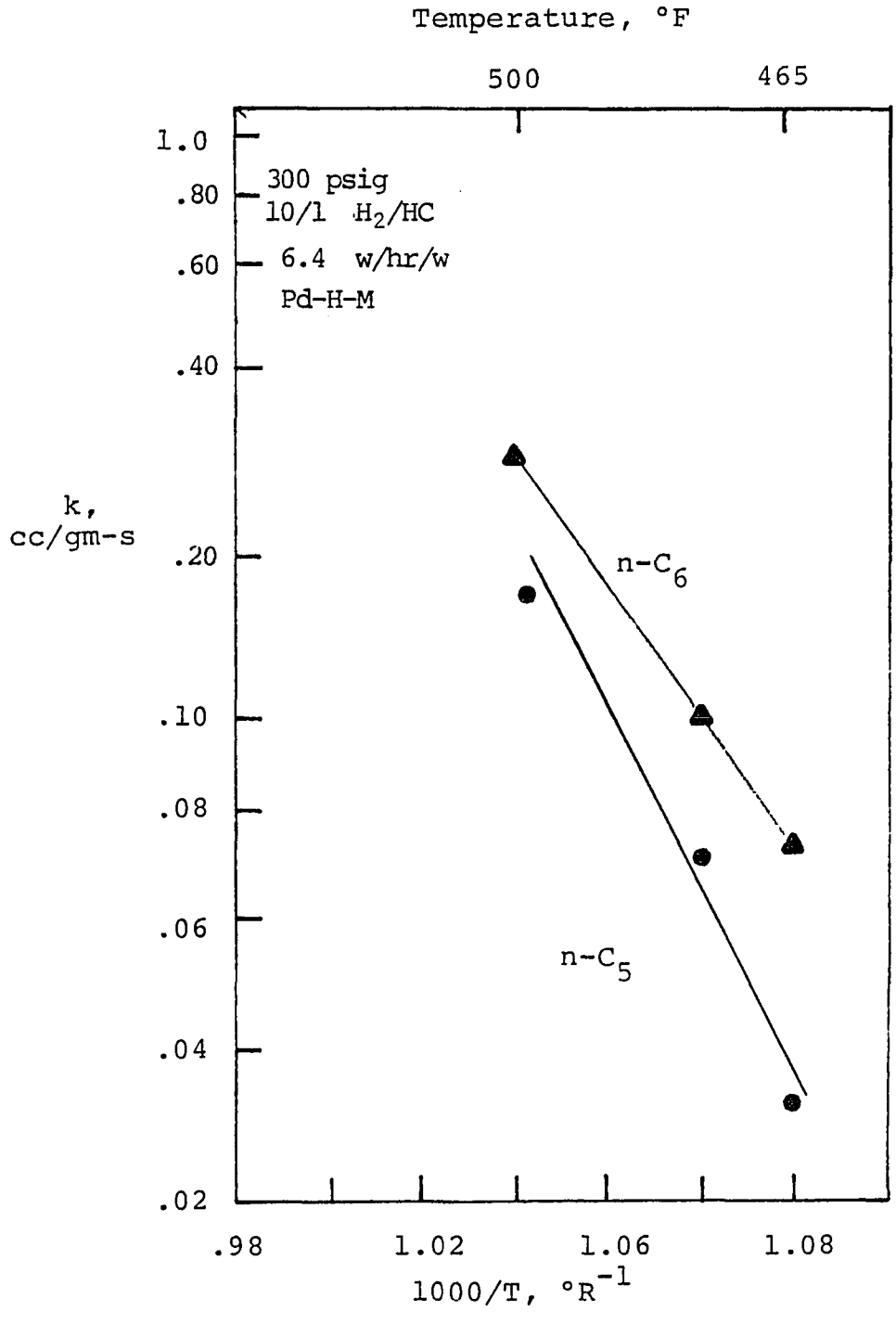

Figure 9. Arrhenius plot of first-order rate constants, pure n-C_5 and C_6.

Reproduced with permission of the copyright owner. Further reproduction prohibited without permission.

obtained on previous studies which also showed $(E_{app})_{n\text{-}C_6} < (E_{app})_{n\text{-}C_5}$ (59). The effect of the hydrogen to hydrocarbon mole ratio, H_2/HC, may be used to test the relative values of the adsorption constants of hydrogen and the hydrocarbon reactants. Figure 10 shows a plot of $k_{C_5}^{-1/2}$ and $k_{C_6}^{-1/2}$ versus $1/(\tilde{R}+1)$ at 200 and 300 psig total pressure. Since these lines had negative intercepts for both pressures, the data indicate that $K_{HC} >> K_{H_2}$. Figure 11 shows a plot of $k_{C_5}^{-1/2}$ and $k_{C_6}^{-1/2}$ versus $\tilde{R}/(\tilde{R}+1)$. This line had a positive abscissa intercept, indicating that $K_{H_2} >> K_{HC}$, confirming the results of Figure 9. This knowledge was valuable in discriminating between two models for the reaction. For example, if the statistically determined adsorption parameters for the hydrocarbon species were much smaller than for hydrogen, such a model would be inconsistent even if the fit were good. In addition, if $K_{HC} >> K_{H_2}$, K_{H_2} may be neglected in some models as a valid simplification of the statistical analysis.

Figures 12 through 19 show the experimentally determined values of the first order rate constant for both C_5 and C_6 hydroisomerization at various conditions. Each figure represents one set of runs at a given temperature and pressure. The H_2/HC ratio was 10/1 to 18/1 and w/hr/w was about 6.4 for all runs. For each set of runs, pure $n\text{-}C_5$ and $n\text{-}C_6$ and three mixtures were isomerized. The rate constants were calculated based on the conversion of normal reactant to isomerized products, as outlined previously.

The general trend of k_{C_5} and k_{C_6} with mixture concentration is constant at both 450° and $465^{\circ}F$. At both temperatures, k_{C_5} decreased when the feed was diluted with $n\text{-}C_6$ while k_{C_6} increased on

Reproduced with permission of the copyright owner. Further reproduction prohibited without permission.

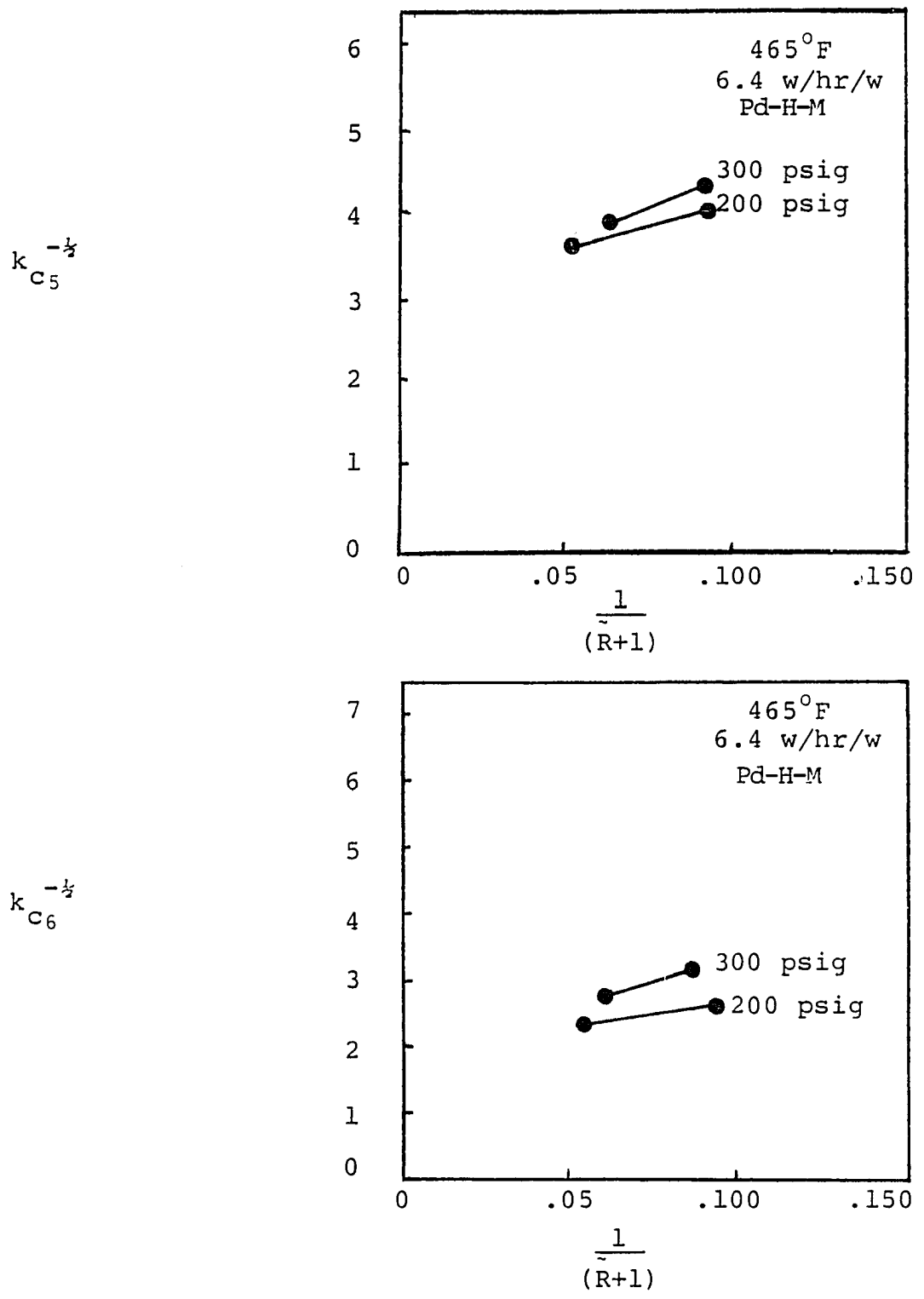

Figure 10. Rate constant versus H_2/HC ratio.

Reproduced with permission of the copyright owner. Further reproduction prohibited without permission.

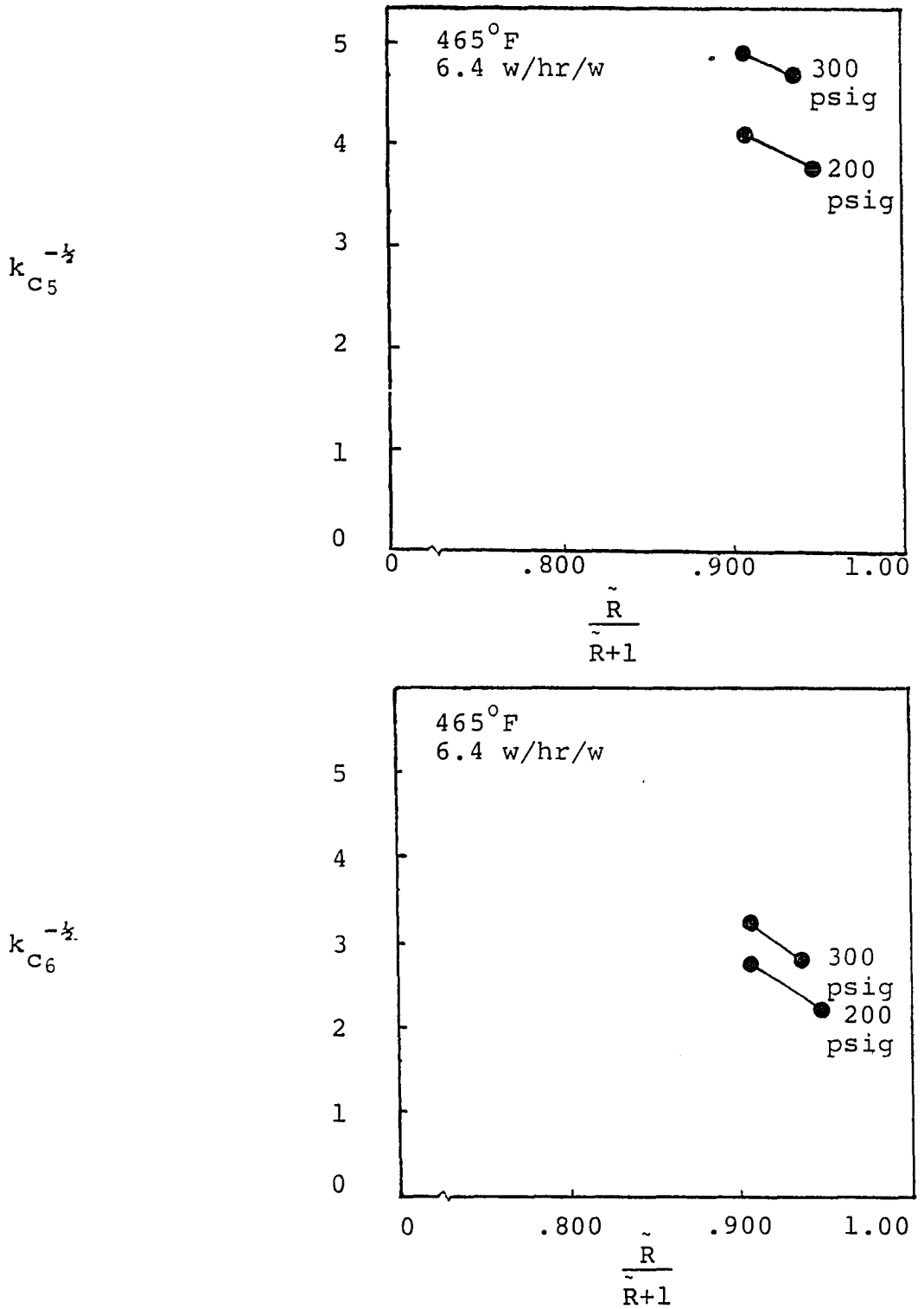

Figure 11. Rate constant versus H_2/HC ratio.

Reproduced with permission of the copyright owner. Further reproduction prohibited without permission.

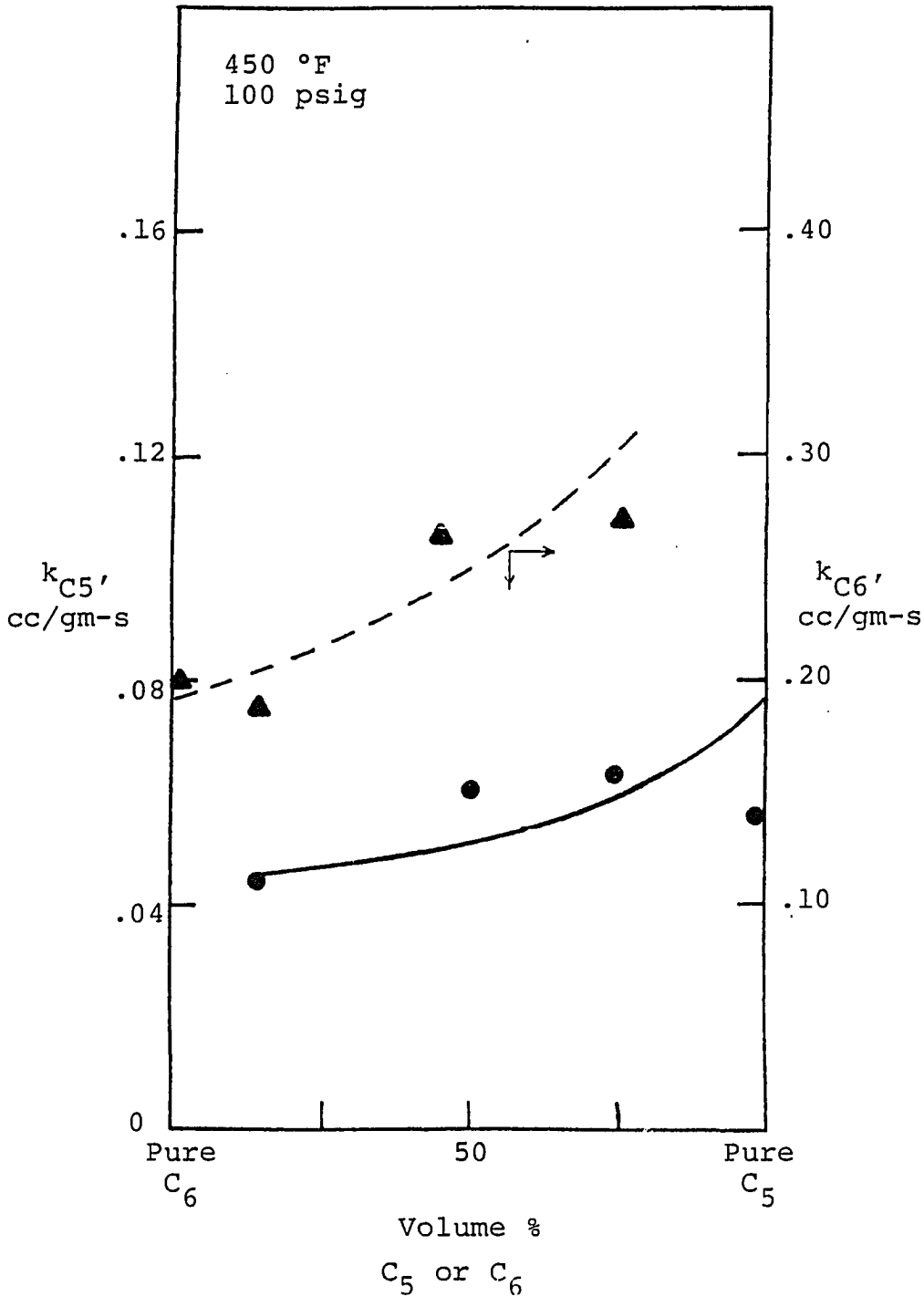

Figure 12. Rate constant versus feed composition.

Reproduced with permission of the copyright owner. Further reproduction prohibited without permission.

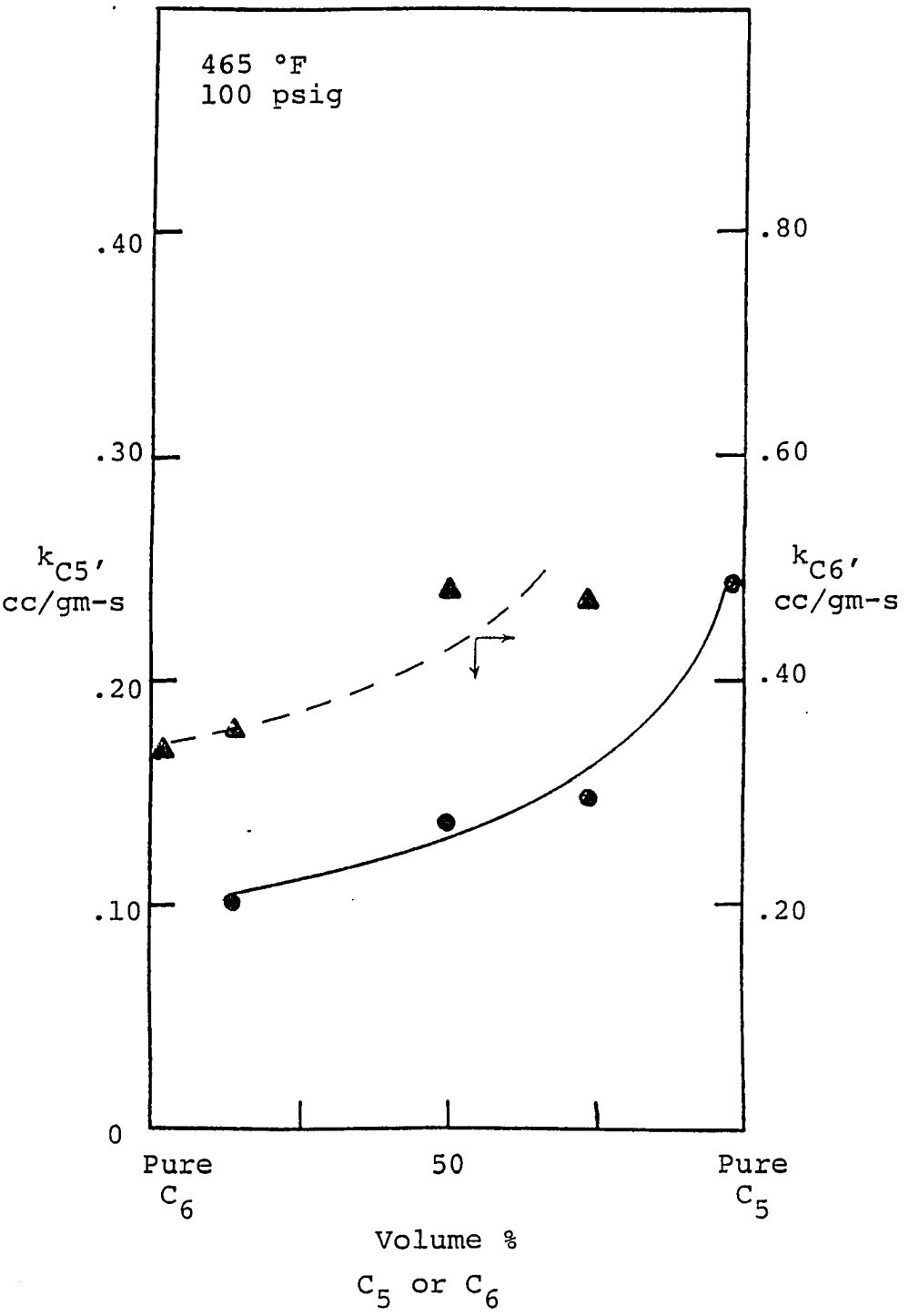

Figure 13. Rate constant versus feed composition.

Reproduced with permission of the copyright owner. Further reproduction prohibited without permission.

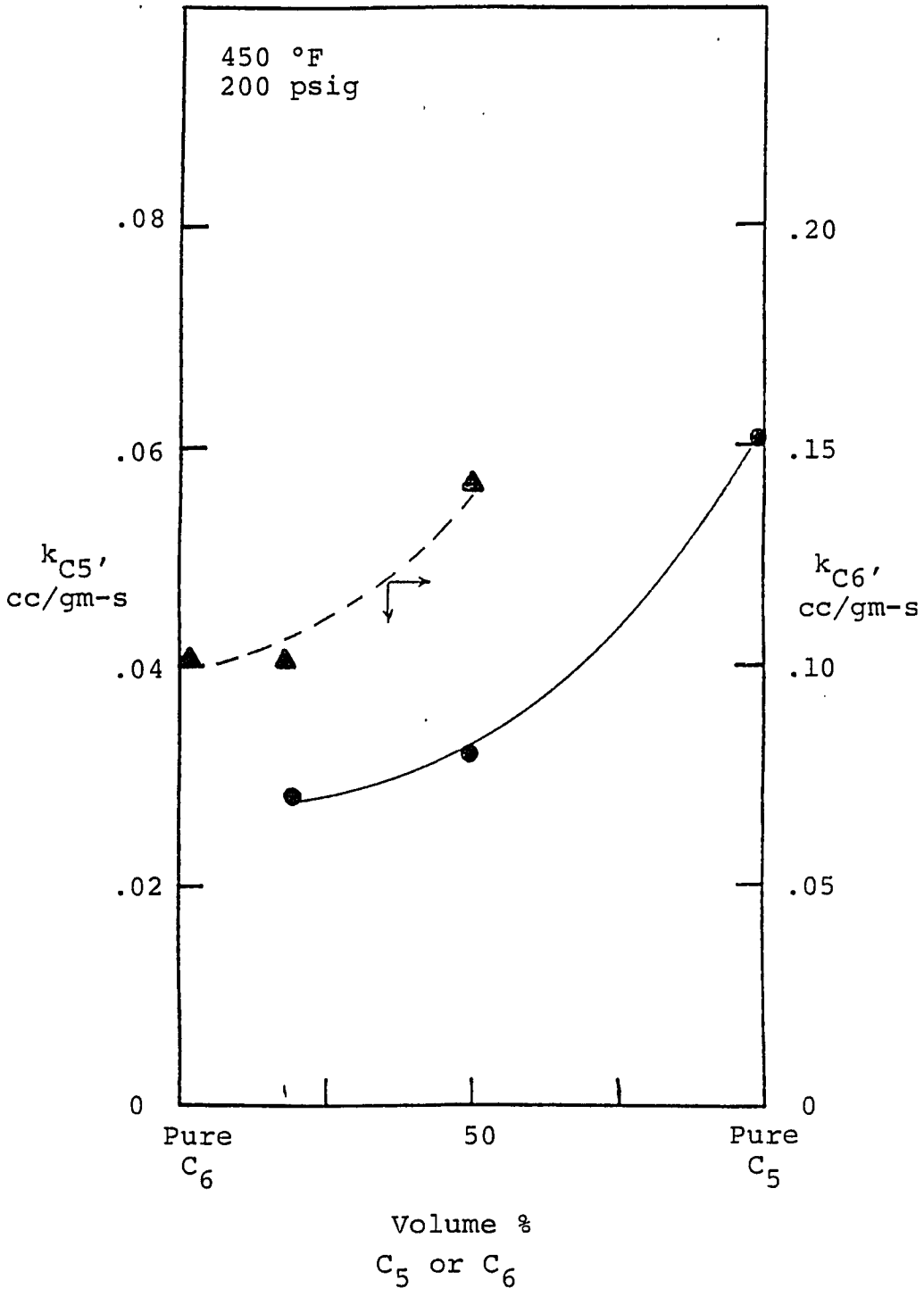

Figure 14. Rate constant versus feed composition.

Reproduced with permission of the copyright owner. Further reproduction prohibited without permission.

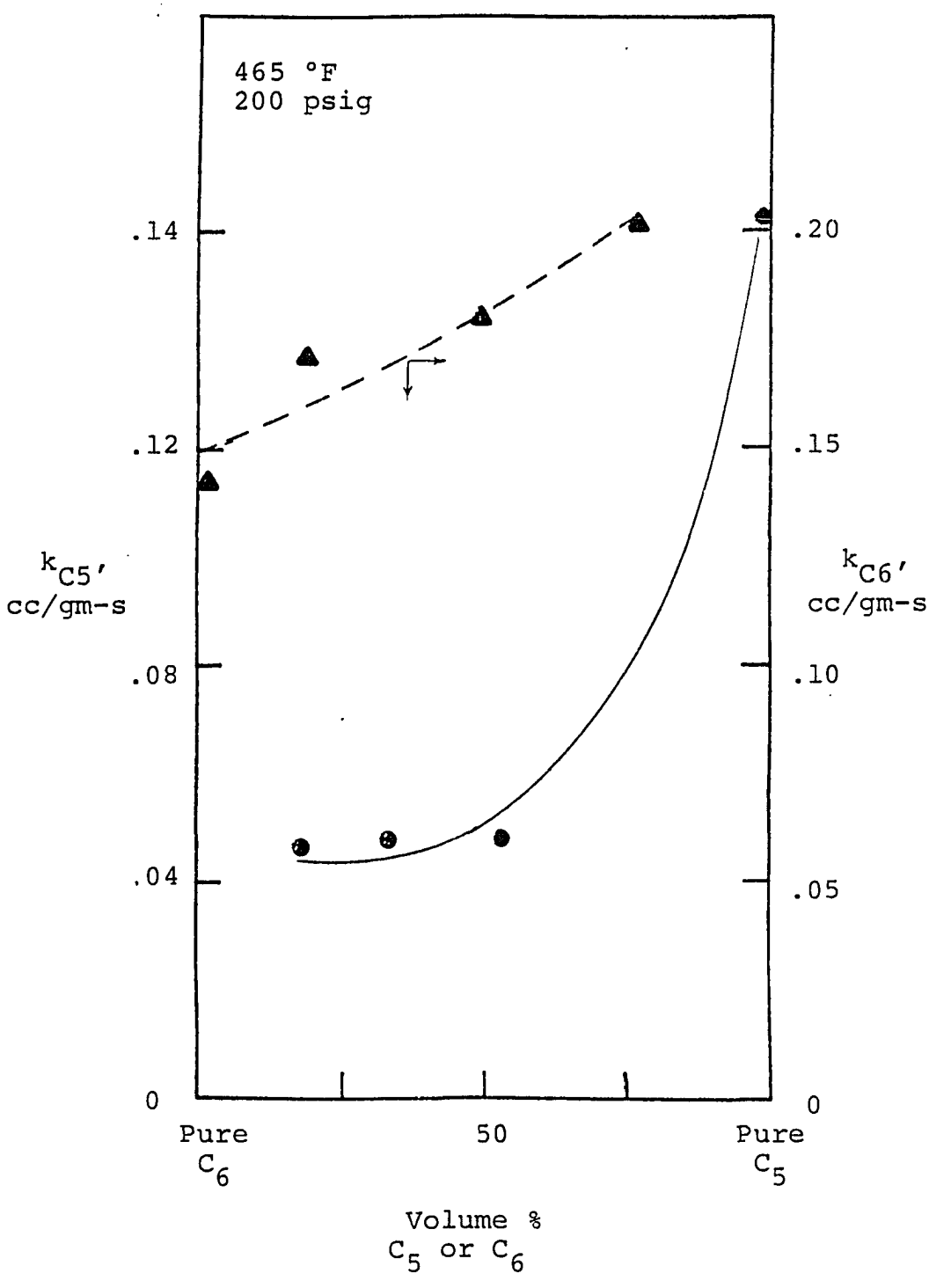

Figure 15. Rate constant versus feed composition.

Reproduced with permission of the copyright owner. Further reproduction prohibited without permission.

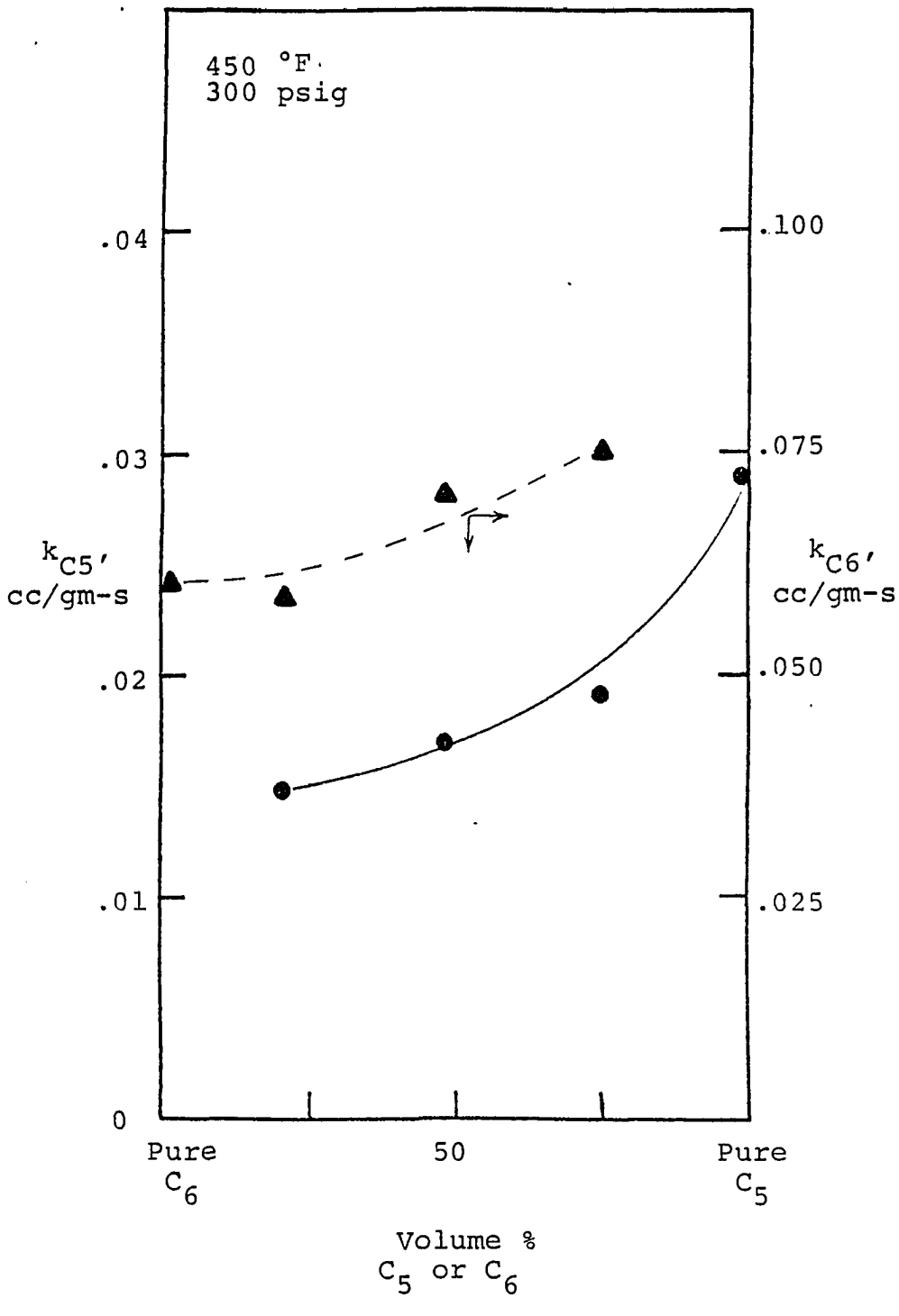

Figure 16. Rate constant versus feed composition.

Reproduced with permission of the copyright owner. Further reproduction prohibited without permission.

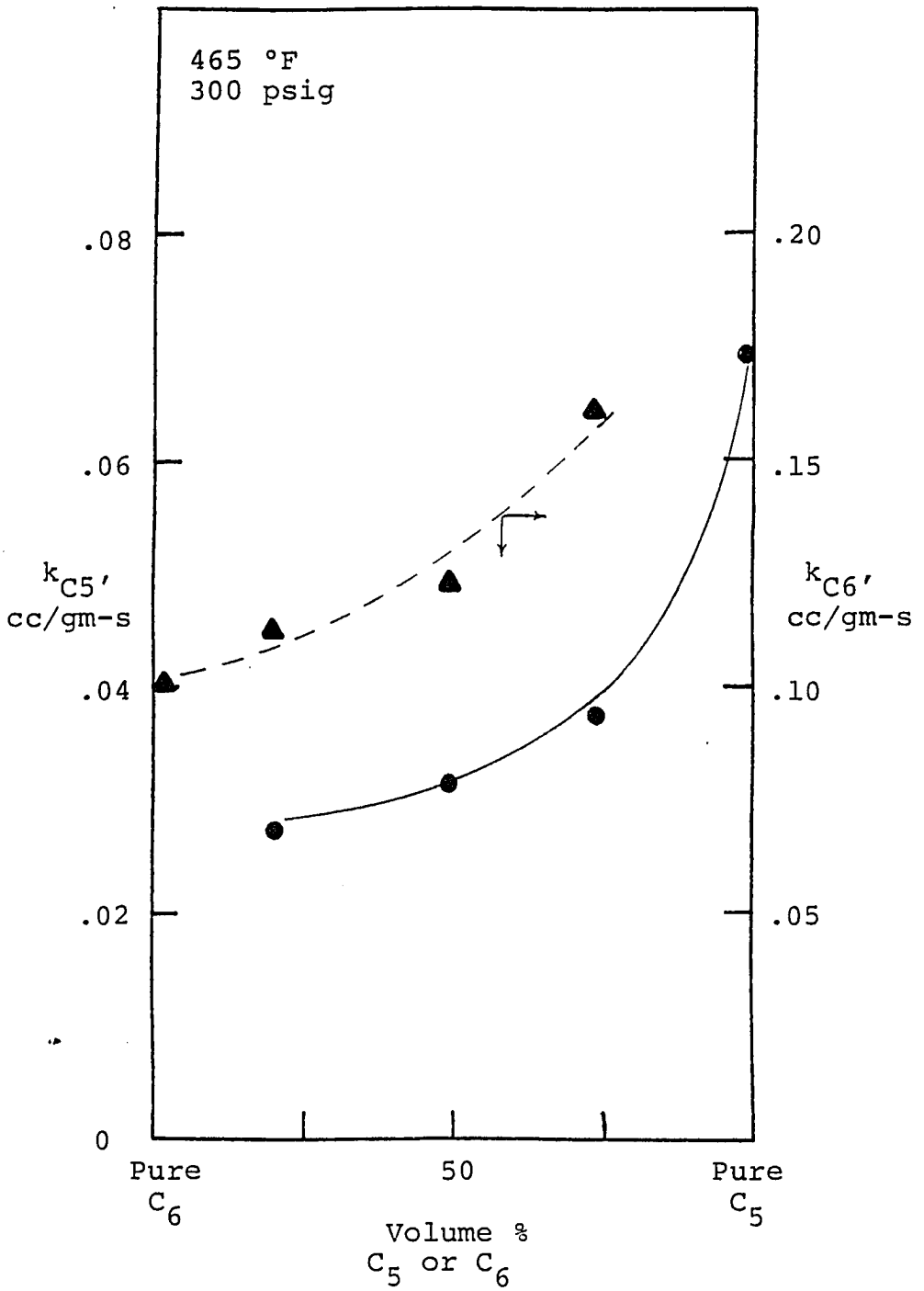

Figure 17. Rate constant versus feed composition.

Reproduced with permission of the copyright owner. Further reproduction prohibited without permission.

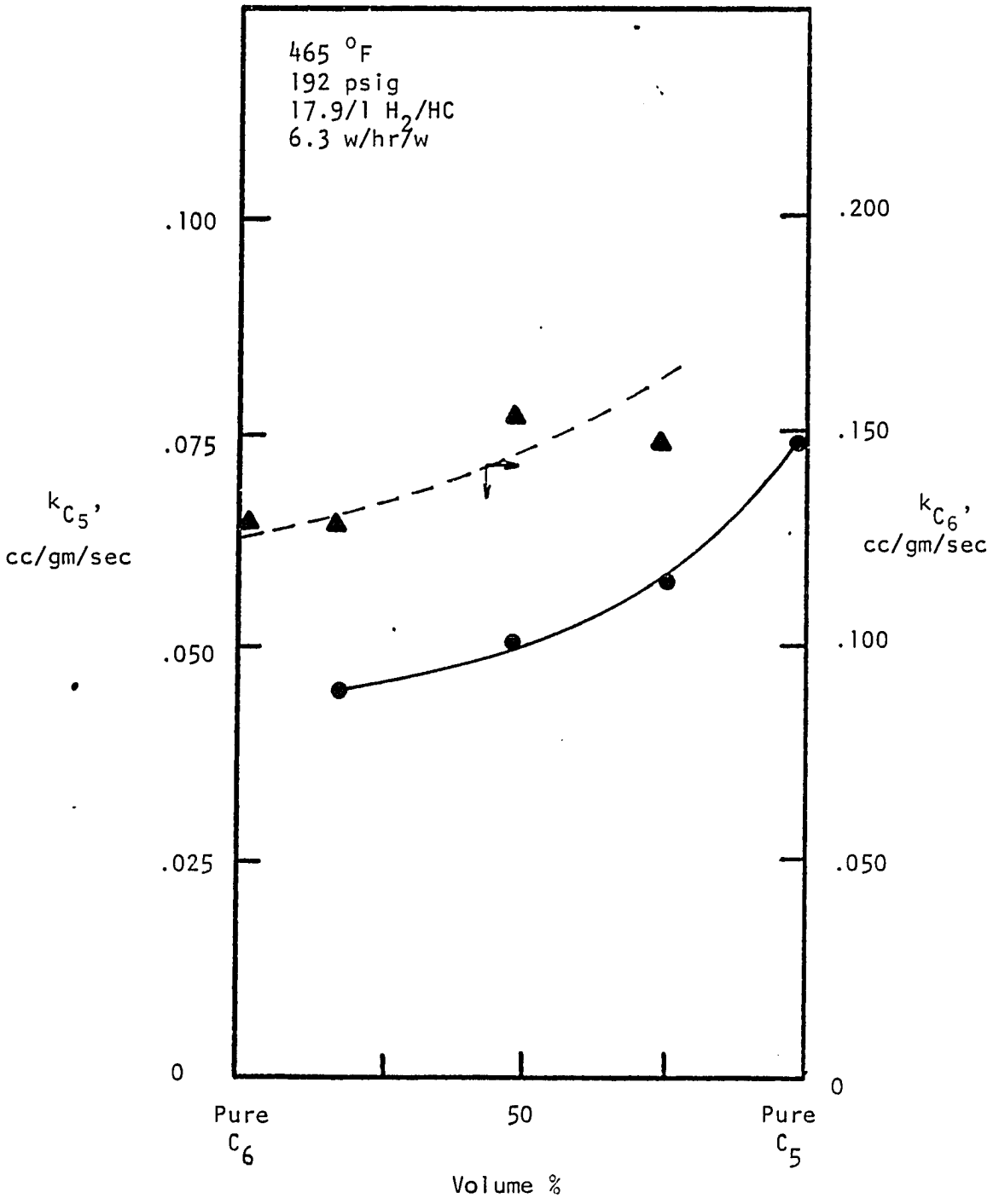

Figure 18. Rate constant versus feed composition.

Reproduced with permission of the copyright owner. Further reproduction prohibited without permission.

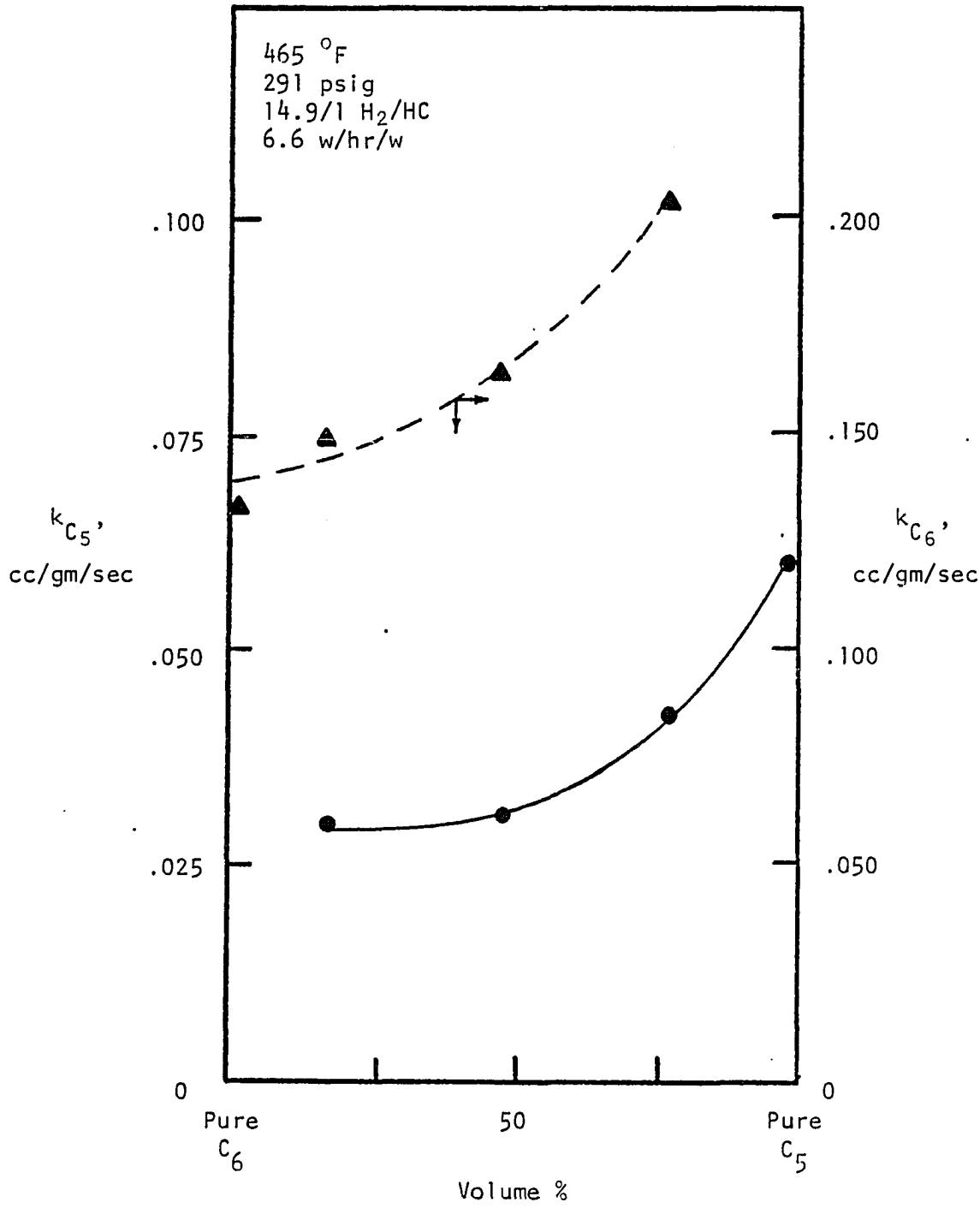

Figure 19. Rate constant versus feed composition.

Reproduced with permission of the copyright owner. Further reproduction prohibited without permission.

dilution. As discussed previously, this would be the result if n-C_6 were more strongly adsorbed than n-C_5. The mean pore diameter of Pd-H-mordenite is 8-10 Å (50). While the molecular diameter of n-C_6 is slightly greater than n-C_5, both molecules are about 5 Å in diameter and pore sieve action would not exclude either species. Thus, pore resistance would not account for the differences in rate constants with dilution.

It can also be noted that the absolute values both k_{C_5} and k_{C_6} decreased with increasing total pressure. This result was consistent with the general Langmuir type model presented earlier, regardless of the rate determining step.

The values of k_{C_6} are greater than k_{C_5} at any given conditions. This phenomena can be explained by postulating that n-C_6 is more strongly adsorbed than n-C_5. Also, the first order rate constant is given by

$$k = \frac{k_o \prod_{i=1}^{m} Ki}{(1 + \Sigma K_i P_i)^2}$$

where k_o is the true surface reaction rate constant. As noted in equation (18), the value of k_o for n-C_6 may be obtained from the intercepts of Figures 7 and 8. From these figures, it can be seen that at 465°F, $(k_o)_{C_5} \simeq .6$ and $(k_o)_{C_6} \simeq 1.0$. Thus, the surface reaction rate of n-C_6 appeared to be greater than that of n-C_5.

It can also be seen that the absolute values of both k_{C_6} and k_{C_5} decreased with increasing H_2/HC ratio = $\tilde{R}$. This may be

Reproduced with permission of the copyright owner. Further reproduction prohibited without permission.

explained by considering the equation

$$k^{-1/2} = k_o^{-1/2} \left[1 + \frac{P_{tot} \tilde{R} K_{H_2} + K_{HC}}{1 + R} \right]$$

At constant total pressure, increasing $\tilde{R}$ will decrease the value of k, provided $K_{H_2} \neq K_{HC}$.

The experimental results as analyzed thus far are consistent with the following:

1. First order reversible kinetics, Figure 6.
2. A dual site mechanism for both n-C_5 and n-C_6 hydroisomerization, Figures 7,8.
3. $(k_o)_{C_6} > (k_o)_{C_5}$, Figures 7,8.
4. $K_{C_6} > K_{C_5}$, Figures 10,11.

This information was used in the formulation of various kinetic models, and in analyzing the results of statistical programs.

The statistical analysis was carried out as follows: The rate constants, k_{C_5} and k_{C_6}, were expressed as functions of partial pressures and parameters to be determined. For example,

$$k_i = \frac{B_4}{(1 + B_1 P_{C_5} + B_2 P_{C_6} + B_3 P_{H_2})^2} \qquad i = C_5, C_6$$

is the model expected from Langmuir adsorption, a dual site mechanism, and dehydrogenation as the rate controlling step. This model may then be subjected to non-linear regression analysis to determine the least-squares values of the parameters, B_i. In this particular model, B_1 corresponds to K_{C_5}, B_2 to K_{C_6}, B_3 to K_{H_2}. Tables 4 through 6

Reproduced with permission of the copyright owner. Further reproduction prohibited without permission.

show the results obtained on the mordenite catalyst for both coupled and individual C_5 and C_6 models. For each of the individual models 20 data points were used, while 40 data points were used in each coupled model.

Table 3 shows the models that were used for individual and coupled modeling. These models were based on both theoretical forms derivable from the kinetic models developed in the previous section (Models 1-6,9-12) and more empirical forms (Models 7,8). Models 7,8 contained Langmuir adsorption denominators with P_i in the numerator. As can be seen from Tables 4-6, the coefficient of P_i in some models became essentially zero. The nature of the statistical program of Daniel and Wood was such that when a coefficient in a denominator approached zero, it indicated that this parameter and corresponding independent variable, if placed in the numerator, may result in a better fit. For this reason, Models 7,8 were tested.

Tables 4-6 show the statistical results obtained on the eight models tested for the data obtained on Pd-H-mordenite.

For the individual (k_{C_5} and k_{C_6}) models, it can be seen by examining the RMS and RRMS that for both k_{C_5} and k_{C_6}, Models 2, 4, 5, 7, 9, and 10 had the lower error terms. For Model 2 in both cases, however, the value of B_1 approached zero while $B_3 > 0$. Since B_1 corresponded to K_{C_5} and B_3 to K_{H_2}, and since it has been shown that $K_{HC} >> K_{H_2}$ this Model was rejected as unrealistic.

Model 7, although its error term was small, had no certainty in any of the parameters, as shown by the low t-values. In addition, it can be seen from the correlation matrix that, for k_{C_5}, the parameters

Reproduced with permission of the copyright owner. Further reproduction prohibited without permission.

Reproduced with permission of the copyright owner. Further reproduction prohibited without permission.

TABLE 3

INDIVIDUAL MODELS

MODEL NUMBER	MODEL	ASSUMPTIONS LEADING TO THE MODEL
1	$k = \frac{B_4}{(1 + B_1 P_{C_5} + B_2 P_{C_6})^{B_3}}$	Dehydrogenation rate controlling, $K_{HC} >> K_{H_2}$, B_3 represents the number of sites.
2	$k = \frac{B_4}{(1 + B_1 P_{C_5} + B_2 P_{C_6} + B_3 P_{H_2})^2}$	Hydrogen rate constant significant, dual site mechanism, dehydrogenation rate controlling.
3	$k = \frac{B_3}{(1 + B_1 P_{C_5} + B_2 P_{C_6})^2}$	Dehydrogenation rate controlling, $K_{HC} >> K_{H_2}$, dual site mechanism.
4	$k = \frac{B_3}{P_{H_2}(1 + B_1 P_{C_5} + B_2 P_{C_6})^2}$	Isomerization rate controlling, $K_{HC} >> K_{H_2}$, dual site mechanism.
5	$k = \frac{B_3}{P_{H_2}(1 + B_1 P_{C_5} + B_2 P_{C_6})}$	Same as 4 but single site mechanism.
6	$k = \frac{B_4}{(1 + B_1 P_{C_5} + B_2 P_{C_6} + B_3 P_{H_2})^{B_5}}$	B_5 defines number of sites, K_{H_2} significant, dehydrogenation rate controlling.

Reproduced with permission of the copyright owner. Further reproduction prohibited without permission.

MODEL NUMBER	MODEL	ASSUMPTIONS LEADING TO THE MODEL
7	$k = \frac{B_4 \, Pi}{(1 + B_1 \, P_{C_5} + B_2 \, P_{C_6} + B_3 \, P_{H_2})^2}$	$i = C_5$ for k_{C_5}, $= C_6$ for k_{C_6}, K_{H_2} significant P_i in numerator is semi-empirical.
8	$k = \frac{B_7 \, Pi^{B_4}}{(1 + B_2 \, P_{C_5} + B_3 \, P_{C_6})^2}$	Same as 7 but with variable exponent.
9	$k = \frac{B_2}{(1 + B_1 \, P_{C_6}) P_{H_2}}$	Single site mechanism, isomerization rate controlling, $K_{C_6} >> K_{H_2}$, K_{C_5}.
10	$k = \frac{B_2}{(1 + B_1 \, P_{C_6})^2 \, P_{H_2}}$	Same as 9 with a dual site mechanism.
11	$k = \frac{B_2}{(1 + B_1 \, P_{C_5}) \, P_{H_2}}$	Same as 9 with $K_{C_5} >> K_{C_6}$, K_{H_2}.
12	$k = \frac{B_2}{(1 + B_1 \, P_{C_5})^2 \, P_{H_2}}$	Same as 11 with a dual site mechanism.

Reproduced with permission of the copyright owner. Further reproduction prohibited without permission.

COUPLED MODELS

MODEL NUMBER	MODEL	ASSUMPTIONS LEADING TO THE MODEL
1	$k = \frac{B_{4,5}}{(1 + B_1 P_{c_5} + B_2 P_{c_6})^{B_3}}$	Dehydrogenation rate controlling, $K_{HC} >> K_{H_2}$ B_3 represents the number of sites.
2	$k = \frac{B_{4,5}}{(1 + B_1 P_{c_5} + B_2 P_{c_6} + B_3 P_{H_2})^2}$	Dehydrogenation rate controlling, K_{H_2} significant, dual site mechanism.
3	$k = \frac{B_{3,4}}{(1 + B_1 P_{c_5} + B_2 P_{c_6})^2}$	Dehydrogenation rate controlling, $K_{HC} >> K_{H_2}$ dual site mechanism.
4	$k = \frac{B_{3,4}}{(1 + B_1 P_{c_5} + B_2 P_{c_6})^2 P_{H_2}}$	Isomerization rate controlling, dual site mechanism, $K_{HC} >> K_{H_2}$.
5	$k = \frac{B_{3,4}}{(1 + B_1 P_{c_5} + B_2 P_{c_6}) P_{H_2}}$	Same as 4 but single site mechanism.
6	$k = \frac{B_{4,5}}{(1 + B_1 P_{c_5} + B_1 P_{c_6} + B_3 P_{H_2})^{B_6}}$	Dehydrogenation rate controlling, B_6 defines number of sites, K_{H_2} significant.

Reproduced with permission of the copyright owner. Further reproduction prohibited without permission.

MODEL NUMBER	MODEL	ASSUMPTIONS LEADING TO THE MODEL
7	$k = \frac{B_{4,5}}{(1 + B_1 P_{c_5} + B_2 P_{c_6} + B_3 P_{H_2})}$	Same as 6 but single site mechanism.
8	$k = \frac{B_{4,5}}{(1 + B_1 P_{c_5} + B_2 P_{c_6} + B_3 P_{H_2})^2 P_{H_2}}$	Isomerization rate controlling, dual site mechanism, K_{H_2} significant.
9	$k = \frac{B_{2,3}}{(1 + B_1 P_{c_6}) P_{H_2}}$	Isomerization rate controlling, single site mechanism, $K_{c_6} >> K_{c_5}, K_{H_2}$.
10	$k = \frac{B_{2,3}}{(1 + B_1 P_{c_6})^2 P_{H_2}}$	Same as 9 but dual site mechanism.
11	$k = \frac{B_{2,3}}{(1 + B_1 P_{c_5}) P_{H_2}}$	Same as 9 but $K_{c_5} >> K_{c_6}, K_{H_2}$.
12	$k = \frac{B_{2,3}}{(1 + B_1 P_{c_5}) P_{H_2}}$	Same as 11 but dual site mechanism.

Reproduced with permission of the copyright owner. Further reproduction prohibited without permission.

TABLE 4

MODEL NUMBER	COEFFICIENT VALUES	CORRELATION MATRIX	95% CONFIDENCE LIMITS	t-VALUE	σ	RMS	RRMS	RSS
	B_1 = 1027.	1.00	$-9.6\times10^4 \rightarrow 9.6\times10^4$	0.0	4.6×10^4			
1	B_2 = 2044.	1.00 1.00	$-1.9\times10^5 \rightarrow 1.9\times10^5$	0.0	9.1×10^4	.0015	.038	.023
	B_3 = 1.28	.133 .128 1.00	.29 → 2.3	2.7	.465			
	B_4 = 21567.	.998 .998 .200 1.00	$-2.6\times10^6 \rightarrow 2.6\times10^6$	0.0	1.22×10^6			
	B_1 = 2.8×10^{-12}	1.00	- .24 → .24	0.0	.113			
2	B_2 = .338	.830 1.00	- .44 → 1.1	.9	.369	.00026	.016	.0041
	B_3 = .0444	.557 .904 1.00	- .04 → .12	1.2	.0375			
	B_4 = 7.21	.712 .967 .979 1.00	-18.2 → 32.6	.6	12.0			
	B_1 = .131	1.00	- .18 → .44	.9	.148			
3	B_2 = .250	.967 1.00	- .24 → .74	1.1	.234	.0014	.038	.024
	B_3 = .865	.994 .980 1.00	-1.6 → 3.4	.7	1.18			
	B_1 = .00933	1.00	- .01 → .029	1.1	.00918			
4	B_2 = .0589	.763 1.00	.021 → .097	3.2	.0182	.00037	.019	.0063
	B_3 = 24.6	.945 .861 1.00	13.6 → 35.5	4.7	5.20			

Reproduced with permission of the copyright owner. Further reproduction prohibited without permission.

MODEL NUMBER	COEFFICIENT VALUES	CORRELATION MATRIX	95% CONFIDENCE LIMITS	t-VALUE	σ	RMS	RRMS	RSS
	B_1 = .0397	1.00	-.042 → .12	1.0	.0389			
5	B_2 = .212	.911 1.00	-.0049 → .43	2.1	.103	.00033	.018	.0056
	B_3 = 30.1	.979 .950 1.00	9.74 → 50.5	3.1	9.66			
	B_1 = .688	1.00	$-2.5\times10^{7} \rightarrow 2.5\times10^{7}$	0.0	1.2×10^{7}			
	B_2 = .444	.991 1.00	$-1.7\times10^{7} \rightarrow 1.7\times10^{7}$	0.0	7.7×10^{6}			
6	B_3 = 1.2×10^{-10}	-.022 -.146 1.00	$-1.7\times10^{4} \rightarrow 1.7\times10^{4}$	0.0	7.9×10^{3}	.0098	.099	.147
	B_4 = 6.39	.651 .748 -.693 1.00	$-1.8\times10^{9} \rightarrow 1.8\times10^{9}$	0.0	8.6×10^{8}			
	B_5 = 9.27	-.434 -.301 -.800 .402 1.00	$-1.3\times10^{8} \rightarrow 1.3\ 10^{8}$	0.0	5.9×10^{7}			
	B_1 = 56.5	1.00	$-1.7\times10^{4} \rightarrow 1.7\times10^{4}$	0.0	8.2×10^{3}			
	B_2 = 4.86	.999 1.00	$-1.5\times10^{3} \rightarrow 1.5\times10^{3}$	0.0	7.1×10^{2}			
7	B_3 = 10.55	1.00 .999 1.00	$-3.3\times10^{3} \rightarrow 3.3\times10^{3}$	0.0	1.6×10^{3}	.00061	.025	.0097
	B_4 = 5.08×10^{4}	1.00 .999 1.00 1.00	$-3.1\times10^{7} \rightarrow 3.1\times10^{7}$	0.0	1.5×10^{7}			
	B_1 = .890	1.00	-1.9 →3.7	.7	1.34			
8	B_2 = .135	.821 1.00	-.41 →.68	.5	.257	.0015	.039	.024
	B_3 = .255	.947 .931 1.00	-.38 →.89	.9	.298			
	B_4 = 6.2×10^{-12}	.302 .789 .550 1.00	-1.1 → 1.1	0.0	.538			

MODEL NUMBER	COEFFICIENT VALUES	CORRELATION MATRIX	95% CONFIDENCE LIMITS	t-VALUE	σ	RMS	RRMS	RSS
9	B_1 = .107	1.00	.049 → .17	3.9	.0277	.00036	.0189	.00643
	B_2 = 19.8	.675 1.00	17.0 → 22.7	14.6	1.36			
10	B_1 = .0427	1.00	.021 → .064	4.2	.0101	.00037	.0194	.00677
	B_2 = 19.5	.658 1.00	16.7 → 22.3	14.6	1.34			
11	B_1 = 1.31×10^{-13}	1.00	-.033 → .033	0.0	.0156	.00099	.0315	.0180
	B_2 = 14.1	.832 1.00	9.5 → 18.7	6.4	2.19			
12	B_1 = 1.05×10^{-13}	1.00	-.017 → .017	0.0	.008	.00099	.0315	.0180
	B_2 = 14.0	.838 1.00	9.3 → 18.6	6.3	2.22			

Reproduced with permission of the copyright owner. Further reproduction prohibited without permission.

Reproduced with permission of the copyright owner. Further reproduction prohibited without permission.

TABLE 5

MODEL NUMBER	COEFFICIENT VALUES	CORRELATION MATRIX	95% CONFIDENCE LIMITS	t-VALUE	σ	RMS	RRMS	RSS
	B_1 = 2.32	1.00	- 392. → 397.	0.0	186.			
	B_2 = 3.98	1.00 1.00	- 675. → 683.	0.0	320.			
1						.011	.11	.18
	B_3 = .935	-.972 -.973 1.00	- 245. → 432.	0.0	160.			
	B_4 = 8.39	1.00 1.00 -.968 1.00	- 1190. → 1200.	.6	563.			
	B_1 = 2.4×10^{-12}	1.00	-.26 → .26	0.0	.124			
	B_2 = .132	.895 1.00	-.34 → .61	.6	.224			
2						.0032	.057	.051
	B_3 = .0356	.577 .820 1.00	-.04 → .11	1.1	.0333			
	B_4 = 13.9	.742 .926 .973 1.00	-40.4 → 68.2	.5	25.6			
	B_1 = .0370	1.00	-.037 → .11	1.1	.0352			
3	B_2 = .0678	.805 1.00	-.024 → .16	1.6	.0436	.0109	.104	.186
	B_3 = .740	.913 .952 1.00	-.18 → 1.7	1.7	.437			
	B_1 = 2.7×10^{-13}	1.00	-.016 → .016	0.0	.00760			
4	B_2 = .0239	.582 1.00	.0033 → .045	2.5	.00976	.0026	.051	.045
	B_3 = 57.3	.808 .894 1.00	36. → 79.	5.7	10.1			

MODEL NUMBER	COEFFICIENT VALUES	CORRELATION MATRIX	95% CONFIDENCE LIMITS	t-VALUE	σ	RMS	RRMS	RSS
	$B_1 = 1.76\times10^{-13}$	1.00	-.037 → .037	0.0	.0174			
5	$B_2 = .0449$	.635 1.00	-.01 → .10	1.7	.0260	.0026	.050	.043
	$B_3 = 53.7$	.818 .922 1.00	31. → 76.	5.0	10.8			
	$B_1 = .0230$	1.00	-135. → 135.	0.0	63.2			
	$B_2 = .442$	.995 1.00	-2700 → 2700.	0.0	1260.			
6	$B_3 = 2\times10^{-15}$	-.951 -.940 1.00	-.23 → .23	0.0	.106	.073	.270	1.09
	$B_4 = 20.3$	.998 .998 -.948 1.00	$-2.3\times10^5 \rightarrow 2.3\times10^5$	0.0	1.1×10^5			
	$B_5 = 7.53$	-.993 -1.00 .935 -.997 1.00	$-1.7\times10^4 \rightarrow 1.7\times10^4$	0.0	8050.			
	$B_1 = 4.6\times10^{-13}$	1.00	-.46 → .46	0.0	.218			
	$B_2 = 1.70$	.691 1.00	-4.9 → 8.3	0.5	3.13			
7	$B_3 = .0303$	.487 .956 1.00	-.085 → .15	0.6	.0543	.0048	.069	.076
	$B_4 = 12.4$	.667 .998 .970 1.00	-79. → 104.	0.3	4.30			
	$B_1 = 1.12$	1.00	-3.2 → 5.4	.5	2.03			
8	$B_2 = .161$	.875 1.00	-.55 → .87	.5	.334	.0015	.039	.024

Reproduced with permission of the copyright owner. Further reproduction prohibited without permission.

MODEL NUMBER	COEFFICIENT VALUES	CORRELATION MATRIX	95% CONFIDENCE LIMITS	t-VALUE	σ	RMS	RRMS	RSS
	$B_3 = .296$	.964 .950 1.00	-.56 → 1.2	.7	.401			
	$B_4 = 5\times10^{-11}$	.387 .783 .582 1.00	-1.2 → 1.2	0.0	.548			
9	$B_1 = .0437$	1.00	.0042 → .083	2.3	.0118	.0024	.0488	.0427
	$B_2 = 54.4$	.905 1.00	42. → 67.	9.2	5.92			
10	$B_1 = .0180$	1.00	.0037 → .032	2.7	.00683	.0024	.0490	.00432
	$B_2 = 53.1$	.879 1.00	42. → 64.	10.2	5.19			
11	$B_1 = 5.53\times10^{-14}$	1.00	-.026 → .026	0.0	.0126	.0042	.0648	.0757
	$B_2 = 43.6$	.727 1.00	36. → 51.	12.0	3.63			
12	$B_1 = 5.88\times10^{-14}$	1.00	-.013 → .013	0.0	.00628	.0040	.0631	.0716
	$B_2 = 42.6$	.730 1.00	35. → 50.	12.0	3.55			

Reproduced with permission of the copyright owner. Further reproduction prohibited without permission.

Reproduced with permission of the copyright owner. Further reproduction prohibited without permission.

TABLE 6

MODEL NUMBER	COEFFICIENT VALUES	CORRELATION MATRIX	95% CONFIDENCE LIMITS	t-VALUE	σ	RMS	RRMS	RSS
	B_1 = 1427.	1.00	$-1.5\times10^5 \rightarrow 1.6\times10^5$	0.0	7.7×10^4			
	B_2 = 2545.	1.00 1.00	$-2.8\times10^5 \rightarrow 2.8\times10^5$	0.0	1.4×10^5			
1	B_3 = .947	.0032 0.0 1.00	.41 →1.5	3.6	.266	.0060	.077	.209
	B_4 = 1172.	.999 .999 .049 1.00	$-1.2\times10^5 \rightarrow 1.2\times10^5$	0.0	5.9×10^4			
	B_5 = 3327.	.999 .999 .049 1.00 1.00	$-3.9\times10^5 \rightarrow 4.0\times10^5$	0.0	1.9×10^5			
	$B_1 = 6.4\times10^{-13}$	1.00	-.32 →.32	0.0	.156			
	B_2 = .233	.874 1.00	-.57 →1.04	.6	.398			
2	B_3 = .0627	.663 .921 1.00	-.088 →.213	.8	.074	.0019	.043	.065
	B_4 = 11.5	.754 .961 .990 1.00	-43. →66.	.4	27.0			
	B_5 = 36.9	.752 .964 .991 .999 1.00	-139. →213.	.4	86.5			
	B_1 = .0410	1.00	-.013 →.095	1.5	.0265			
	B_2 = .0757	.827 1.00	.0068 →.15	2.2	.0340			
3	B_3 = .250	.827 .817 1.00	.0036 →.496	2.1	.121	.0059	.077	.213
	B_4 = .811	.921 .956 .862 1.00	.099 →1.5	2.3	.351			

Reproduced with permission of the copyright owner. Further reproduction prohibited without permission.

MODEL NUMBER	COEFFICIENT VALUES	CORRELATION MATRIX	95% CONFIDENCE LIMITS	t-VALUE	σ	RMS	RRMS	RSS
4	$B_1 = 3.0\times10^{-13}$	1.00	-.011 → .011	0.0	.00516	.0015	.038	.054
	$B_2 = .0254$	.590 1.00	.011 → .04	3.6	.00709			
	$B_3 = 17.9$	.736 .613 1.00	12. → 24.	6.2	2.87			
	$B_4 = 58.2$	.801 .894 .705 1.00	44. → 73.	8.0	7.24			
5	$B_1 = 1.9\times10^{-13}$	1.00	-.025 → .025	0.0	.0122	.0014	.038	.052
	$B_2 = .0620$	.674 1.00	.017 → .11	2.8	.0224			
	$B_3 = 18.2$	.792 .703 1.00	12. → 25.	5.6	3.25			
	$B_4 = 59.7$	.827 .932 .771 1.00	42. → 78.	6.8	8.80			
6	$B_1 = 7.0\times10^{-13}$	1.00	-.38 → .38	0.0	.185	.0013	.036	.044
	$B_2 = .358$	.644 1.00	-5.8 → 6.5	0.1	3.04			
	$B_3 = .0686$	.601 .998 1.00	-1.1 → 1.2	0.1	.575			
	$B_4 = 5.15$	.637 .999 .999 1.00	-97. → 108.	0.1	50.4			
	$B_5 = 16.7$	.636 .999 .999 1.00 1.00	-316. → 349.	0.1	163.			
	$B_6 = 1.57$	-.530 .984 -.990 -.982 .983 1.00	-.301 → 3.4	1.7	.918			

MODEL NUMBER	COEFFICIENT VALUES	CORRELATION MATRIX	95% CONFIDENCE LIMITS	t-VALUE	σ	RMS	RRMS	RSS
	$B_1 = 7.7\times10^{-13}$	1.00	-1.2 → 1.2	0.0	.571			
	$B_2 = 1.34$	.703 1.00	-11. → 14.	.2	6.17			
7	$B_3 = .137$	.623 .991 1.00	-1.1 → 1.4	.2	.602	.0022	.047	.076
	$B_4 = 2.68$	.668 .997 .998 1.00	-21. → 26.	,2	11.6			
	$B_5 = 8.56$	.665 .997 .998 1.00 1.00	-67. → 84.	.2	37.2			
	$B_1 = 5.7\times10^{-14}$	1.00	-.04 → .04	0.0	.0197			
	$B_2 = .0385$	.882 1.00	-.0094 → .087	1.6	.0236			
8	$B_3 = .00297$	-.428 -.289 1.00	.00041 → .0055	2.4	.00126	.0021	.045	.073
	$B_4 = 36.0$	.682 .725 .265 1.00	12. → 60.	3.1	11.6			
	$B_5 = 115.8$	.695 .804 .288 .911 1.00	46. → 186.	3.4	34.4			
	$B_1 = .0511$	1.00	.022 → .081	3.5	.0145			
9	$B_2 = 17.5$	.371 1.00	14. → 21.	9.3	1.88	.0014	.0373	.051
	$B_3 = 56.5$	.896 .333 1.00	47. → 66.	12.6	4.49			

Reproduced with permission of the copyright owner. Further reproduction prohibited without permission.

Reproduced with permission of the copyright owner. Further reproduction prohibited without permission.

MODEL NUMBER	COEFFICIENT VALUES	CORRELATION MATRIX	95% CONFIDENCE LIMITS	t-VALUE	σ	RMS	RRMS	RSS
	$B_1 = .0205$	1.00	.0101 → .031	4.0	.00514			
10	$B_2 = 17.1$	.328 1.00	13. → 21.	9.3	1.84	.0014	.0376	.052
	$B_3 = 54.8$	.868 .285 1.00	47. → 63.	13.9	3.94			
	$B_1 = 9.14\times10^{-14}$	1.00	-.018 → .018	0.0	.00907			
11	$B_2 = 14.4$	.491 1.00	10. → 19.	6.5	2.21	.0025	.0500	.0925
	$B_3 = 43.3$	.700 .344 1.00	38. → 49.	16.1	2.69			
	$B_1 = 1.51\times10^{-13}$	1.00	-.0094 → .0094	0.0	.00462			
12	$B_2 = 13.5$	.488 1.00	9.2 → 18.	6.4	2.12	.0023	.0481	.0857
	$B_3 = 40.8$	.703 .344 1.00	36. → 46.	15.7	2.60			

were not independent. For the k_{C_6} case, the parameters showed independence with the exception that B_3 and B_4 were related to B_2. However, t-values for all parameters were less than .6 indicating a very low degree of confidence in the parameter values. On the basis of statistical uncertainty, Model 7 was rejected.

Models 4 and 5 were identical with the exception of the exponent of the adsorption term. Models 9 and 10 were also related in the same way. Both of these sets of models were derivable from the assumptions of isomerization rate controlling and $K_{HC} >> K_{H_2}$. Model 4 indicated a dual site mechanism while Model 5 indicated a single site mechanism. Similarly, Model 9 was a single and model 10 a dual site mechanism. Models 9 and 10 further assumed $K_{C_6} >> K_{C_5}$, as shown from qualitative considerations discussed earlier. While it has been shown earlier in this section that the data indicated a dual site mechanism, it would be expected that statistical analysis of these sets of models would yield the same result.

For k_{C_5}, Model 4 resulted in a higher t-value for all three parameters than Model 5. Although the RMS and RRMS were higher for model 4, it can be seen that the differences were very small, especially when compared to the values obtained on other models. The correlation matrix for Model 4 showed that no parameter was correlated above the .95 level while Model 5 resulted in B_3 correlated with B_1 and B_2 at .95 or above. This indicated that in Model 4 the parameters are more independent. It is important to note that both Models 4 and 5 were consistent with the qualitative observation made earlier that $K_{C_5} < K_{C_6}$. That is, to the extent that B_1 and B_2 correspond to K_{C_5} and K_{C_6}, Models 4 and 5 result in valid values for B_1 and B_2,

Reproduced with permission of the copyright owner. Further reproduction prohibited without permission.

namely $B_1 < B_2$. Based on the higher t-values of the Model 4 parameters and the relative independence of the parameters, it is judged that Model 4 is superior.

Models 9 and 10 would be expected to demonstrate the same relationship as Models 4 and 5. It can be seen that the error terms of Models 9 and 10 were essentially equal to each other and to those of Models 4 and 5. However, as with Models 4 and 5, the dual site Model, 10, had a higher t-value for B_1, with the t-values for B_2 being equal. In addition, the B_1-B_2 correlation was less, .658 versus .675, for Model 10. On the basis of more certainty and independence of the parameters, Model 10 was superior.

Now, for k_{C_5}, Models 4 and 10 must be compared. It can be seen that if it is assumed that $K_{C_6} >> K_{C_5}$, Model 4 becomes Model 10. The two models are thus not contradictory but complementary, both being derivable from the same assumptions with only the above mentioned difference. It can be seen that B_1 in Model 4, corresponding to K_{C_5}, had a low t-value and includes zero in the 95% confidence limits. On this basis, it was impossible to reject the hypothesis that B_1 was zero at the .95 level. Thus, statistically, Model 10 was superior. The t-values for both B_1 and B_2 of Model 10 are 3.9 and 14.6, indicating that the null hypothesis may be rejected well above the .99 confidence level. Thus, for k_{C_5} models, it can be seen that Model 10 was both statistically superior and was consistent with the qualitative and quantitative conclusions presented earlier in this section, namely $K_{C_6} >> K_{C_5}$ or K_{H_2}, dual site mechanism, and isomerization rate controlling.

Reproduced with permission of the copyright owner. Further reproduction prohibited without permission.

For k_{C_6}, Models 4, 5, 9, and 10 must also be compared, other models being ruled out as indicated earlier. For example, it can be seen that for Model 8, $B_4 \rightarrow 0$ which reduced Model 8 to the same form as Model 3. However, the RMS and RRMS for Model 3 were much higher than for Models 4, 5, 9, and 10. Models 8 and 3 were thus rejected. Models 1, 2, 6, 7, and 12 may be rejected on the basis of higher error terms. Models 4 and 5 both implied that $B_1 \rightarrow 0$. Note that this resulted in a low t-value for B_1. Thus Models 4 and 5 were inadequate. However, they indicated that a better fit may be obtained by deleting B_1 from the model altogether. Models 9 and 10 resulted from the assumption that $K_{C_6} >> K_{C_5}$, as indicated by the results of Models 4 and 5. Models 9 and 10 for k_{C_6} were derived assuming single and dual site kinetics, respectively, with isomerization rate controlling, as stated earlier. Even though both these models had only two parameters, which is fewer than any of the others, the error term was smaller than for any other proposed model for k_{C_6} except Model 8, which had four parameters. Model 8 had been ruled out previously on the basis of low t-values for all parameters. Thus, Models 9 and 10 were the best realistic representations of the data. It should also be noted that zero was not included in the 95% confidence limits of the parameters for both Models 9 and 10 as was the case for k_{C_5}. In order to distinguish between Models 9 and 10, examine first the correlation matrix. Model 10 showed the B_1-B_2 correlation to be less than for Model 9, .879 to .905. Model 10 had higher t-values for both B_1 and B_2. Since the RRMS and RMS were essentially the same for Models 9 and 10, Model 10 was seen as the superior statistical representation of the data. Note that Model 10 was derivable from a dual site mechanism whereas Model 9

Reproduced with permission of the copyright owner. Further reproduction prohibited without permission.

resulted from a single site mechanism. Model 10 being a better fit was thus consistent with the results indicated earlier in this section.

It was concluded that for both k_{C_5} and k_{C_6}, Model 10 was the superior model.

For the coupled models as shown in Table 6, it can be seen that Models 1, 2, 6, and 7 may be rejected based on the t-values of the parameters. Of the remaining models, Model 3 had a RMS and RRMS more than twice that of Model 4, 5, or 8. It was rejected on the basis of a less adequate fit of the data. Of Models 4, 5, 8, 11, and 12 it can be seen in each case, $B_1 \rightarrow 0$. This indicated that $K_{C_5} << K_{C_6}$ for the coupled models as was the case for k_{C_6} alone. Models 9 and 10 had the lowest RRMS and RMS of any model except the model which had been rejected above. The error terms of Models 9 and 10 were essentially equal and cannot be distinguished on that basis. However, as was the case with the individual models, Model 10, corresponding to a dual site mechanism, had higher t-values for B_1 and B_3 (B_2 t-value being equal) than Model 9. In addition, the correlation matrix showed greater independence among all of the parameter relationships. Thus, the statistical analysis indicated that Model 10 was superior. This was to be expected since a dual site mechanism was also consistent with results presented earlier in this section.

Now, the individual and coupled Model 10 results must be compared. Such a comparison should reveal the validity of the coupling procedure. From Tables 4, 5, and 6, it can be seen that for Model 10 the values of the parameters $B_1 \rightarrow B_3$ were of the same order. The results

Reproduced with permission of the copyright owner. Further reproduction prohibited without permission.

are shown below for convenience.

	From k_{C_5} Data	From k_{C_6} Data	From Coupled Data
B_1	.0427	.0180	.0205
B_2	19.5	53.1	17.5
B_3	____	____	54.8

Note that B_2 for k_{C_5} data corresponds to B_2 for the coupled data while B_2 for k_{C_6} data corresponds to B_3 for the coupled data. It can be seen that B_1 for the coupled data lies between the other two values as expected. In addition, note the close correspondence of B_2 for k_{C_5}, 19.5, and B_2 for the coupled data, 17.5. The same was true for B_2 for k_{C_6} data and B_3 for the coupled data, 53.1 versus 54.8. This indicated that the coupling procedure was valid and did not contradict results obtained by individual analysis.

Reproduced with permission of the copyright owner. Further reproduction prohibited without permission.

Faujasite Experimental Results

As with the mordenite catalyst, pure component runs were carried out on the Pd-H-faujasite to establish the baseline activity of this particular catalyst. Table 7 shows the comparison of the Pd-H-faujasite used in this study with similar catalysts. It can be seen that the catalyst used in this study had an activity comparable to those used in previous studies. It should be noted that the isomerization activity of this Pd-H-faujasite, as with the mordenite discussed earlier,was strongly dependent on the preparation technique. Thus, some scatter in rate constant values from batch to batch was inevitable.

Table 8 and Figure 20 show a comparison of the activation energy indicated by this study for the isomerization of $n\text{-}c_5$ compared with results obtained on similar catalysts studied at LSU. It can be seen that the catalyst used in this study had an activation energy for $n\text{-}c_5$ isomerization of 44 kcal/g-mole which is comparable to that obtained on similar catalysts in previous studies.

The relative magnitudes of the hydrocarbon and hydrogen adsorption constants may be evaluated by examining the effect of the hydrogen to hydrocarbon ratio, H_2/HC, as discussed earlier. Figure 21 shows a plot of $k_{c_5}^{-1/2}$ and $k_{c_6}^{-1/2}$ versus $1/(\tilde{R}+1)$ at 200 and 300 psig total pressure. Figure 22 shows a plot of $k_{c_5}^{-1/2}$ and $k_{c_6}^{-1/2}$ versus $\tilde{R}/(\tilde{R}+1)$ at 200 psig and 300 psig. As discussed earlier, if $K_{HC} >> K_{H_2}$, then Figure 21 should yield a straight line with a negative abscissa intercept and Figure 22 should not. This was the case. These results were

Reproduced with permission of the copyright owner. Further reproduction prohibited without permission.

TABLE 7

$n\text{-}c_5$ rate constants, Pd-H-Faujasite

INVESTIGATOR	PRESSURE, psia	TEMP., °F	w/hr/w, hr^{-1}	H_2/HC	k_{c_5}, cc/gm/sec
Habibe	465	555	8.5	6.2	.156
		500	8.5	6.0	.0119
This Study	465	500	6.2	10.1	.014
Strickland	465	550	7.7	10.1	.0691
		500	3.2	10.4	.0171

Reproduced with permission of the copyright owner. Further reproduction prohibited without permission.

TABLE 8

Activation energies for n-C_5 hydroisomerization on Pd-H-Faujasite

INVESTIGATOR	TEMPERATURE RANGE, °F	ACTIVATION ENERGY, kcal/g-mole
Habibe	500-550	53
Strickland	450-600	40
This Study	450-500	44

Reproduced with permission of the copyright owner. Further reproduction prohibited without permission.

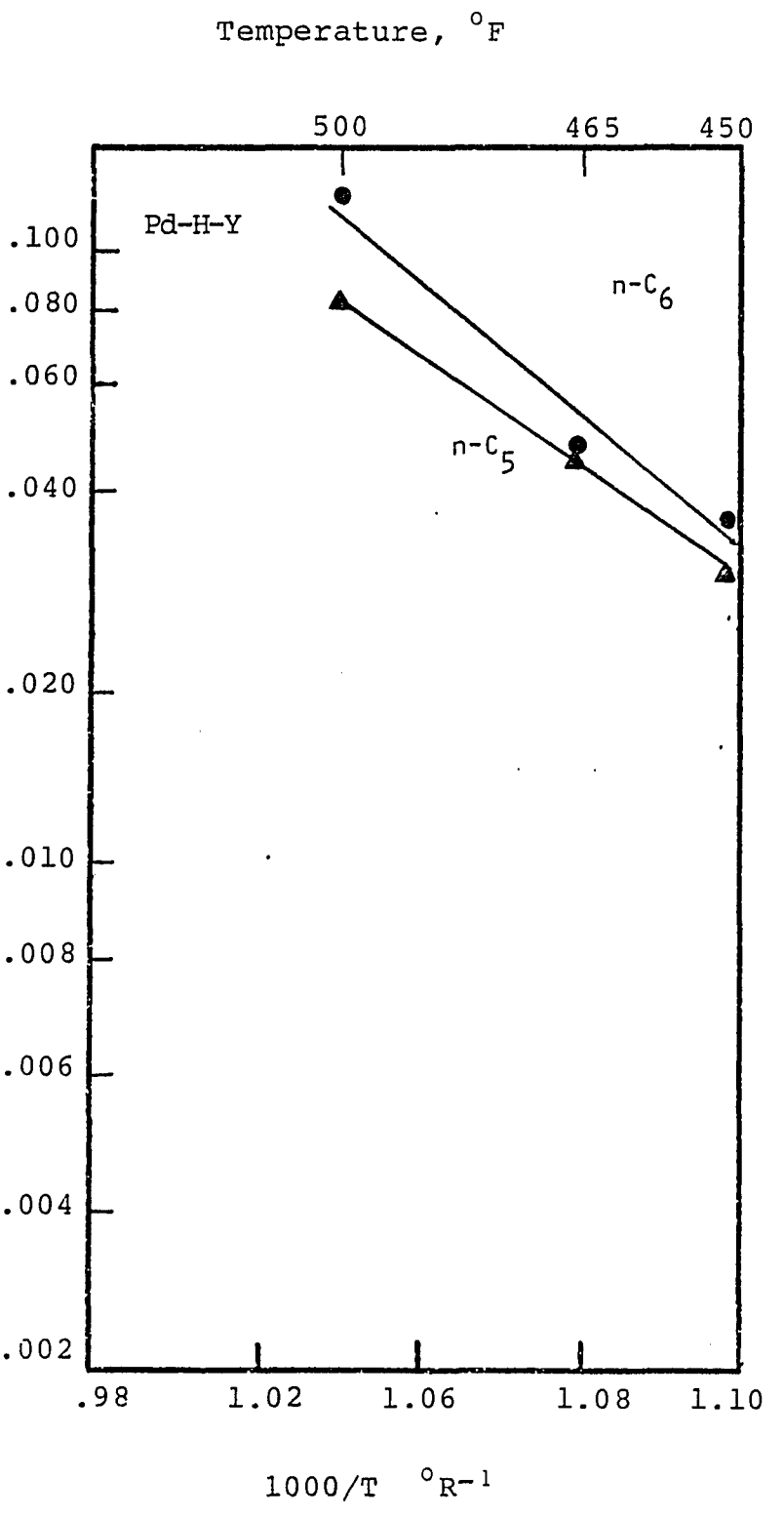

Figure 20. Arrhenius plot of first-order rate constants

Reproduced with permission of the copyright owner. Further reproduction prohibited without permission.

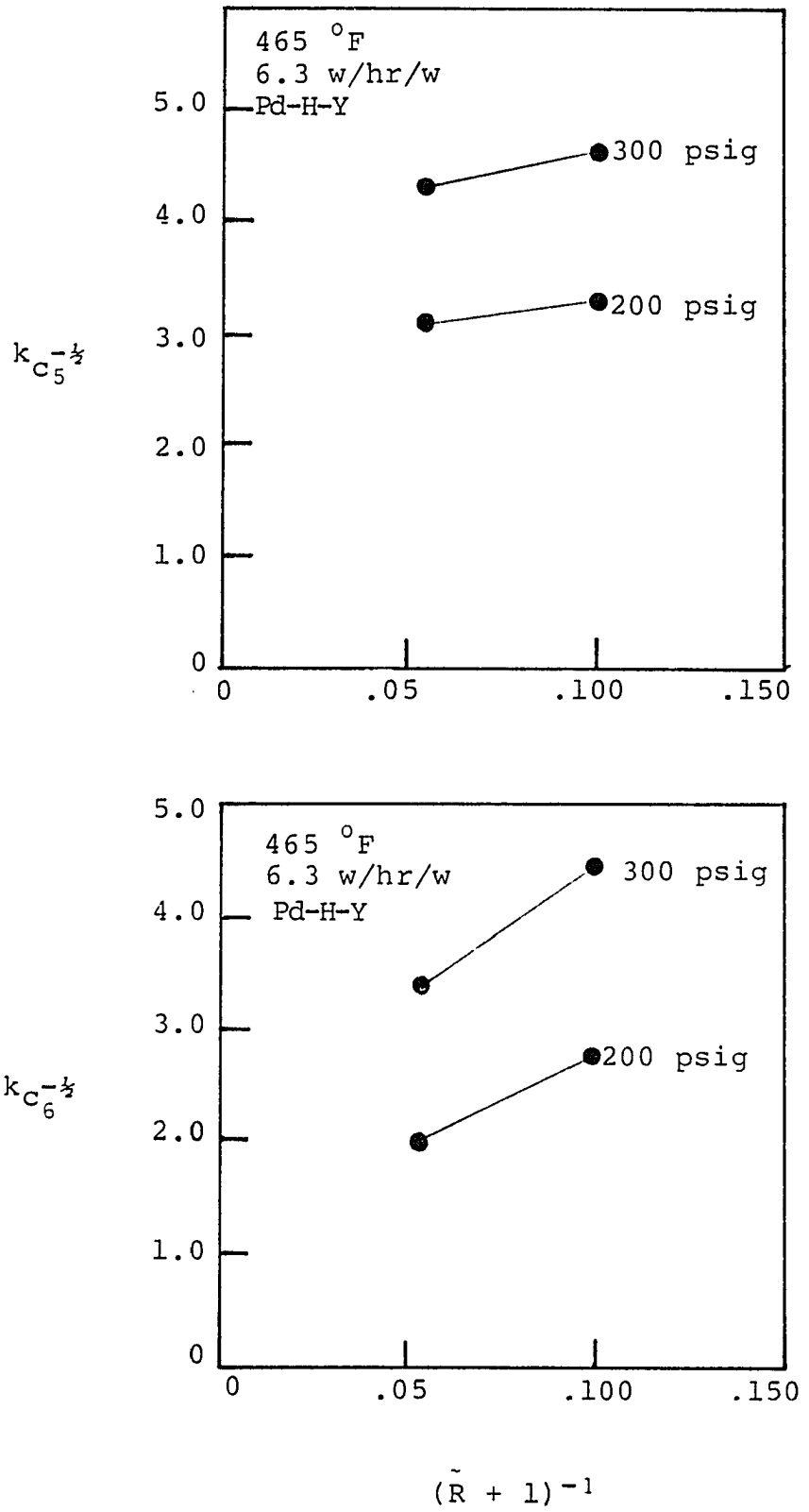

Figure 21. Rate constant versus H_2/HC ratio

Reproduced with permission of the copyright owner. Further reproduction prohibited without permission.

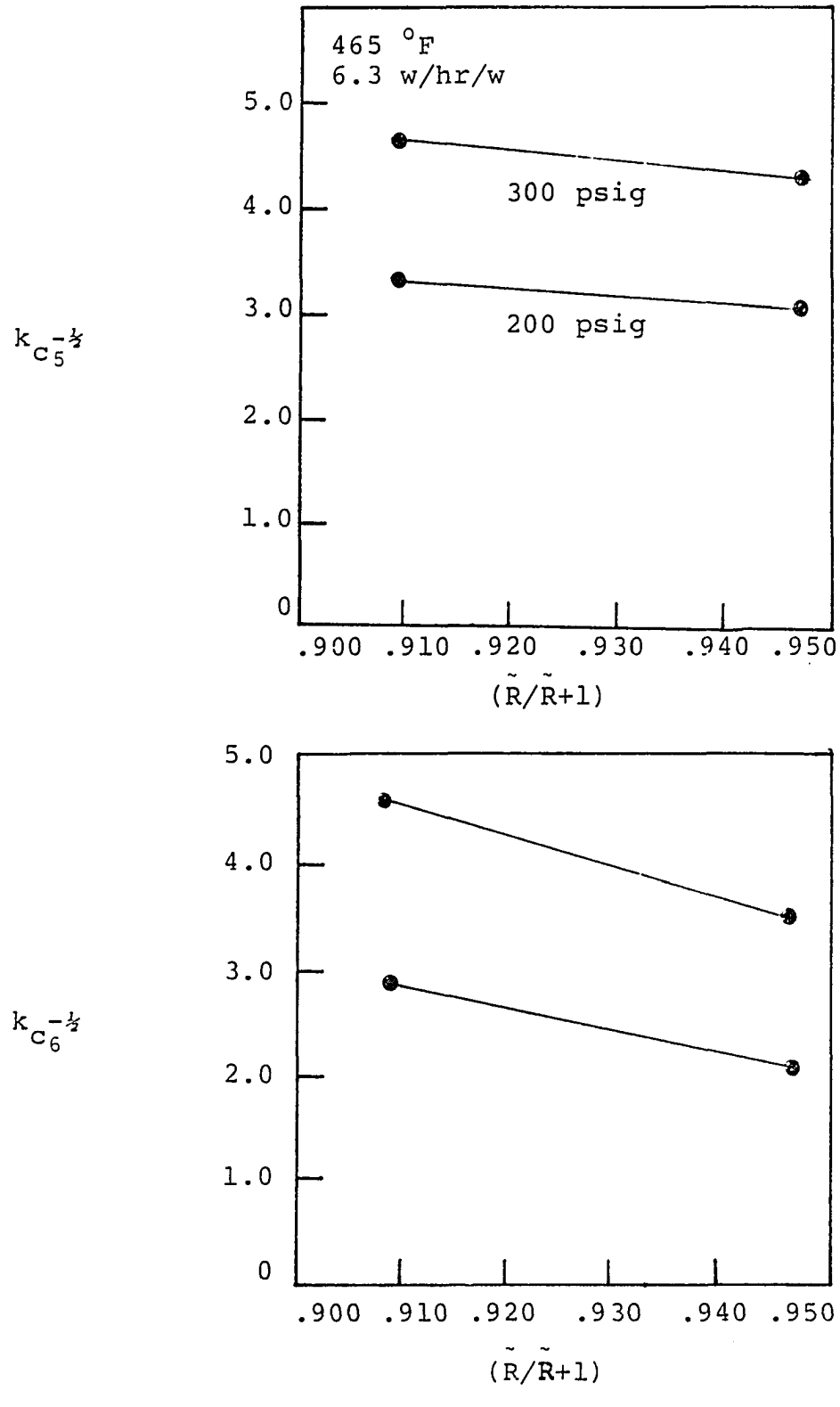

Figure 22. Rate constant versus H_2/HC ratio.

Reproduced with permission of the copyright owner. Further reproduction prohibited without permission.

consistent with those obtained on the mordenite catalyst as shown in Figures 21 and 22 and indicated that the relative magnitudes of the hydrogen and hydrocarbon adsorption paramaters was the same on both catalysts.

Under the simplifying assumptions discussed earlier, a plot of $k^{-1/n}$ vs P_{tot} should give a straight line with a positive intercept for the correct value of n, where n is the number of sites involved in the surface reaction. Figures 23 and 24 show the results of such a plot for an n of 1 and 2. The plot of both $(k_{c_5})^{-\frac{1}{2}}$ and $(k_{c_6})^{-\frac{1}{2}}$ both have positive intercepts whereas $(k_{c_5})^{-1}$ and $(k_{c_6})^{-1}$ both had negative intercepts. The data were thus consistent with the assumption of a dual site mechanism.

Previous studies (44,56) had shown that Pd-H-mordenite and Pd-H-faujasite may both be considered to isomerize through a dual site mechanism, and that the assumption of first order reversible kinetics is valid. Thus this study did not duplicate the experiments to verify first order kinetics on the faujasite catalyst but concentrated on examining the mechanism of isomerization of mixtures and comparing these results to Pd-H-mordenite.

Figures 25 through 30 show the results obtained on mixtures of n-C_5 and n-C_6 at 465°F, 6.4 w/hr/w, pressures from 100 to 300 psig, and H_2/HC ratios from 10/1 to 18/1. These runs were carried out in the same manner as those over the mordenite catalyst, i.e., a pure n-C_5 and n-C_6 run and three mixture runs were done at each temperature and pressure. Several general trends may be noted.

Reproduced with permission of the copyright owner. Further reproduction prohibited without permission.

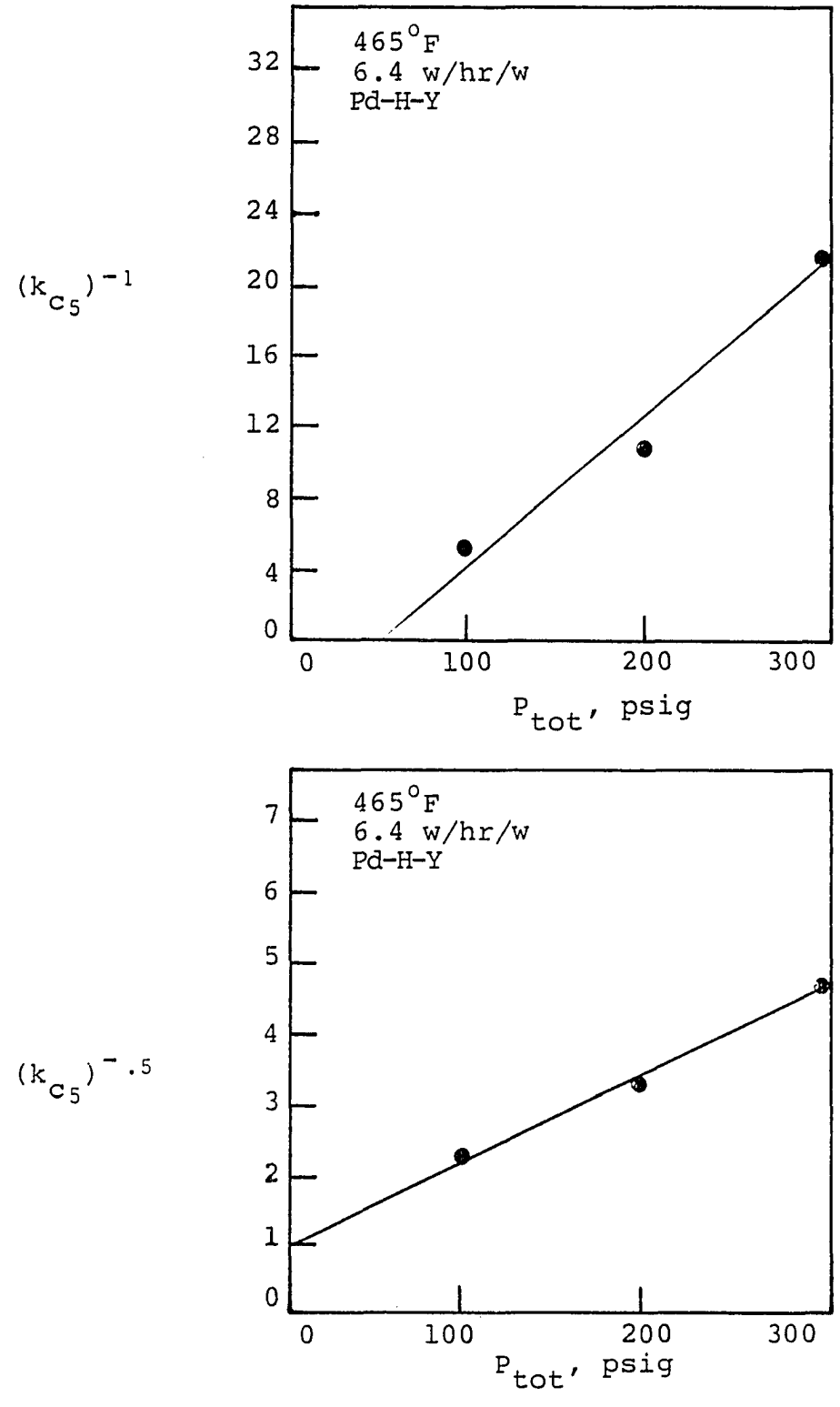

Figure 23. Test for a dual site mechanism, n-C_5.

Reproduced with permission of the copyright owner. Further reproduction prohibited without permission.

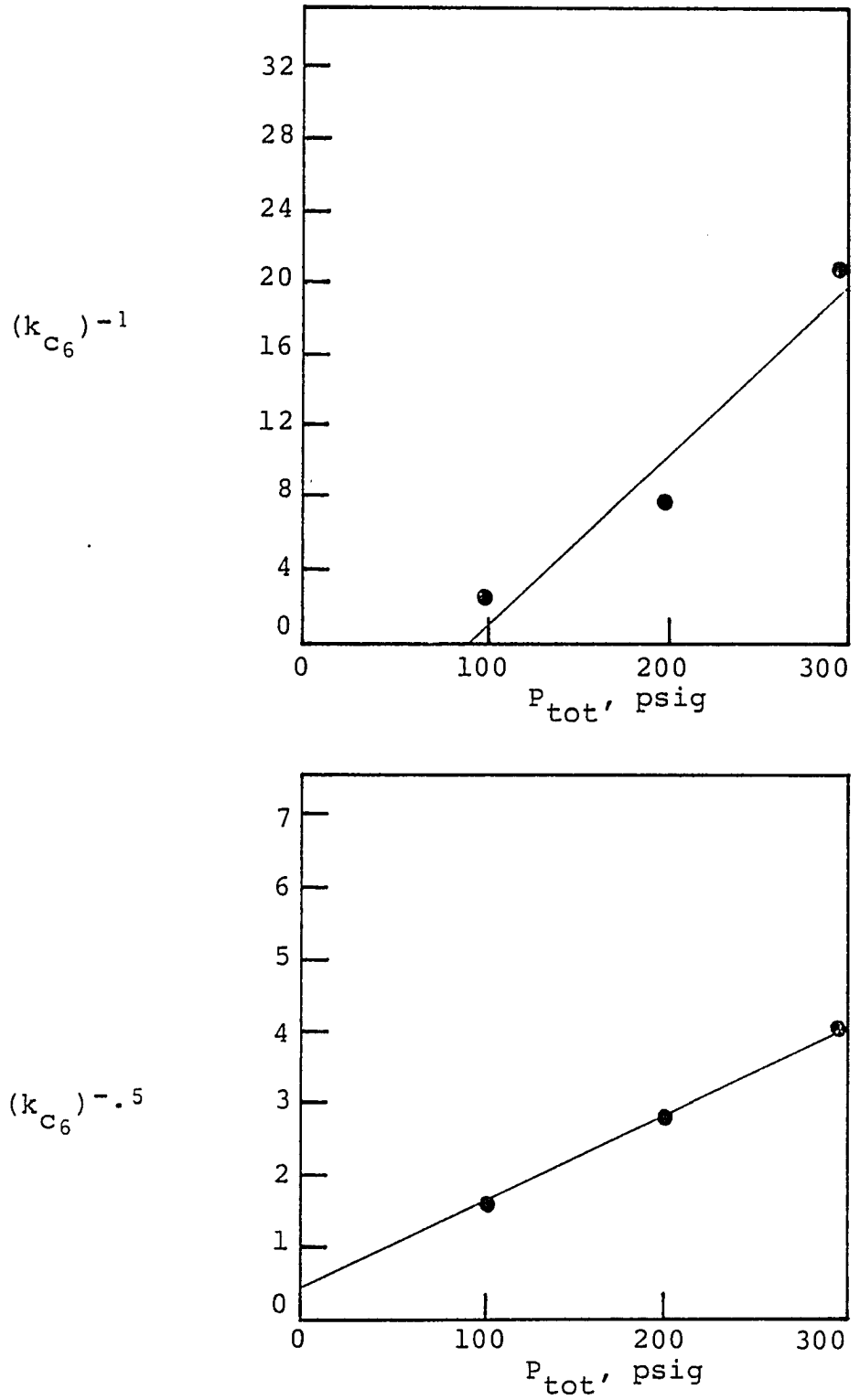

Figure 24. Test for a dual site mechanism, n-C_6.

Reproduced with permission of the copyright owner. Further reproduction prohibited without permission.

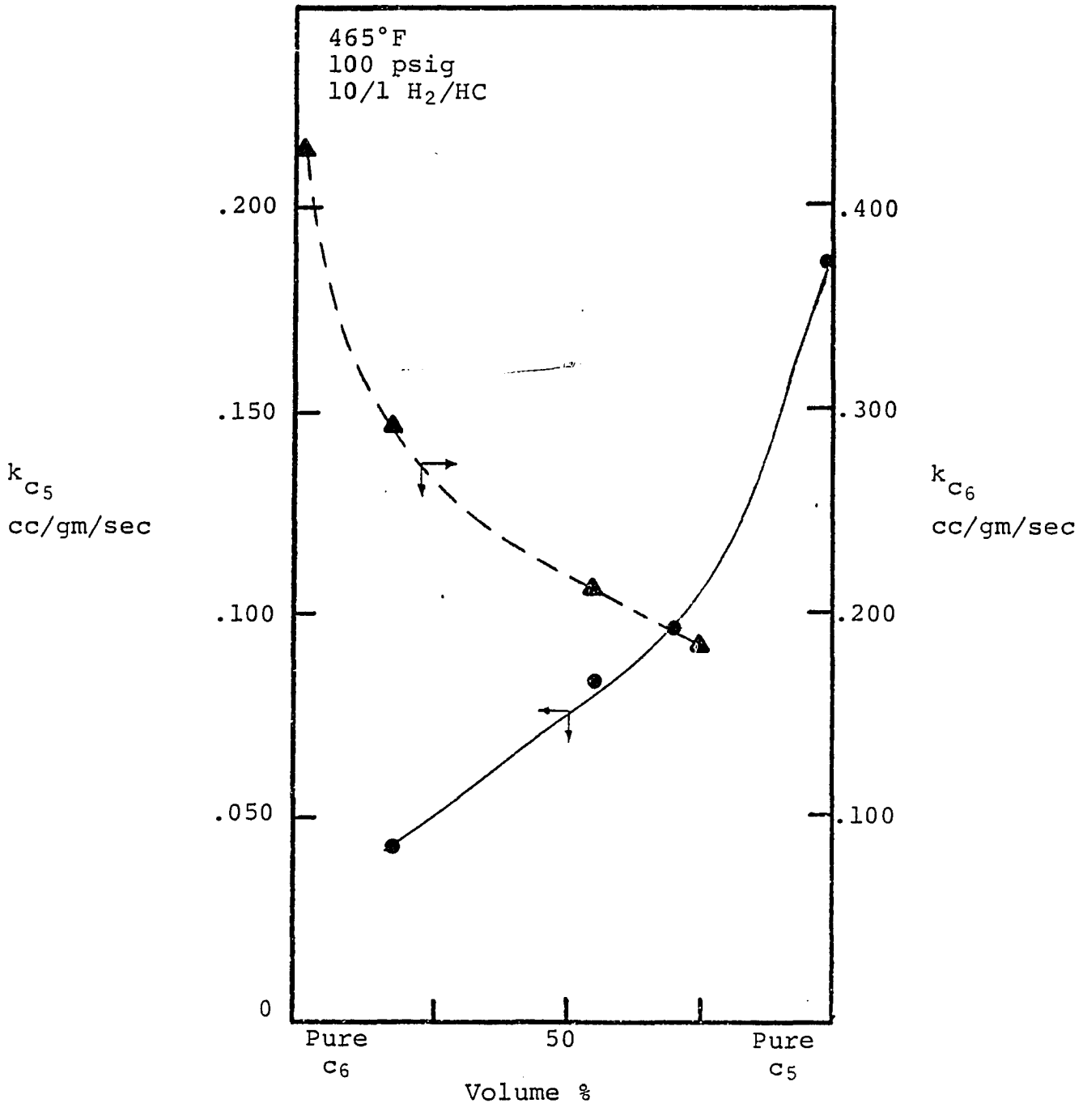

Figure 25. Rate constant versus feed concentration.

Reproduced with permission of the copyright owner. Further reproduction prohibited without permission.

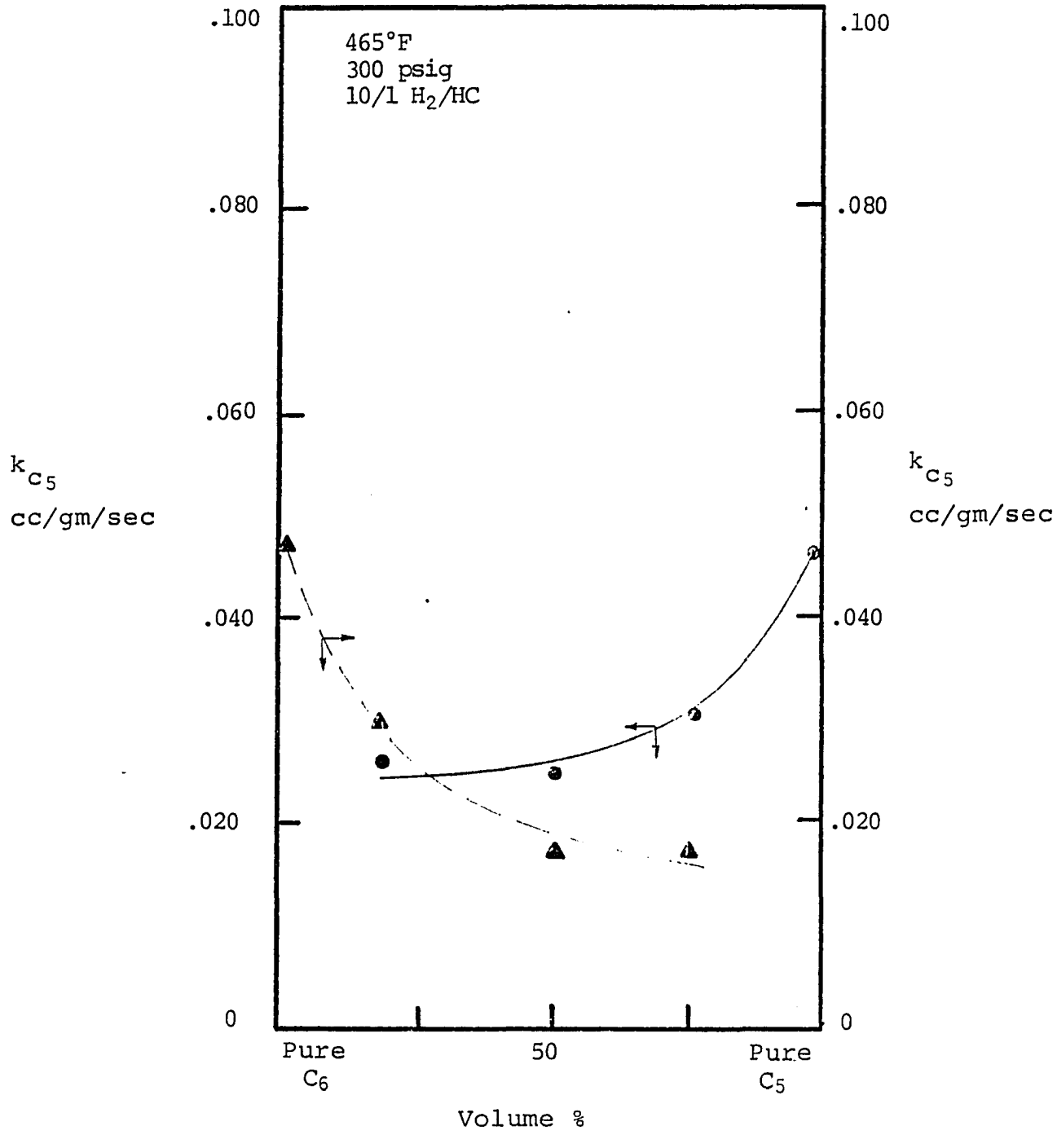

Figure 26. Rate constant versus feed concentration.

Reproduced with permission of the copyright owner. Further reproduction prohibited without permission.

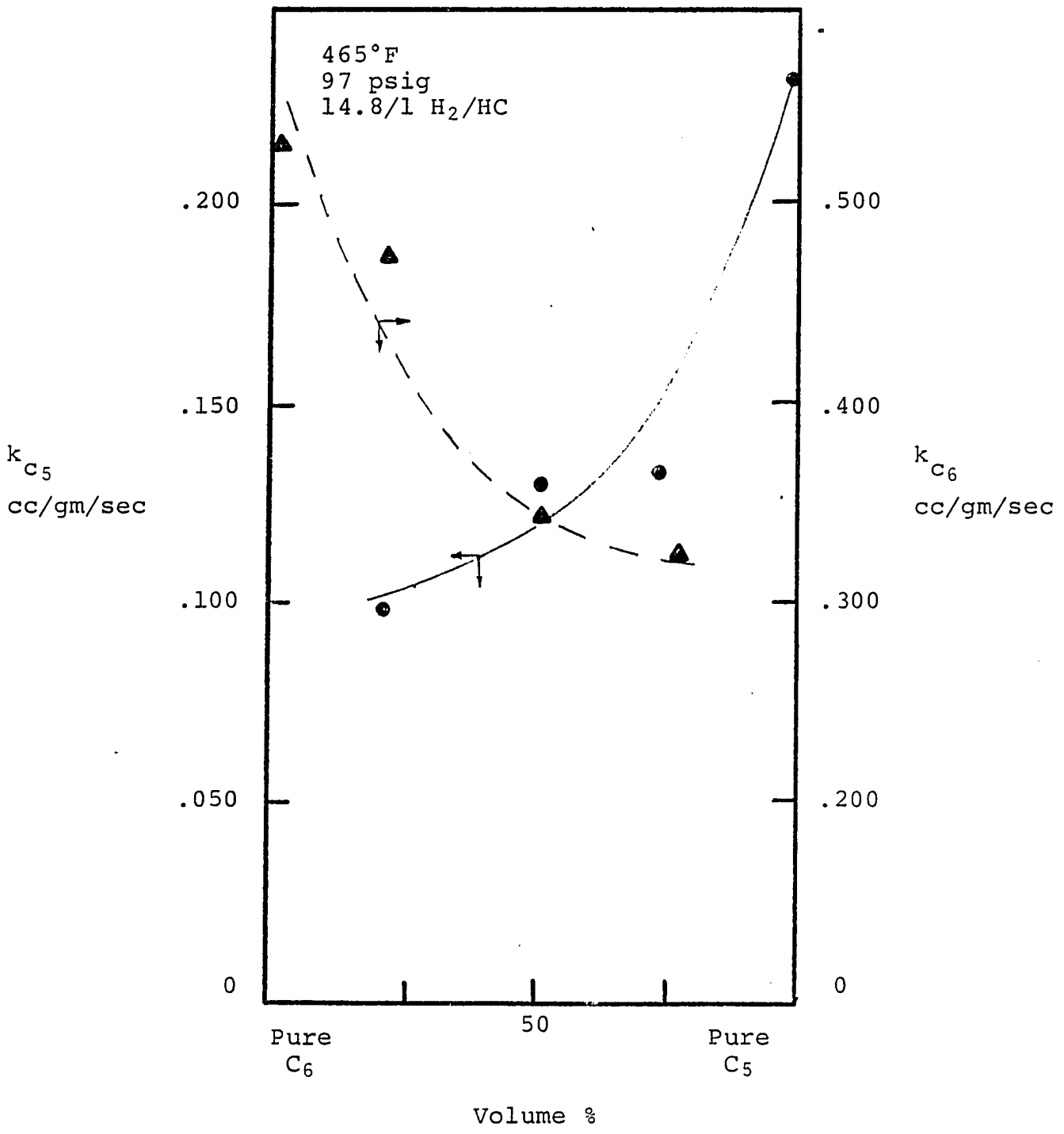

Figure 27. Rate constant versus feed concentration.

Reproduced with permission of the copyright owner. Further reproduction prohibited without permission.

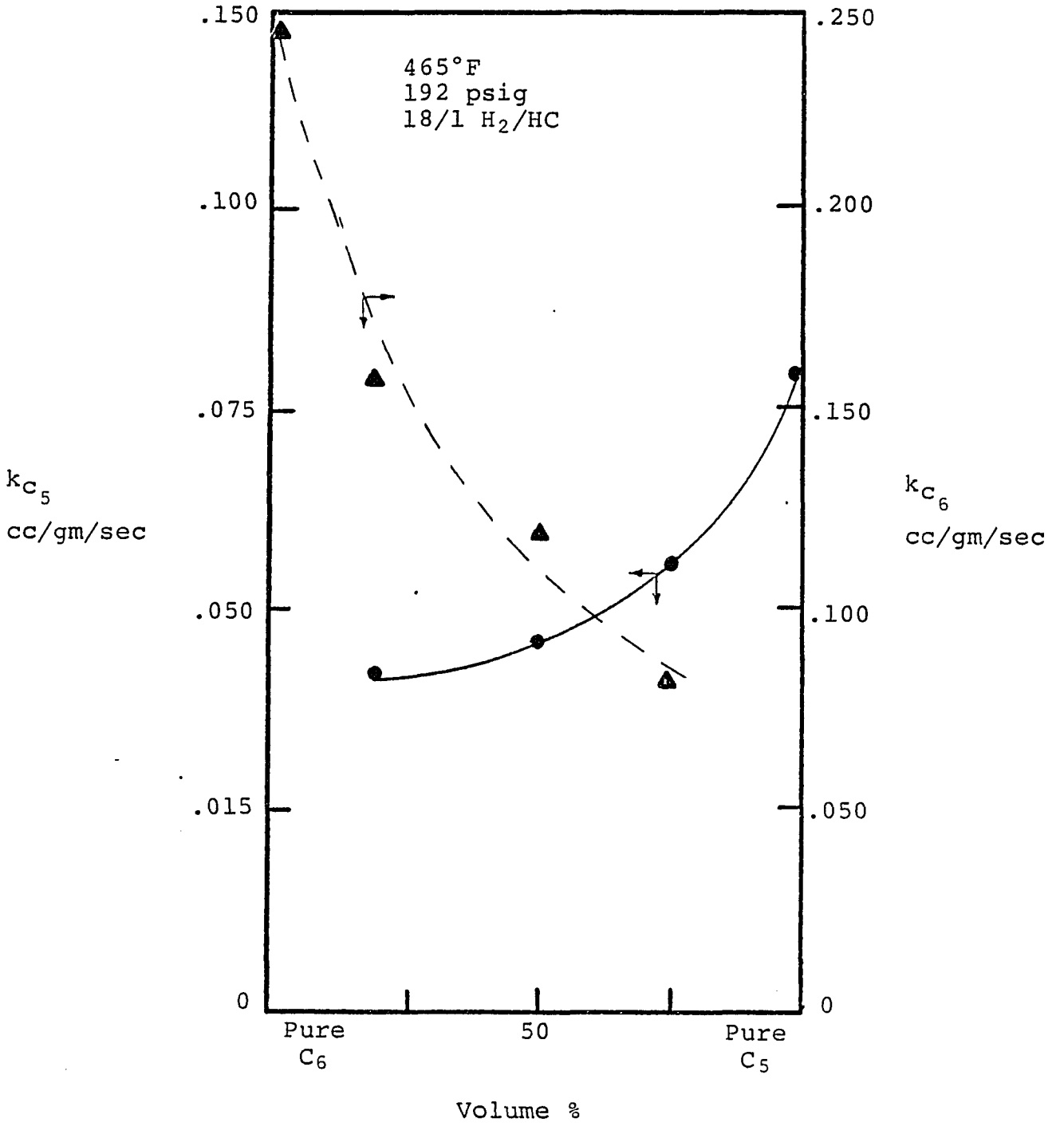

Figure 28. Rate constant versus feed concentration.

Reproduced with permission of the copyright owner. Further reproduction prohibited without permission.

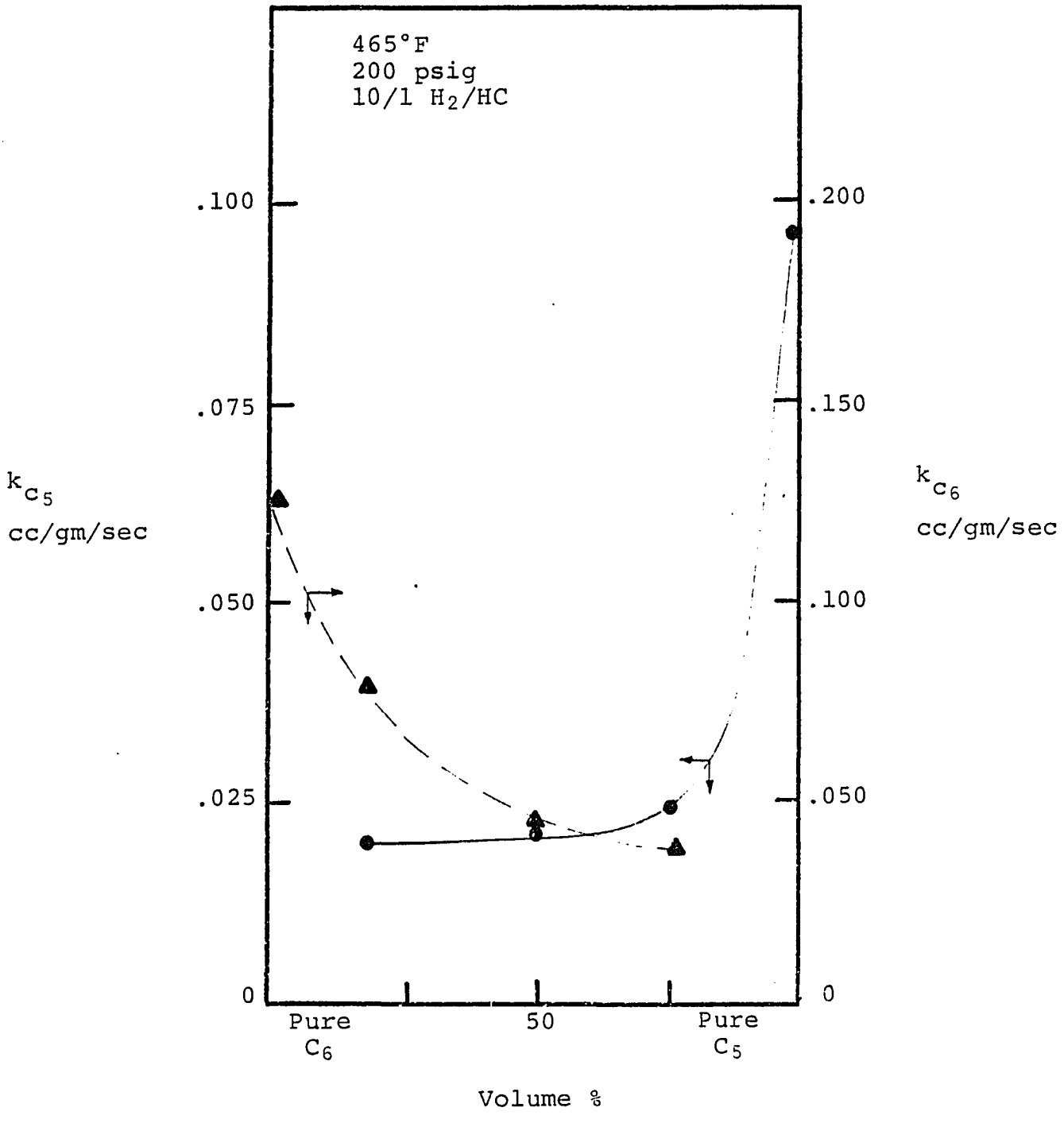

Figure 29. Rate constant versus feed concentration.

Reproduced with permission of the copyright owner. Further reproduction prohibited without permission.

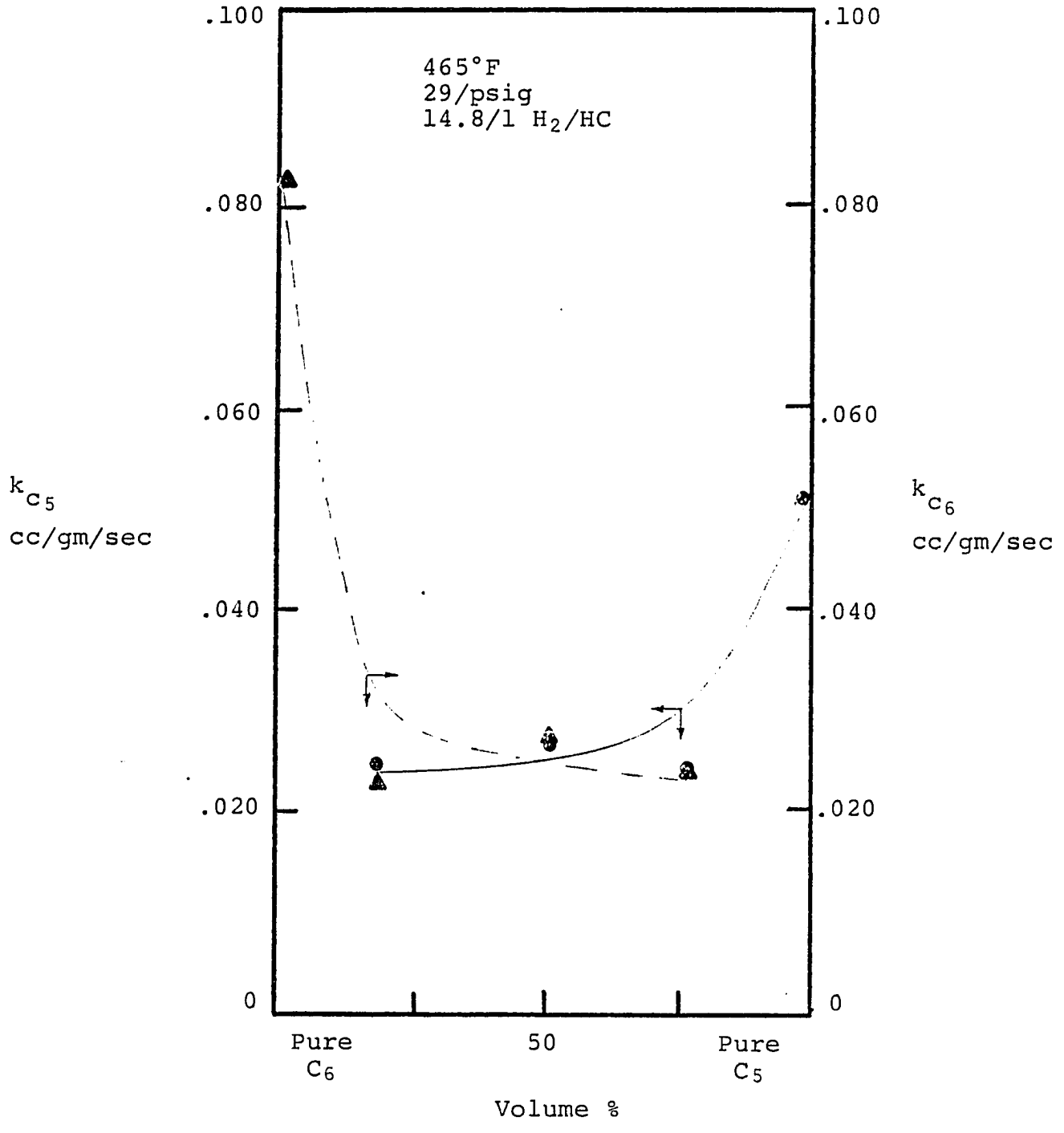

Figure 30. Rate constant versus feed concentration.

Reproduced with permission of the copyright owner. Further reproduction prohibited without permission.

Both k_{c_5} and k_{c_6} decreased on dilution. This was in contrast to the mordenite catalyst on which k_{c_6} increased on dilution while k_{c_5} decreased. On the Pd-H-faujasite catalyst, the results thus indicated a competitive interaction between C_5 and C_6 on the catalysts surface. It may be said that n-C_5 and n-C_6 had approximately the same adsorption affinity on the faujasite catalyst. Otherwise, the rate constant of the preferentially adsorbed hydrocarbon would increase on dilution. The pore diameter of the faujasite was 8Å, comparable to that of the mordenite. Thus, differences in adsorption between the mordenite and faujasite must be due to another cause, perhaps differences in the types of active centers involved in surface reaction.

The results also show that the values of both k_{c_5} and k_{c_6} decrease with increasing total pressure. This same result was observed on the mordenite. This was expected from the Langmuir form of rate constant:

$$k_j = \frac{\bar{k}}{[1 + \Sigma\, Ki\, Pi]^n} \qquad \begin{matrix} j=c_5,c_6 \\ i=c_5,c_6,H_2 \end{matrix}$$

since, as the P_i's are increased, the denominator gets larger and k_j gets smaller.

As with the mordenite catalyst, the absolute values of k_{c_6} were greater than for k_{c_5}. This may be due to a larger true surface reaction rate constant for n-C_6 than n-C_5. i.e., $(k_o)_{c_6} \geq (k_o)_{c_5}$. From equation (18) the value of k_o may be obtained from the intercepts of Figures 23 and 24 From these Figures, it can be seen that $(k_o)_{c_5} \simeq 1.0$ whereas $(k_o)_{c_6} \simeq 4.9$. Thus, the data indicated that indeed the inherent surface reaction rate constant for n-C_6 was greater than that for n-C_5. The same result was

Reproduced with permission of the copyright owner. Further reproduction prohibited without permission.

obtained on the mordenite catalyst.

Finally, it can be seen that the absolute value of both k_{c_5} and k_{c_6} decreased with increasing H_2/HC ratio, $\tilde{R}$. This was consistent with equation (18) developed earlier showing the functional dependence of the rate constant on $\tilde{R}$ at a given P_{tot},

$$k^{-\frac{1}{2}} = \bar{k}^{-\frac{1}{2}} \left[1 + \frac{P_{tot} (\tilde{R} K_{H2} + K_{HC})}{1 + \tilde{R}} \right] .$$

As $\tilde{R}$ increases at constant P_{tot}, k must decrease unless $K_{H_2} = K_{HC}$. It has been shown that $K_{HC} >> K_{H_2}$ and thus k must decrease with increasing $\tilde{R}$.

In summary, it can be said that the data on the Pd-H faujasite are consistent with the following:

1. First order reversible kinetics (44,56).
2. Dual site mechanism for both n-C_5 and n-C_6 hydroisomerization, Figures 23,24.
3. $(k_o)_{c_6} > (k_o)_{c_5}$, Figures 23,24.
4. $K_{c_5} \simeq K_{c_6}$, Figures 25-30.
5. $K_{HC} >> K_{H_2}$, Figures 21,22.

These results were identical to those obtained on the mordenite catalyst with the exception of the relative magnitudes of the n-C_5 and n-C_6 adsorption constants. On the mordenite, $K_{c_6} >> K_{c_5}$ while $K_{c_6} \simeq K_{c_5}$ on the faujasite.

The information obtained from the statistical analysis of the experimental results may be used to formulate and judge the rate constant and partial pressure relationships. The statistical analysis was carried out in the same manner as described earlier for the mordenite

Reproduced with permission of the copyright owner. Further reproduction prohibited without permission.

catalyst. Various models, shown in Table 3, were postulated as functional forms for k (P_i) based on assumptions about the number of sites involved in the mechanism, the relative values of the adsorption parameters, and the rate controlling step. Both individual and coupled models were used.

Tables 9-11 show the results for the Pd-H-faujasite catalyst. On each individual model, twenty-four data points were used and the coupled models thus used forty-eight points.

On the individual n-C_5 models, Table 9, examination of the RMS and RRMS showed that Models 2, 4, 5, and 6 resulted in substantially better representations of the data than the remaining models. Of these four models, only Model 4 did not include zero in the 95% confidence limits of any of the coefficients. In addition, even though Model 2 had four parameters and Model 6 had five, neither resulted in a significantly better fit than Model 4 which has only three parameters. Model 6 may be ruled out by virtue of the low t-values for four of the five coefficients. Low t-values result from parameter values which approach zero, since the t-value is equal to the parameter value divided by σ. For Model 5, while the t-values were non-zero, zero is within the B_1 confidence limits. There was also a .98 correlation between B_1 and B_3. On this basis, Model 5 was rejected. For Model 2, zero was within 3 of 4 parameter confidence limits. Also, there were low t-values for B_1 and B_2. Thus Model 2 was rejected in favor of Model 4.

While Model 4 may be judged to be the best of the twelve models in describing the relationship between the simplified pentane rate constant and the partial pressures of the reactants, it was noted that B_1 and B_3 were correlated at the .948 level. However, the B_1-B_2 and

Reproduced with permission of the copyright owner. Further reproduction prohibited without permission.

Reproduced with permission of the copyright owner. Further reproduction prohibited without permission.

TABLE 9

MODEL NUMBER	COEFFICIENT VALUES	CORRELATION MATRIX	95% CONFIDENCE LIMITS	t-VALUE	σ	RMS	RRMS	RSS
1	B_1 = 179.	1.00	-9400. → 9700.	0.0	4570.	.000532	.0230	.0106
	B_2 = 467.	1.00 1.00	-2400. → 25000.	0.0	11900.			
	B_3 = 1.28	.009 .005 1.00	.895 → 1.7	7.0	.184			
	B_4 = 2094.	.999 .999 .049 1.00	140,000 → 140,000	0.0	67,900.			
2	B_1 = .0733	1.00	-.021 → .017	1.6	.0453	.000258	.0160	.00516
	B_2 = .419	.771 1.00	.011 → .072	2.9	.146			
	B_3 = .0141	.279 .735 1.00	-.00016→ .028	2.1	.00684			
	B_4 = 1.935	.638 .924 .913 1.00	-.048 → 4.4	1.7	1.16			
3	B_1 = .151	1.00	.014 → .29	2.3	.0659	.00053	.0231	.0112
	B_2 = .387	.930 1.00	.11 → .67	2.9	.135			
	B_3 = .931	.990 .953 1.00	-.042 → 1.9	2.0	.468			
4	B_1 = .0273	1.00	.00084→ .041	2.2	.00956	.000280	.0167	.0591
	B_2 = .143	.736 1.00	.088 → .20	5.3	.0268			
	B_3 = 28.7	.948 .831 1.00	19.1 → 38.	6.2	4.62			

MODEL NUMBER	COEFFICIENT MATRIX	CORRELATION LIMITS	95% CONFIDENCE LIMITS	VALUE	σ	RMS	RRMS	RSS
	B_1 = .0727	1.00	-.014 → .16	1.8	.0416			
5	B_2 = .529	.905 1.00	.19 → .87	3.2	.165	.000234	.0153	.00491
	B_3 = 34.5	.980 .940 1.00	18. → 51.	4.3	8.09			
	B_1 = 38.1	1.00	-2700· → 2800.	0.0	1330.			
	B_2 = 222.	1.00 1.00	-16000·→ 16000.	0.0	7720.			
6	B_3 = 7.34	1.00 1.00 1.00 1.00	-531· → 546.	0.0	257.	.000248	.0158	.00472
	B_4 = .724	1.00 1.00 1.00 1.00	-770000→ 780000.	0.0	371000.			
	B_5 = 1.50	-.123 -.125 -.121 -.103 1.00	1.2 → 1.8	9.9	.151			
	B_1 = 19.5	1.00	-1100. → 1100.	0.0	525.			
	B_2 = 18.3	1.00 1.00	-1000. → 1000.	0.0	490.			
7	B_3 = .552	1.00 1.00 1.00	-30. → 32.	0.0	14.9	.000858	.0293	.0172
	B_4 = 1008.	1.00 1.00 1.00 1.00	-110000→ 110000.	0.0	53000.			
	B_1 = .0325	1.00	.082 → .57	2.8	.117			
	B_2 = .00507	.0374 1.00	-.0043 → .14	1.1	.0047			
8	B_3 = .184	.600 .628 1.00	.061 → .31	3.1	.0590	.000763	.0276	.0153

Reproduced with permission of the copyright owner. Further reproduction prohibited without permission.

MODEL NUMBER	COEFFICIENT VALUES	CORRELATION MATRIX	95% CONFIDENCE LIMITS	t-VALUE	σ	RMS	RRMS	RSS
	$B_4 = 2.16\times10^{-12}$	-.459 .862 .288 1.00	-.61 → .61	0.0	.290			
9	B_1 = .254	1.00	.15 → .36	5.3	.0483	.000347	.0186	.00764
	B_2 = 19.8	.617 1.00	.17 → 22.	17.6	1.12			
10	B_1 = .0971	1.00	.063 → .13	5.8	.0167	.000378	.0194	.00830
	B_2 = 19.4	.606 1.00	17. → 21.	17.0	1.14			
11	$B_1 = 3.93\times10^{-13}$	1.00	-.041 → .041	0.0	.0196	.00158	.0397	.0347
	B_2 = 12.0	.806 1.00	7.7 → 16.	5.8	2.08			
12	$B_1 = 2.37\times10^{-14}$	1.00	-.048 → .048	0.0	.0230	.00278	.0527	.0611
	B_2 = 6.81	.806 1.00	1.1 → 13.	2.5	2.76			

Reproduced with permission of the copyright owner. Further reproduction prohibited without permission.

Reproduced with permission of the copyright owner. Further reproduction prohibited without permission.

TABLE 10

MODEL NUMBER	COEFFICIENT VALUES	CORRELATION MATRIX	95% CONFIDENCE LIMITS	t-VALUE	σ	RMS	RRMS	RSS
	B_1 = .0666	1.00	-.16 → .30	.6	.111			
	B_2 = .0380	.999 1.00	-.096 → .17	.6	.0640			
1						.00172	.0415	.0344
	B_3 = 5.46	-.997 -.996 1.00	- 7.6 → 19.	.9	6.26			
	B_4 = 2.00	.944 .951 -.921 1.00	-.17 → 4.2	1.9	1.04			
	B_1 = 2.02	1.00	-2.6 → 6.7	.9	2.23			
	B_2 = .875	.997 1.00	-1.2 → 2.9	.9	.992			
2						.000505	.0225	.0101
	B_3 = .0792	.988 .978 1.00	-.12 → .28	.8	.0947			
	B_4 = 133.	.998 .993 .996 1.00	-470. → 736.	.5	289.			
	B_1 = .752	1.00	-.043 → 1.55	2.0	.382			
3	B_2 = .440	.988 1.00	-.067 → .95	1.8	.244	.00187	.0432	.0393
	B_3 = 9.49	.992 .998 1.00	-7.5 → 27.	1.2	8.18			
	B_1 = .181	1.00	.14 → .22	9.7	.0186			
4	B_2 = .0732	.897 1.00	.051 → .096	6.8	.0107	.000313	.0177	.00658

Reproduced with permission of the copyright owner. Further reproduction prohibited without permission.

MODEL NUMBER	COEFFICIENT VALUES	CORRELATION MATRIX	95% CONFIDENCE LIMITS	t-VALUE	σ	RMS	RRMS	RSS
	B_3 = 132.	.935 .982 1.00	101. → 163.	8.8	15.0			
	B_1 = 2.68	1.00	-3.5 → 8.8	.9	2.96			
5	B_2 = 1.08	.998 1.00	-1.6 → 3.7	.9	1.27	.000497	.0223	.0104
	B_3 = 506.	.999 1.00 1.00	-599. → 1600.	1.0	532.			
	B_1 = .0464	1.00	-.035 → .13	1.2	.0390			
	B_2 = .0197	.996 1.00	-.016 → .055	1.2	.0169			
6	B_3 = .00151	.984 .973 1.00	-.0013 → .0043	1.1	.00133	.000319	.0179	.00606
	B_4 = 2.49	.957 .957 .964 1.00	-.90 → 4.1	3.3	.762			
	B_5 = 5.87	-.997 -.991 -.990 -.946 1.00	-1.2 → 13.	1.7	3.39			
	B_1 = 20.0	1.00	-1200. → 1200.	0.0	581.			
	B_2 = 32.0	1.00 1.00	-1900. → 2000.	0.0	939.			
7	B_3 = .322	.999 .999 1.00	-19. → 20.	0.0	9.42	.00601	.0775	.120
	B_4 = 4203.	.999 1.00 1.00 1.00	-500000. → 510000.	0.0	240000.			

MODEL NUMBER	COEFFICIENT VALUES	CORRELATION MATRIX	95% CONFIDENCE LIMITS	t-VALUE	σ	RMS	RRMS	RSS
8	B_1 = 2.60	1.00	-.47 → 5.7	1.8	1.47	.00246	.0496	.0493
	B_2 = .340	.952 1.00	-.0088 → .69	2.0	.167			
	B_3 = .177	.854 .940 1.00	-.16 → .52	1.1	.163			
	B_4 = 3.58×10^{-13}	.566 .746 .910 1.00	-.64 → .64	0.0	.308			
9	B_1 = .00783	1.00	-.042 → .57	.3	.0239	.00996	.0998	.219
	B_2 = 32.7	.837 1.00	20. → 45.	5.5	5.97			
10	B_1 = .00412	1.00	-.019 → .027	.4	.0112	.00995	.0997	.219
	B_2 = 32.8	.828 1.00	21. → 45.	5.6	5.84			
11	B_1 = .165	1.00	.065 → .27	3.4	.0484	.00385	.0621	.0848
	B_2 = 45.9	.655 1.00	34. → 53.	13.0	3.54			
12	B_1 = .0682	1.00	.0330 → .103	4.0	.0169	.00374	.0611	.0822
	B_2 = 45.6	.630 1.00	39. → 53.	13.6	3.37			

Reproduced with permission of the copyright owner. Further reproduction prohibited without permission.

Reproduced with permission of the copyright owner. Further reproduction prohibited without permission.

TABLE 11

MODEL NUMBER	COEFFICIENT VALUES	CORRELATION MATRIX	95% CONFIDENCE LIMITS	t-VALUE	σ	RMS	RRMS	RRS
	B_1 = 2.45	1.00	-34. → 39.	.1	18.0			
	B_2 = 1.63	1.00 1.00	-23. → 26.	.1	12.1			
1	B_3 = 1.78	-.971 -.970 1.00	.34 → 3.2	2.5	.711	.00236	.0486	.101
	B_4 = 18.5	.999 .999 -.958 1.00	-366. → 403.	.1	19.0			
	B_5 = 47.8	.999 .999 -.958 1.00 1.00	-947. → 1000.	.1	49.3			
	B_1 = 2.74	1.00	-14. → 19.	.3	8.22			
	B_2 = 1.43	.999 1.00	-7.3 → 10.	.3	4.32			
2	B_3 = .126	.995 .991 1.00	-.67 → .93	.3	.397	.00161	.0401	.0691
	B_4 = 120	.999 .997 .998 1.00	-13000.→ 15000.	.2	706.			
	B_5 = 312	.999 .997 .998 1.00 1.00	-3400.→ 4000.	.2	1840.			
	B_1 = .703	1.00	-.095 → 1.5	1.8	.396			
	B_2 = .463	.989 1.00	-.10 → 1.0	1.7	.279			
3	B_3 = 3.75	.988 .987 1.00	-3.5 → 11.	1.0	3.59	.00228	.0477	.100
	B_4 = 9.75	.993 .998 .988 1.00	-8.9 → 28.	1.1	9.24			

MODEL NUMBER	COEFFICIENT VALUES	CORRELATION MATRIX	CONFIDENCE LIMITS	t-VALUE	σ	RMS	RRMS	RSS
4	B_1 = .155	1.00	.083 → .23	4.4	.0355	.00153	.0391	.0673
	B_2 = .0744	.901 1.00	.028 → .12	3.2	.0230			
	B_3 = 48.3	.891 .881 1.00	22. → 74.	3.8	12.9			
	B_4 = 127.	.940 .981 .892 1.00	65. → 188.	4.1	30.7			
5	B_1 = 18.7	1.00	-441. → 478.	.1	228.	.00153	.0391	.0674
	B_2 = 9.37	1.00 1.00	-223. → 242.	.1	115.			
	B_3 = 1475.	1.00 1.00 1.00	-34000. → 37000.	.1	17800.			
	B_4 = 3802.	1.00 1.00 1.00 1.00	89000. → 96000.	.1	45800			
6	B_1 = .594	1.00	-4.7 → 5.9	.2	2.61	.00164	.0404	.0687
	B_2 = .307	.999 1.00	-2.4 → 3.1	.2	1.36			
	B_3 = .0259	.997 .996 1.00	- .21 → .26	.2	.118			
	B_4 = 9.44	.997 .996 .998 1.00	-107. → 126.	.2	57.8			
	B_5 = 24.6	.997 .997 .998 .999 1.00	-280. → 329.	.2	151.			
	B_6 = 2.17	-.988 -.987 -.984 -.975 -.976 1.00 -.15	→ 4.5	1.9	1.15			

Reproduced with permission of the copyright owner. Further reproduction prohibited without permission.

MODEL NUMBER	COEFFICIENT VALUES	CORRELATION MATRIX	95% CONFIDENCE LIMITS	t-VALUE	σ	RMS	RRMS	RSS
	$B_1 = 5.66\times10^{12}$	1.00	$-3.9\times10^{14} \rightarrow 4.03\times10^{14}$	0.0	1.97×10^{14}			
	$B_2 = 2.17\times10^{12}$	1.00 1.00	$-1.5\times10^{14} \rightarrow 1.6\times10^{14}$	0.0	7.56×10^{13}			
7	$B_3 = 8.20\times10^{10}$	1.00 1.00 1.00	$-5.7\times10^{12} \rightarrow 5.8\times10^{12}$	0.0	2.84×10^{12}	.00376	.0613	.162
	$B_4 = 4.25\times10^{12}$	1.00 1.00 1.00 1.00	$-2.9\times10^{14} \rightarrow 3.0\times10^{14}$	0.0	1.47×10^{14}			
	$B_5 = 1.06\times10^{13}$	1.00 1.00 1.00 1.00 1.00	$-7.3\times10^{14} \rightarrow 7.5\times10^{14}$	0.0	3.66×10^{14}			
	$B_1 = .163$	1.00	.086 → .24	4.2	.0386			
	$B_2 = .0816$	.882 1.00	.028 → .13	3.1	.0258			
8	$B_3 = 3.93\times10^{-14}$	.023 -.213 1.00	-.0031 → .0031	0.0	.00154	.00157	.0396	.0674
	$B_4 = 51.3$	.800 .661 .478 1.00	18. → 84.	3.1	16.3			
	$B_5 = 134.$	.824 .717 .510 .924 1.00	54. → 215.	3.4	40.1			
	$B_1 = .0158$	1.00	-.024 → .056	.8	.0200			
9	$B_2 = 12.9$	.340 1.00	7.6 → 18.	4.9	2.61	.00553	.0744	.249
	$B_3 = 34.3$	.839 .285 1.00	24. → 44.	7.3	4.69			

Reproduced with permission of the copyright owner. Further reproduction prohibited without permission.

MODEL NUMBER	COEFFICIENT VALUES	CORRELATION MATRIX	95% CONFIDENCE LIMITS	t-VALUE	σ	RMS	RRMS	RSS
	B_1 = .00779	1.00	-.01 → .026	.9	.00882			
10	B_2 = 12.8	.319 1.00	7.7 → 18.	5.0	2.59	.00552	.0743	.249
	B_3 = 34.4	.823 .263 1.00	25. → 43.	7.6	4.50			
	B_1 = .133	1.00	.058 → .21	3.6	.0373			
11	B_2 = 18.2	.495 1.00	11. → 25.	5.3	3.42	.00325	.0570	.146
	B_3 = 44.2	.655 .324 1.00	38. → 51.	14.1	3.14			
	B_1 = .0539	1.00	.027 → .081	4.1	.0133			
12	B_2 = 17.7	.465 1.00	11. → 24.	5.3	3.31	.00327	.0572	.147
	B_3 = 43.6	.629 .293 1.00	38. → 50.	14.5	3.01			

Reproduced with permission of the copyright owner. Further reproduction prohibited without permission.

B_3 - B_2 correlations were only .736 and .831, respectively, indicating relative independence among these parameters. Also note that zero is not included in the 95% confidence limits of any of the coefficients of Model 4. In addition, the t-values of the coefficients were ≥ 2.2, indicating a $\geq .961$ probability of rejecting the null hypothesis i.e., the hypothesis that the coefficients are different from zero. Model 4 was thus considered to be the best representation of the data for k_{c_5}.

For the individual k_{c_6} models, shown in Table 10, it can be seen that Models 4, 6, 11, and 12 have RMS and RRMS values which were significantly lower than those for the remaining models. In discriminating among these four models, it was noted that the t-values for Model 6 were ≤ 1.7 with the exception of B_4, that zero was in the 95% confidence limits of each coefficient, and that all five parameters were highly correlated. Model 6 was thus rejected.

Models 11 and 12 both have RMS and RRMS values which were 19 and 23% respectively, higher than for Model 4, indicating a poorer fit of the data.

In addition, the t-values for B_1, corresponding to the C_5 adsorption parameter for Models 4, 11, and 12 were higher for Model 4 (9.7) than for Models 11 (3.4) or 12 (4.0). It should be noted, however, that the t-values for the numerator, proportional to $(k_o)_{c_6}$, were higher in Models 11 (13.0) and 12 (13.6) than for Model 4 (8.8). On the basis of the lower error values for Model 4, although the remaining bases of comparison are equivalent on balance, Model 4 was judged to be the representation of the k_{c_6} rate constant.

Reproduced with permission of the copyright owner. Further reproduction prohibited without permission.

The coupled model results are shown in Table 11. On the basis of RMS and RRMS, models 2, 4, 5, 6, and 8 were superior to the remaining models. Further discrimination can be made by examining the t-values of these models. Models 2, 5, and 6 each had both low t-values for the parameters and a very high degree of correlation among all the parameters. These models are thus rejected. Model 8 shows that B_3, corresponding to the n-C_6 adsorption parameter, approached zero, and thus had a low t-value. Since earlier qualitative results indicate the approximate equivalence of K_{c_5} and K_{c_6}, Model 8 was rejected as unrealistic.

Thus, Model 4 was the most accurate representation of the coupled data, as it is for the individual models. The 95% confidence limits for this model did not include zero for any of the four coefficients. Although B_2 and B_4 were correlated at the .981 level, the remaining correlations were satisfactory. The t-values for the parameters were all $\geq$ 3.2, indicating a $\geq$ .997 probability of rejecting the null hypothesis. Thus, not only was Model 4 the best of the models, it was also an acceptable fit of the data.

Comparison of the individual and coupled models showed the following for Model 4:

	From k_{c_5} Data	From k_{c_6} Data	From Coupled Data
B_1	.0273	.181	.155
B_2	.143	.0732	.0744
B_3	28.7	132.	48.3
B_4	____	____	127.

Reproduced with permission of the copyright owner. Further reproduction prohibited without permission.

B_4 for the coupled model corresponds to B_3 for the k_{c_6} data while B_3 for the coupled model corresponds to B_3 for the k_{c_5} data. Note that the values of B_1 and B_2 from the coupled model lie between those of the k_{c_5} and k_{c_6} data as expected. However, these values were much closer to the k_{c_6} model values than to the k_{c_5} values. Since the relative values of B_1 and B_2 , corresponding to K_{c_5} and K_{c_6} respectively, were reversed in the two individual models, the fact that the coupled data showed that $B_1 > B_2$, as do the k_{c_6} data, indicated that the data were best represented by $B_1 > B_2$. The difference in B_1 and B_2, namely $B_1 = 2.1\ B_2$, was not as great as on the mordenite catalyst. There, $B_1 \not\gg B_2$ and B_2 could be deleted from the model.

It may thus be concluded that the faujasite data may be modelled by assuming a dual site mechanism, $K_{H_2} << K_{HC}$, K_{c_5} of the same order as K_{c_6}, and surface reaction rate controlling. Further, the data indicate that B_1, corresponding to K_{c_5}, was approximately twice the value of B_2, corresponding to K_{c_6}.

Reproduced with permission of the copyright owner. Further reproduction prohibited without permission.

Comparison of the Mordenite and Faujasite Catalysts

Having modelled the results on both the mordenite and faujasite catalysts, a comparison was made of the reaction and adsorption phenomena as indicated by both the models and the additional analysis discussed earlier.

First, the results showed that at 465°F, 6.4 w/hr/w and at pressures of 100, 200, and 300 psig, Pd-H-mordenite was a more active catalyst for hydroisomerization of n-C_5, n-C_6, and mixtures of the two. Table 12 shows a comparison of the results on each catalyst. For the pure component runs on both n-C_5 and n-C_6, there were no distinct trends of the mordenite and faujasite rate constants with pressure or H_2/HC ratio. However, for 3 out of 5 n-C_5 runs and 3 of 5 n-C_6 runs, the mordenite catalyst was more active.

For the mixture runs, Table 12 showed that the mordenite catalyst was more active over the entire range of conditions of total pressure and H_2/HC used in this study. However, it can be seen that there was no general trend of the rate constants on the mordenite versus the faujasite with total pressure or H_2/HC ratio. It may thus be concluded that the Pd-H-mordenite catalyst used in this study was more active for hydroismerization of n-C_5, n-C_6, and mixtures of the two than was the Pd-H-faujasite.

Comparison of the statistical models which describe the reactions on each catalyst showed that the mordenite exhibits preferential adsorption of n-C_6 such that the adsorption parameter of n-C_5 can be neglected. On the faujasite catalyst, both n-C_5 and n-C_6 adsorption parameters must be included in the model. The models for the hydroisomerization reactions on each catalyst are shown below for convenience.

Reproduced with permission of the copyright owner. Further reproduction prohibited without permission.

TABLE 12

Comparison of the Results of Pd-H-Mordenite and Pd-H Faujasite Hydroisomerization at 465°F

Total Pressure, psig	C_5/C_6 Volume Ratio	H_2/HC	Mordenite k_{c_5}	Mordenite k_{c_6}	Faujasite k_{c_5}	Faujasite k_{c_6}
100	Pure C_5	10/1	.241	-	.187	-
200	Pure C_5	10/1	.061	-	.091	-
192	Pure C_5	17.8/1	.073	-	.079	-
300	Pure C_5	10/1	.071	-	.046	-
291	Pure C_5	14.7/1	.058	-	.053	-
100	Pure C_6	10/1	-	.337	-	.431
200	Pure C_6	10/1	-	.143	-	.125
192	Pure C_6	17.8/1	-	.127	-	.246
300	Pure C_6	10/1	-	.100	-	.047
291	Pure C_6	14.7/1	-	.133	-	.083
100	15/85	10/1	.101	.374	.042	.293
	50/50	10/1	.137	.519	.095	.208
	75/25	10/1	.143	.507	.081	.183
200	15/85	10/1	.046	.171	.020	.078
	50/50	10/1	.048	.179	.021	.043
	75/25	10/1	-	-	.024	.038
192	15/85	17.8/1	.045	.125	.042	.156
	50/50	17.8/1	.050	.152	.045	.118
	75/25	17.8/1	.058	.144	.055	.080
300	15/85	10/1	.029	.115	.026	.029
	50/50	10/1	.032	.125	.024	.017
	75/25	10/1	.038	.162	.030	.018
292	15/85	14.8/1	.030	.150	.025	.053
	50/50	14.8/1	.033	.165	.027	.031
	75/25	14.8/1	.043	.205	.024	.032

Reproduced with permission of the copyright owner. Further reproduction prohibited without permission.

Model Number	Mordenite	Model Number	Faujasite

Individual Models

$$10 \quad k_{c_5} = \frac{19.5}{(1+.0427\ P_{c_6})^2} \qquad 4 \quad k_{c_5} = \frac{28.7}{(1+.0273\ P_{c_5}+.143\ P_{c_6})^2}$$

$$10 \quad k_{c_6} = \frac{53.1}{(1+.0180\ P_{c_6})^2} \qquad 4 \quad k_{c_6} = \frac{132.}{(1+.181\ P_{c_5}+.0732\ P_{c_6})^2}$$

Coupled Models

$$10 \quad k_{c_5} = \frac{17.1}{(1+.0205\ P_{c_6})^2} \qquad 4 \quad k_{c_5} = \frac{48.3}{(1+.155\ P_{c_5}+.0744\ P_{c_6})^2}$$

$$10 \quad k_{c_6} = \frac{54.8}{(1+.0205\ P_{c_6})^2} \qquad 4 \quad k_{c_6} = \frac{127.}{(1+.155\ P_{c_5}+.0744\ P_{c_6})^2}$$

On the mordenite catalyst, both qualitative considerations and the statistical analysis, as shown and discussed earlier, indicated that $K_{c_6} >> K_{c_5}$. On the faujasite, both K_{c_5} and K_{c_6} must be included in the model. This may account for the anomalous effects observed on both catalysts. On the mordenite, the increase in k_{c_6} on dilution of n-C_6 with n-C_5 may be explained by the preferential adsorption of n-C_6, i.e., the predominance of n-C_6 in competing for active sites. This hypothesis was strengthened by the statistical analysis which showed that the model corresponding to the predominance of n-C_6 adsorption was the most accurate. Interestingly, the faujasite data required that both adsorption parameters be included,which indicated both n-C_5 and n-C_6 adsorption were

Reproduced with permission of the copyright owner. Further reproduction prohibited without permission.

important with neither species predominating. This competition for active sites may cause the observed decrease in the rate constant for both adsorbing species on dilution. It has been shown that this observed decrease occurred at each pressure and H_2/HC ratio examined in this study.

On both catalysts, the individual results indicate that the numerator, which was proportional to the surface reaction rate constant, was greater for n-C_6 than for n-C_5 isomerization. Comparison of the coupled models indicated that while the true surface reaction rate constants for both n-C_5 and n-C_6, proportional to the numerators of the models, were greater on the faujasite than the mordenite, the larger adsorption terms, i.e. the denominators, caused the simplified rate constants on the faujasite to be lower at a given set of conditions.

Thus, the differences in the performance of the two catalysts may be explained by qualitative considerations and statistically determined models. The results of these two methods of analysis were consistent and complementary.

Reproduced with permission of the copyright owner. Further reproduction prohibited without permission.

Conclusions

Based on the results of the analysis discussed in this study, the following conclusions may be made.

1. The data obtained in the hydroisomerization of n-C_5 and n-C_6 mixtures and pure components on both the Pd-H-mordenite and Pd-H-faujasite used in this study are consistent with a model derived assuming a dual site mechanism, with isomerization rate-controlling, and hydrocarbon adsorption parameters much greater than hydrogen adsorption parameters.
2. Further, the results indicate that on the mordenite, the hexane adsorption parameter is much greater than that of pentane, while on the faujasite the hexane adsorption parameter is of the same order as that of pentane.
3. The Pd-H-mordenite catalyst is more active for hydroisomerization of n-C_5 and n-C_6 mixtures than the Pd-H-faujasite catalyst over the entire range of pressures and H_2/HC ratios used in this study.
4. Both catalysts exhibit anomalous effects in hydroisomerization of n-C_5 and n-C_6 mixtures. On the mordenite catalyst, the simplified hexane isomerization rate constant increases while that of pentane decreases on dilution. On the faujasite, both rate constants decrease. On the mordenite, the anomaly is attributed to the preferential adsorption of n-C_6. On the faujasite, competition between the adsorbents appears to result in a decrease in both the hexane and pentane rate constants on dilution.

Reproduced with permission of the copyright owner. Further reproduction prohibited without permission.

Recommendations

The following recommendations for further work may be made based on the results of this study.

1. Investigate the adsorption of the n-C_5 and n-C_6 on both Pd-H-mordenite and Pd-H-faujasite on zeolites with varying pore geometry to relate adsorption more generally to structure. Since adsorption appears to affect the rate constants on both catalysts used in this study a more detailed examination of the effects of structural parameters and reaction conditions on the adsorption mechanism would be illustrative. Part of such a study could be the relationship between the equilibrium adsorption constants and values obtained in a kinetic study.
2. Study the effect of aromatics on hydroisomerization of n-paraffins on mordenite and faujasite catalysts. Since typical feedstocks for isomerization in a refinery would contain aromatics, the effect of various concentrations of aromatics on adsorption and reaction at low molecular weight n-paraffins is appropriate.
3. Further examine the effect of structural parameters such as pore geometry and configuration, parameters, and surface activity especially as related to the acidity of the zeolite on the reaction of n-C_5 and n-C_6. The negative interaction seen in this study may be related to effects of catalyst preparation on the strength and distribution of active sites, both metallic and acidic.

Reproduced with permission of the copyright owner. Further reproduction prohibited without permission.

4. Examine the reactions of n-C_5 and n-C_6 using isomers of these paraffins as feeds. Since the data were consistent with isomerization being rate controlling on both the mordenite and faujasite, interaction between isomers of the two feeds may be important in explaining the observed synergism. Such interaction as well as a more detailed mechanism of reaction, may be described more fully by such a study, with conversions of each isomer held to differential levels in order to understand the mechanism of isomerization.

Reproduced with permission of the copyright owner. Further reproduction prohibited without permission.

References

1. Kouwenhoven, H. W., and Langhout, W. C., "Shell's Hydro-Isomerization Process", Chem. Eng. Progress, 67, 4, April 1971, p. 65-70.

2. Chick, D. J., Katzer, J. R., and Gates, B. C., "Deactivation of Pd-H-Mordenite Catalyst during n-C_6 Isomerization", ACS Symposium Series, 1977, p. 515-527.

3. Minachev, K. M., Garanin, V. I., Kharlamov, V. V., and Isakova, T. A., Kinetika i Kataliz, 13, 5, Sept. 1972, p. 991-1000.

4. Bolton, A. P., and Larewala, M. A., "A Mechanism for the Isomerization of Hexanes Using Zeolite Catalysts", J. Catalysis, 18, 1970, p. 1-11.

5. Belden, D. H., Haensel, V., Starnes, W. G., and Zabor, R. C., "Upgrading C_5 and C_6 Paraffins by the Penex Process for Hydroisomerization", O.I and Gas J., 55, 40, May 20, 1957, p. 142-6.

6. Breck, D. W., Zeolite Molecular Sieves, John Wiley & Sons, New York, 1974.

7. Smith, V. J., "Faujasite-Type Structures: The Aluminosilicate Framework: Positions of Cations and Molecules: Nomenclature", Advances in Chemistry Series, 101, 1971, p. 171.

8. Saito, M., and Iwasaki, T., "Isomerization of Pentanes on Platinum/Rare Earth Hydrogen Zeolite Y Catalysts", Bulletin of the Japanese Petroleum Inst., 18, 2, Nov. 1976, p. 117-126.

9. Minachev, K. M., Garanin, V. I., Kharmolov, V. V., Piguzova, L. I., and Vitukima, A. S., "Effect of Treatment Conditions of Pd-Zeolite Catalysts on Activity and Selectivity in Isomerization of Hexane", Petroleum Chemistry USSR, 9, 6, 1969, p. 227-231.

10. Yashima, T., Iwase, O., and Hara, N., Chem. Lett., 1975, p. 1215.

11. Namba, S., Iwase, O., Takahashi, N., Yashima, T., and Hara, N., J. Catalysis 56, 1979, p. 445.

12. Namba, S., and Yashima, T., Chem. Lett., 1978, p. 1261.

13. Maile, J. N., and Weisz, P. B., U. S. Patent 3,280,212 assigned to Mobil Oil Corp., Aug. 18, 1964.

14. Gray, J. A., and Cobb, J. T., J. Catalysis, 36, 1975, p. 126.

Reproduced with permission of the copyright owner. Further reproduction prohibited without permission.

15. Braun, G., Fetting, F., and Schoeneberger, H., "Isomerization of n-Hexane and n-Pentane Over Various Bifunctional Zeolite Catalysts", ACS Symposium Series, 40, 1977, p. 504-14.

16. Choudary, N., and Saraf, D. N., I & EC Prod. Res. Div., 14, 2, 1975, p. 75.

17. Ward, J. W., Hydrocarbon Proc., Sept. 1975, p. 102.

18. Topchieva, K. V., and Dorogochinshaya, V. A., "Isomerization of n-Hexane on Platinized Type Y Zeolite Binder-Free Bead Catalysts", Khimiya i Tekhrologiya Topliv i Mosel, 11 Nov. 1973, p. 6-8.

19. Yeginzarov, Y. G., "Isomerization of n-Pentane on a Catalyst Containing Zeolite", Pet. Chem. USSR,15, 6, 1975, p. 804-7.

20. Garanin, V. I., Minachev, K. M., and Isakova, T. A., "Isomerization of n-C_5 on Y Zeolite Containing Palladium", Pet. Chem. USSR, 12, 4, 1972, p. 129-134.

21. Barron, Y., Maire, G., Muller, J. M., and Gault, F. G., J. Catalysis, 7, 1967, p. 315.

22. Anderson, J. R., and Avery, N. R., J. Catalysis, 9, 1967, p. 95.

23. Weeks, T. J., and Bolton, A. P., "Hydroisomerization and Hydrocracking of n-Pentane (3-C^{13}) with Type Y Zeolite", J. Chem. Soc., Faraday Trans. 1, 73, 11, 1977, p. 1681-5.

24. Bolton, A. P., Ladd, I. R., and Weeks, T. J., Proc. 6th Int. Contress on Catalysis (London), paper A22.

25. Minachev, K. M., Garanin, V. R., Kharlamov T. A., Isakova, T. A. and Sanderov, E. E., Izv. Akad. Nauk SSR, Ser. Khim., 1969, p. 1737.

26. Mills, G. A., Heinemonn, H., Millekin, T. H., and Obbad, A. G., Ind. Eng. Chem., 45, 1953, p. 134.

27. Kurchi, V. M., Garanin, V. I., and Minachev. K. M., Kinetika i Kataliz, 9, 1968, p. 571.

28. Kouwenhoven, H. W., and Van Helden, H. J. A., British Patent 1,189,850, April 29, 1970.

29. Kouwenhoven, H. W., and Van Zijill Longhout, W. C., "Shell Hydroisomerization Process for C_5/C_6 Fractions", 68th AICHE National Meeting, Houston, 1971.

30. Kouwenhoven, H. W., and Van Zijill Langhout, W. C., Chem. Eng. Prog., 67, 4, 1971, p. 65.

31. Kouwenhoven, H. W., and Van Zijill Langhout, W. C., Petrol. and

Reproduced with permission of the copyright owner. Further reproduction prohibited without permission.

Petrochem. Inter., 11, 11, 1971, p. 64.

32. Kouwenhoven, H. W., Advances Chem. Ser., 121, 1973, p. 529.

33. Bryant, P. A., Ph.D. Dissertation, Louisiana State University, 1966.

34. Benesi, H. A., U. S. Patent 3,527,835, Sept. 8, 1970.

35. Voorhies, A., and Bryant, P. A., AICHE J., 14, 1968, p. 852.

36. Beecher, R., Voorhies, A., and Eberly, P. E., Ind. Eng. Chem., Prod. Res. Div., 7, 1968, p. 203.

37. Kranich, W. L., Ma, Y. H., Sand, L. B., Weiss, A. H., and Zweibel, I., International Conference on Molecular Sieve Zeolites, Worcester, Mass., 1970.

38. Eberly, P. E., Kimberlin, C. N., and Voorhies, A., "Effect of S_iO_2/Al_2O_3 Ratio on Physicochemical Properties of Mordenite for n- Pentane Isomerization", J. Catalysis, 22, 3, 1971, p. 419-26.

39. Lopez, G., Perot, G., Gueguen, C., and Guisnet, M., "Isomerization and Cracking of Saturated Hydrocarbons on H-Mordenite and Pt-H-Mordenite Catalysts", Acta. Phys. Chem., 24, 1-2, 1978, p. 207-13.

40. Gray, J. A., and Cobb, J. T., "Hydroisomerization and Hydrocracking of n- Pentane Over Various Mordenite Catalysts", J. Catalysis, 36, 1975, p. 125-141.

41. Yashima, T., and Hara, N., J. Catalysis, 27, 1972, p. 329.

42. Bryant, D. E., and Krovich, W. L., J. Catlysis, 8, 1967, p. 8.

43. Minachev, K. M., Garanin, V. I., Isakova, I., Kharlamov, V., and Bogomolov, V., Adv. Chem. Ser., 102, 1971, p. 441.

44. Beecher, R. G., and Voorhies, A., Ind. Eng. Chem., Prod. Res. Div., 8, 1969, p. 366.

45. Lanewala, M. A., Pichert, P. E., and Bolton, P. A., J. Catalysis, 9, 1967, p. 95.

46. Boudart, M., Adv. Cat. Rel. Subj., 20, 1969, p. 153.

47. Hougen, O. A., and Watson, K. M., Chemical Process Principles, Part III, Kinetics and Catalysis, John Wiley and Sons, New York, 1947.

48. Petersen, E. E., Chemical Reaction Analysis, Prentice-Hall, Inc., Englewood Cliffs, N. J., 1965.

49. Weisz, P. B., "Zeolites New Horizons in Catalysis", Chem. Tech., Aug., 1973., p. 498-505.

Reproduced with permission of the copyright owner. Further reproduction prohibited without permission.

50. Spry, J. C., and Sawyer, W. H., "Configurational Diffusion Effects in Catalytic Demetallization of Petroleum Feedstocks", paper presented at the 68th Annual AICHE Meeting, Los Angeles, Nov., 1975.

51. Bosanquet, C. H., British TA Report BR-507, Sept. 27, 1944.

52. Wilke, C. R., and Lee, C. Y., "Estimation of Diffusion Coefficients for Gases and Vapors", Ind. Eng. Chem., 47, 1955, p. 1253.

53. Hopper, J. R., "A Study of the Catalytic Hydroisomerization Reactions of n-C_6 and Cyclohexane over Structurally Modified Mordenites", Ph.D. Dissertation, Dept. of Chemical Engineering, Louisiana State University, 1969.

54. Levenspiel, O., and Bischoff, K. B., "Patterns of Flow in Chemical Process Vessels", Advances in Chemical Engineering, Vol. 4, 1963, Vol. 4, 1963, p. 95-198.

55. Luzarraga, M. G., "Hydroisomerization and Hydrocracking of Cyclohexane Over a Faujasite Catalyst", Ph.D. Dissertation, Dept. of Chemical Engineering, Louisiana State University, 1971.

56. Hatcher, W. J., "Hydroisomerization of n-C_6 and Cyclohexane over a Zeolite Catalyst", Ph.D. Dissertation, Dept. of Chemical Engineering, Louisiana State University, 1968.

57. Perry, J. E., ed., Chemical Engineer's Handbook, McGraw-Hill Book Co., Inc., New York, 1974.

58. Prausnitz, J. M., Molecular Thermodynamics of Fluid Phase Equilibria, Prentice-Hall, Englewood Cliffs, N.J., 1969.

59. Habibe, O. D., "Hydroisomerization of n-C_6 and Cyclohexane Over Zeolite Catalysts", M.S. Thesis, Dept. of Chemical Engineering, Louisiana State University, 1973.

60. Strickland, R. W., "Hydroisomerization of n-C_5 and Cyclohexane Mixtures Over Faujasite Catalysts", M.S. Thesis, Dept. of Chemical Engineering, Louisiana State University, 1974.

61. Levenspiel, O., Chemical Reaction Engineering, 2nd ed., John Wiley and Sons, New York, 1972.

62. Daniel, C., and Wood, F. S., Fitting Equations to Data, Wiley-Interscience, New York, 1971.

63. Voorhies, A., and Hopper, J. R., "Hydroisomerization of Cyclohexane and n- Pentane Over a Series of Catalysts with Varying Silica-Alumina Ratios", Ind. Eng. Chem., Prod. Res. Div., 11, 3, 1972, p. 294-8.

Reproduced with permission of the copyright owner. Further reproduction prohibited without permission.

64. Reid, R.C., and Sherwood, T.K., The Properties of Gases and Liquids, McGraw-Hill Book Co., Inc. New York, 1958.

65. Livesay, H.S.,"Hydroisomerization of n-C_5, Cyclohexane, and Benzene Mixtures Over a Modified Pd-H-Mordenite Zeolite Catalyst", Masters Thesis, Dept. of Chemical Engineering, Louisiana State University, 1978.

66. Weller, S.W., and Bauer, J.M., "Studies of the Catalytic and Chemical Properties of Acid-Extracted Mordenite", Preprint 62, Annual AICHE Meeting, Washington, D.C., 1969.

Reproduced with permission of the copyright owner. Further reproduction prohibited without permission.

APPENDIX 1

SAMPLE CALCULATIONS

A. Experimental Conditions

Run Number	MI-37
Catalyst volume, cc	4.26
Catalyst weight, gm	2.0012
Barometric pressure, in. Hg	30.08
Room temperature, °F	74
Reactor temperature, °F	465
Reactor pressure, psig	97
H_2 flow rate data	
Average WTM reading, sec/o.05 ft^3	87.4
Average WTM temperature, °F	74.3
Normal Pentane flow rate, cc/hr	20.0
Normal Hexane flow rate, cc/hr	20.0
Average gas flow rate, sec/0.05 ft^3	82.4
Average WTM temperature, °F	74.4

B. Analytical Data (Gas Chromatograph)

Component	Hydrogen Free Mole % (from Gas Chromatograph)
Isopentane	2.09
Normal Pentane	36.69
2,2 Dimethyl Butane	0.0
2 Methyl Pentane	10.23
3 Methyl Pentane	2.79
Normal Hexane	45.70

Reproduced with permission of the copyright owner. Further reproduction prohibited without permission.

C. Calculated Process Conditions

1. Hydrocarbon feed rates

$$\text{Normal Pentane} = \frac{(20.0\ \text{cc/hr})\ (0.6262\ \text{gm/cc})}{(72.15\ \text{gm/g-mole})} = 0.1736\ \text{g-mole/hr}$$

$$\text{Normal Hexane} = \frac{(20.0\ \text{cc/hr})\ (.6601\ \text{gm/cc}}{(84.16\ \text{gm/g-mole})} = 0.1569\ \text{g-mole/hr}$$

2. Corrected barometric pressure

Temperature of barometer: (74-32.0) /1.8 = 23.3°C

$$\text{Corrected pressure} = 30.08\ [\ 1 - \frac{0.000164(23.3)}{1+0.000182(23.3)}] = 29.97\ \text{in Hg}$$

3. Hydrogen flow rate

$$\frac{(14.72\ \text{psia})\ (453.6\ \text{g-mole/lb mole})(3600\ \text{sec/hr})\ (29.97-.875)\ \text{in Hg}}{(29.92\ \text{in Hg})(10.73\ \text{psia ft}^3/\text{lb mole °R})\ (20-.05\ \text{ft}^3/\text{ft}^3)\ (87.46\ \text{sec}/.05\ \text{ft}^3)}$$

$$\frac{}{(460+74.3)°R} = 2.335\ \text{g-mole/hr}$$

4. Hydrogen/hydrocarbon molar ratio

$$2.335/(0.1736 + 0.1569) = 14.89$$

5. Feed w/hr/w and v/hr/v

$$\text{w/hr/w} = \frac{[(20.0)\ (.6262) + (20.0)\ (.6601)]\text{gm/hr}}{(2.0012\ \text{gm})} = 6.55\ \text{gm/hr/gm cat}$$

$$\text{v/hr/v} = (20.0 + 20.0)/4.26 = 9.39\ \text{cc/hr/cc cat}$$

6. Molar gas density in reactor

$$\frac{(97 + 14.7)\ \text{psia}\ (453.6\ \text{g-mole.lb mole})}{(10.73\ \text{psia ft}^3/\text{lb mole°R})\ (460+465)°R\ (28312.6\ \text{cc/ft}^3)} = 1.803\times10^{-4}\ \text{g-mole/cc}$$

7. Superficial residence time

$$\frac{(1.8038\times10^{-4}\ \text{g-mole/cc})\ (4.26\ \text{cc})\ (3600\ \text{sec/hr})}{(2.335 + .1736 + .1569)\ \text{g-mole/hr}} = 1.11\ \text{sec}$$

8. Superficial gas velocity

$$\frac{4.26\ \text{cc}}{(1.96\ \text{cm}^2)\ (1.11\ \text{sec})} = 1.96\ \text{cm/sec}$$

Reproduced with permission of the copyright owner. Further reproduction prohibited without permission.

D. Material Balance Calculations

Basis: 1 hour

1. Hydrocarbon atoms in hydrocarbon feed

$12(.1736) + 14\ (.1569) = 4.280$ gm atoms H

2. Carbon atoms in hydrocarbon feed

$5(.1736) + 6(.1569) = 1.809$ gm atoms C

3. Gm atoms C per mole of hydrocarbon product

Component	Average Mole Fraction	x Gm atoms/g mole	= Gm atoms C
IC5	.0209	5	0.1045
NC5	.3669	5	1.8345
22DMB	.0000	6	0.000
2MP	.1023	6	0.6138
3MP	.0279	6	0.1674
NC6	.4570	6	2.7420
			5.4622

4. Calculated g-moles of hydrocarbon product

1.809 gm atom C/5.4622 gm atom C/g mole = .3312 g-moles

5. Gram atoms H per g-mole of hydrocarbon product

Component	Average Mole Fraction	x Gm atoms/ g mole	= Gm atoms H
IC5	.0209	12	0.3348
NC5	.3669	12	4.4028
22DMB	.0000	14	0.0000
2MP	.1023	14	1.4322
NC6	.0279	14	.1722
	.4570	14	6.3980
			12.7400

6. Calculated H_2 in product streams

$2.335\ [4.280-.3312(12.0)] = 2.4878$ g-mole H_2

7. Calculated g-moles of product gas

$2.4878+.3312 = 2.8190$ = g-moles

8. Observed g-moles of product gas

$$\frac{(14.7)(453.6)(3600)}{(29.92)(10.73)(20)}\left[\frac{(29.97-.876)}{(82.4)(460+74.4)}\right] = 2.4701 \text{ g-moles/hr}$$

Reproduced with permission of the copyright owner. Further reproduction prohibited without permission.

E. Reaction Rate Constants

$$k = \frac{-Yi*V}{W_c t_H} \quad \ln\left(1 - \frac{Y_i}{Y_i^*}\right)$$

1. Normal pentane

$$k = \frac{-(.807)}{(.475)(1.11)} \quad \ln\left(1 - \frac{.0539}{.807}\right) = .107 \text{ cc/gm/sec}$$

2. Normal Hexane

$$k = \frac{-(.840)}{(.47)(1.11)} \quad \ln\left(1 - \frac{.2217}{.840}\right) = .492 \text{ cc/gm/sec}$$

F. GC Factors

Component	Factor
Isopentane	1.580
n-Pentane	1.495
2,2-DMButane	1.352
2-MPentane	1.308
3-MPentane	1.318
n-Hexane	1.278

Reproduced with permission of the copyright owner. Further reproduction prohibited without permission.

APPENDIX 2

List of Computer Program for

Calculation of n-C_6 and Mixture Runs

Reproduced with permission of the copyright owner. Further reproduction prohibited without permission.

```
// EXEC EYFORT3,PARM.FORT=(NOSOURCE,NOMAP),PARM.LKED=LET
//FORT.SYSPRINT DD DUMMY
      DIMENSION XIC5(7),XNC5(7),X22DMB(7),X2MP(7),X3MP(7),
     XNC6(7)
      DIMENSION RUNNO(2)
      DIMENSION CATYP(2)
      DATA STP/'    '/
  666 CONTINUE
      READ(5,999)RUNNO
      IF(RUNNO(1).EQ.STP)CALL EXIT
      READ(5,999)CATYP
  999 FORMAT(2A4)
      READ(5,998)XC5R,XC6R
  998 FORMAT(8F10.0)
      READ(5,1)XM
    1 FORMAT(8F10.0)
      N=XM
      READ(5,2)PRES,CATWT,DCAT,HFLOWI,AVGAS
    2 FORMAT(5F10.0)
      CTVOL=CATWT/DCAT
      READ(5,3)TTEMP,YC5,YC6,C5VFR,C6VFR
    3 FORMAT(5F10.0)
      READ(5,4)PBAR,TBAR,TWTMA,TWTMB
    4 FORMAT(4F10.0)
      TWTMAK=273.16+5.*(TWTMA-32.)/9.
      TARG=647.27-TWTMAK
      ARG=TARG*(3.2438+TARG*.00587+(TARG**3)*1.17E-08)/
     1(TWTMAK*(1.+TARG*.00219))
      PWTMA=218.17*(10.**(-ARG))*29.92
      TWTMBK=273.16+5.*(TWTMB-32.)/9.
      TBRG=647.27-TWTMBK
      BRG=TBRG*(3.2438+TBRG*.00587+(TBRG**3)*1.17E-08)/
     1(TWTMBK*(1.+TBRG*.00219))
      PWTMB=218.17*(10.**(-BRG))*29.92
      READ(5,6)(XIC5(I),I=1,N)
      READ(5,6)(XNC5(I),I=1,N)
      READ(5,6)(X22DMB(I),I=1,N)
      READ(5,6)(X2MP(I),I=1,N)
      READ(5,6)(X3MP(I),I=1,N)
      READ(5,6)(XNC6(I),I=1,N)
    6 FORMAT(8F10.0)
      TPRES=PRES+14.7
      GMNC5=(C5VFR*.6262)/72.15
      GMNC6=(C6VFR*.6631)/86.18
      TMOLE=GMNC5+GMNC6
      PENT=GMNC5/TMOLE
      HEX=GMNC6/TMOLE
      TEMPC=(TBAR-32.)/1.8
      PBARC=PBAR*(1.-(.000164*TEMPC)/(1.+.000182*TEMPC))
      HRATE=3732.1*(PBARC-PWTMA)/HFLOWI/(460.+TWTMA)
      H2CR=HRATE/(GMNC5+GMNC6)
      PPH2=H2CR/(H2CR+1.)*TPRES
```

Reproduced with permission of the copyright owner. Further reproduction prohibited without permission.

```
      PPC5=PENT/(H2CR+1.)*TPRES
      PPC6=HEX/(H2CR+1.)*TPRES
      WHSV=(C5VFR*.6252+C6VFR*.6601)/CATWT
      VHSV=(C5VFR+C6VFR)/CTVOL
      GDEN=TPRES*453.6/10.73/28312.6/(460.+TTEMP)
      THOLD=GDEN*CTVOL*3600./(GMNC5+GMNC6+HRATE)
      AIC5=0.
      ANC5=0.
      A22DMB=0.
      A2MP=0.
      A3MP=0.
      ANC6=0.
      DO 50 I=1,N
      AIC5=AIC5+XIC5(I)
      ANC5=ANC5+XNC5(I)
      A22DMB=A22DMB+X22DMB(I)
      A2MP=A2MP+X2MP(I)
      A3MP=A3MP+X3MP(I)
      ANC6=ANC6+XNC6(I)
   50 CONTINUE
      AIC5=AIC5/XM
      ANC5=ANC5/XM
      A22DMB=A22DMB/XM
      A2MP=A2MP/XM
      A3MP=A3MP/XM
      ANC6=ANC6/XM
      HATOM=12.*GMNC5+14.*GMNC6
      CATOM=5.*GMNC5+6.*GMNC6
      TCATOM=(5.*AIC5+5.*ANC5+6.*A22DMB+6.*A2MP+6.*A3MP+
      6.*ANC6)/100.
      THATOM=(12.*AIC5+12.*ANC5+14.*A22DMB+14.*A2MP+14.*
      A3MP+14.*ANC6)
     1/100.
      GMHCP=CATOM/TCATOM
      GMH2P=HRATE+0.5*(HATOM-GMHCP*THATOM)
      CGMPG=GMH2P+GMHCP
      AGMPG=3732.1*(PBARC-PWTMB)/AVGAS/(460.+TWTMB)
      XMATB=AGMPG/CGMPG*100.
      SUMIC5=AIC5/(AIC5+ANC5)
      XKC5=(YC5/(THOLD*DCAT)*ALOG(1.-SUMIC5/YC5))*(-1.)*XC5R
      SUMIC6=(A22DMB+A2MP+A3MP)/(ANC6+A22DMB+A2MP+A3MP)
      XKC6=(YC6/(THOLD*DCAT)*ALOG(1.-SUMIC6/YC6))*(-1.)*XC6R
      WRITE(6,777)
  777 FORMAT(1H1)
      WRITE(6,199)RUNNO
  199 FORMAT(50X,'RUN       ',2A4)
      WRITE(6,1001)
      WRITE(6,1001)
      WRITE(6,1001)
      WRITE(6,1001)
 1001 FORMAT('                    ')
      WRITE(6,102)TTEMP
  102 FORMAT(20X,'TEMPERATURE',17X,F10.0,7X,'DEG F')
```

Reproduced with permission of the copyright owner. Further reproduction prohibited without permission.

```
      WRITE(6,103)PRES
  103 FORMAT(20X,'PRESSURE',20X,F10.0,7X,'PSIG')
      WRITE(6,104)CATWT
  104 FORMAT(20X,'CATALYST WEIGHT',16X,F10.3,4X,'GRAMS')
      WRITE(6,880)CATYP
  880 FORMAT(20X,'CATALYST TYPE',21X,2A4)
      WRITE(6,1001)
      WRITE(6,106)
  106 FORMAT(20X,'HYDROCARBON FEED COMPOSITION')
      WRITE(6,1001)
      WRITE(6,116)
  116 FORMAT(51X,'MOLE FRACTION',4X,'PARTIAL PRESSURE')
      WRITE(6,107)PENT,PPC5
  107 FORMAT(20X,'NORMAL PENTANE',15X,F10.2,4X,F10.2,2X,'PSIA')
      WRITE(6,108)HEX,PPC6
  108 FORMAT(20X,'NORMAL HEXANE',16X,F10.2,4X,F10.2,2X,'PSIA')
      WRITE(6,1001)
      WRITE(6,110)H2CR
  110 FORMAT(20X,'H2/HYDROCARBON MOLE RATIO',4X,F10.2)
      WRITE(6,115)PPH2
  115 FORMAT(20X,'HYDROGEN PRESSURE',11X,F10.1,3X,'PSIA')
      WRITE(6,113)THOLD
  113 FORMAT(20X,'SUPERFICIAL RESIDENCE TIME',3X,F10.2,2X,
     'SEC')
      WRITE(6,114)XMATB
  114 FORMAT(20X,'MATERIAL BALANCE',13X,F10.2,2X,'PERCENT')
      WRITE(6,1001)
      WRITE(6,1001)
      WRITE(6,1001)
      WRITE(6,1001)
      WRITE(6,1001)
      WRITE(6,1001)
      WRITE(6,1001)
      WRITE(6,1001)
      WRITE(6,120)
  120 FORMAT(20X,'MOLES PRODUCT/100 MOLES FEED')
      WRITE(6,1001)
      WRITE(6,1001)
      WRITE(6,121)AIC5
  121 FORMAT(20X,'ISO C5',F10.2)
      WRITE(6,122)ANC5
  122 FORMAT(20X,'N C5',2X,F10.2)
      WRITE(6,123)A22DMB
  123 FORMAT(20X,'22DMB',1X,F10.2)
      WRITE(6,124)A2MP
  124 FORMAT(20X,'2MP',3X,F10.2)
      WRITE(6,125)A3MP
  125 FORMAT(20X,'3MP',3X,F10.2)
      WRITE(6,126)ANC6
  126 FORMAT(20X,'NC6',3X,F10.2)
      WRITE(6,1001)
      WRITE(6,130)XKC5
  130 FORMAT(20X,'C5 RATE CONSTANT',15X,F10.3,2X,'CC/GM/SEC')
      WRITE(6,1001)
      WRITE(6,131)XKC6
  131 FORMAT(20X,'C6 RATE CONSTANT',15X,F10.3,2X,'CC/GM/SEC')
      GO TO 666
      END
```

Reproduced with permission of the copyright owner. Further reproduction prohibited without permission.

APPENDIX 3

List of Computer Program for Calculation of n-C_5 Runs

Reproduced with permission of the copyright owner. Further reproduction prohibited without permission.

```
// EXEC EYFORT3,PARM.FORT=(NOSOURCE,NOMAP),PARM.LKED=LET
//FORT.SYSPRINT DD DUMMY
      DIMENSION XIC5(7),XNC5(7),X22DMB(7),X2MP(7),X3MP(7),
      XNC6(7)
      DIMENSION CATYP(2)
      DIMENSION RUNNO(2)
      DATA STP/*    */
  666 CONTINUE
      READ(5,999)RUNNO
      IF(RUNNO(1).EQ.STP)CALL EXIT
      READ(5,999)CATYP
  999 FORMAT(3A4)
      READ(5,998)XC5R,XC6R
  998 FORMAT(8F10.0)
      READ(5,1)XM
    1 FORMAT(8F10.0)
      N=XM
      READ(5,2)PRES,CATWT,DCAT,HFLOWI,AVGAS
    2 FORMAT(5F10.0)
      CTVOL=CATWT/DCAT
      READ(5,3)TTEMP,YC5,YC6,C5VFR,C6VFR
    3 FORMAT(5F10.0)
      READ(5,4)PBAR,TBAR,TWTMA,TWTMB
    4 FORMAT(4F10.0)
      TWTMAK=273.16+5.*(TWTMA-32.)/9.
      TARG=647.27-TWTMAK
      ARG=TARG*(3.2438+TARG*.00587+(TARG**3)*1.17E-08)/
     1(TWTMAK*(1.+TARG*.00219))
      PWTMA=218.17*(10.**(-ARG))*29.92
      TWTMBK=273.16+5.*(TWTMB-32.)/9.
      TBRG=647.27-TWTMBK
      BRG=TBRG*(3.2438+TBRG*.00587+(TBRG**3)*1.17E-08)/
     1(TWTMBK*(1.+TBRG*.00219))
      PWTMB=218.17*(10.**(-BRG))*29.92
      READ(5,6)(XIC5(I),I=1,N)
      READ(5,6)(XNC5(I),I=1,N)
    6 FORMAT(8F10.0)
      TPRES=PRES+14.7
      GMNC5=C5VFR*.6262/72.15
      GMNC6=C6VFR*.6601/86.18
      TMOLE=GMNC5+GMNC6
      PENT=GMNC5/TMOLE
      HEX=GMNC6/TMOLE
      TEMPC=(TBAR-32.)/1.8
      PBARC=PBAR*(1.-(.000164*TEMPC)/(1.+.000182*TEMPC))
      HRATE=3732.1*(PBARC-PWTMA)/HFLOWI/(460.+TWTMA)
      H2CR=HRATE/(GMNC5+GMNC6)
      PPH2=H2CR/(H2CR+1.)*TPRES
      PPC5=PENT/(H2CR+1.)*TPRES
      PPC6=HEX/(H2CR+1.)*TPRES
      WHSV=(C5VFR*.6262+C6VFR*.6601)/CATWT
      VHSV=(C5VFR+C6VFR)/CTVOL
```

Reproduced with permission of the copyright owner. Further reproduction prohibited without permission.

```
      GDEN=TPRES*453.6/10.73/28312.6/(460.+TTEMP)
      THOLD=GDEN*CTVOL*3600./(GMNC5+GMNC6+HRATE)
      AIC5=0.
      ANC5=0.
      DO 50 I=1,N
      AIC5=AIC5+XIC5(I)
      ANC5=ANC5+XNC5(I)
   50 CONTINUE
      AIC5=AIC5/XM
      ANC5=ANC5/XM
      HATOM=12.*GMNC5
      CATOM=5.*GMNC5
      TCATOM=(5.*AIC5+5.*ANC5)/100.
      THATOM=(12.*AIC5+12.*ANC5)/100.
      GMHCP=CATOM/TCATOM
      GMH2P=HRATE+0.5*(HATOM-GMHCP*THATOM)
      CGMPG=GMH2P+GMHCP
      AGMPG=3732.1*(PBARG-PWTMB)/AVGAS/(460.+TWTMB)
      XMATB=AGMPG/CGMPG*100.
      SUMIC5=AIC5/100.
      XKC5=(YC5/(THOLD*DCAT)*ALOG(1.-SUMIC5/YC5))*(-1.)*XC5R
      WRITE(6,777)
  777 FORMAT(1H1)
      WRITE(6,199)RUNNO
  199 FORMAT(50X,'RUN       ',3A4)
      WRITE(6,1001)
      WRITE(6,1001)
      WRITE(6,1001)
      WRITE(6,1001)
 1001 FORMAT('             ')
      WRITE(6,102)TTEMP
  102 FORMAT(20X,'TEMPERATURE',17X,F10.0,7X,'DEG F')
      WRITE(6,103)PRES
  103 FORMAT(20X,'PRESSURE',20X,F10.0,7X,'PSIG')
      WRITE(6,104)CATWT
  104 FORMAT(20X,'CATALYST WEIGHT',16X,F10.3,4X,'GRAMS')
      WRITE(6,880)CATYP
  880 FORMAT(20X,'CATALYST TYPE',21X,2A4)
      WRITE(6,1001)
      WRITE(6,106)
  106 FORMAT(20X,'HYDROCARBON FEED COMPOSITION')
      WRITE(6,1001)
      WRITE(6,116)
  116 FORMAT(51X,'MOLE FRACTION',4X,'PARTIAL PRESSURE')
      WRITE(6,107)PENT,PPC5
  107 FORMAT(20X,'NORMAL PENTANE',15X,F10.2,4X,F10.2,2X,'PSIA')
      WRITE(6,108)HEX,PPC6
  108 FORMAT(20X,'NORMAL HEXANE',16X,F10.2,4X,F10.2,2X,'PSIA')
      WRITE(6,1001)
      WRITE(6,110)H2CR
  110 FORMAT(20X,'H2/HYDROCARBON MOLE RATIO',4X,F10.2)
      WRITE(6,115)PPH2
  115 FORMAT(20X,'HYDROGEN PRESSURE',11X,F10.1,3X,'PSIA')
```

Reproduced with permission of the copyright owner. Further reproduction prohibited without permission.

```
      WRITE(6,111)WHSV
  111 FORMAT(20X,'WEIGHT HOURLY SPACE VELOCITY',1X,F10.2,
     2X,'W/HR/W')
      WRITE(6,113)THOLD
  113 FORMAT(20X,'SUPERFICIAL RESIDENCE TIME',3X,F10.2,2X,
     'SEC')
      WRITE(6,114)XMATB
  114 FORMAT(20X,'MATERIAL BALANCE',13X,F10.2,2X,'PERCENT')
      WRITE(6,1001)
      WRITE(6,1001)
      WRITE(6,1001)
      WRITE(6,1001)
      WRITE(6,1001)
      WRITE(6,1001)
      WRITE(6,1001)
      WRITE(6,120)
  120 FORMAT(20X,'MOLES PRODUCT/100 MOLES FEED')
      WRITE(6,1001)
      WRITE(6,1001)
      WRITE(6,121)AIC5
  121 FORMAT(20X,'ISO C5',F10.2)
      WRITE(6,122)ANC5
  122 FORMAT(20X,'N C5',2X,F10.2)
      WRITE(6,1001)
      WRITE(6,130)XKC5
  130 FORMAT(20X,'C5 RATE CONSTANT',15X,F10.3,2X,'CC/GM/SEC')
      WRITE(6,1001)
      GO TO 666
      END
//LKED.SYSPRINT DD DUMMY
//GO.SYSIN DD *
```

Reproduced with permission of the copyright owner. Further reproduction prohibited without permission.

APPENDIX 4

Detailed Run Data and Results

Reproduced with permission of the copyright owner. Further reproduction prohibited without permission.

RUN C61-5

TEMPERATURE	465.	DEG F
PRESSURE	200.	PSIG
CATALYST WEIGHT	2.000	GRAMS
CATALYST TYPE	LJJ 289	

HYDROCARBON FEED COMPOSITION

	MOLE FRACTION	PARTIAL PRESS
NORMAL PENTANE	0.0	0.0 PSIA
NORMAL HEXANE	1.00	19.29 PSIA

H2/HYDROCARBON MOLE RATIO	10.14	
HYDROGEN PRESSURE	195.4	PSIA
WEIGHT HOURLY SPACE VELOCITY	6.60	W/HR/W
SUPERFICIAL RESIDENCE TIME	2.44	SEC
MATERIAL BALANCE	99.40	PERCENT

MOLES PRODUCT/100 MOLES FEED

ISO C5	0.14
N C5	2.15
22DMB	0.63
2MP	12.03
3MP	5.39
NC6	79.65

C5 RATE CONSTANT	0.0	CC/GM/SEC
C6 RATE CONSTANT	0.143	CC/GM/SEC

Reproduced with permission of the copyright owner. Further reproduction prohibited without permission.

RUN C61-7

TEMPERATURE	465.	DEG F
PRESSURE	300.	PSIG
CATALYST WEIGHT	2.000	GRAMS
CATALYST TYPE	LJJ 289	

HYDROCARBON FEED COMPOSITION

	MOLE FRACTION	PARTIAL PRESS
NORMAL PENTANE	0.0	0.0 PSIA
NORMAL HEXANE	1.00	27.98 PSIA

H2/HYDROCARBON MOLE RATIO	10.25	
HYDROGEN PRESSURE	286.7	PSIA
WEIGHT HOURLY SPACE VELOCITY	6.60	W/HR/W
SUPERFICIAL RESIDENCE TIME	3.54	SEC
MATERIAL BALANCE	98.62	PERCENT

MOLES PRODUCT/100 MOLES FEED

ISO C5	0.19
N C5	3.03
22DMB	0.48
2MP	12.24
3MP	5.42
NC6	78.63

C5 RATE CONSTANT	0.0	CC/GM/SEC
C6 RATE CONSTANT	0.100	CC/GM/SEC

Reproduced with permission of the copyright owner. Further reproduction prohibited without permission.

RUN C61-8

TEMPERATURE	465.	DEG F
PRESSURE	100.	PSIG
CATALYST WEIGHT	2.000	GRAMS
CATALYST TYPE	LJJ 289	

HYDROCARBON FEED COMPOSITION

	MOLE FRACTION	PARTIAL PRESS
NORMAL PENTANE	0.0	0.0 PSIA
NORMAL HEXANE	1.00	10.61 PSIA

H2/HYDROCARBON MOLE RATIO	9.91	
HYDROGEN PRESSURE	104.1	PSIA
WEIGHT HOURLY SPACE VELOCITY	6.60	W/HR/W
SUPERFICIAL RESIDENCE TIME	1.34	SEC
MATERIAL BALANCE	99.38	PERCENT

MOLES PRODUCT/100 MOLES FEED

ISO C5	0.11
N C5	0.80
22DMB	1.19
2MP	16.95
3MP	4.81
NC6	76.15

C5 RATE CONSTANT	0.0	CC/GM/SEC
C6 RATE CONSTANT	0.337	CC/GM/SEC

Reproduced with permission of the copyright owner. Further reproduction prohibited without permission.

RUN C61-14

TEMPERATURE	465.	DEG F
PRESSURE	192.	PSIG
CATALYST WEIGHT	2.002	GRAMS
CATALYST TYPE	LJJ 289	

HYDROCARBON FEED COMPOSITION

	MOLE FRACTION	PARTIAL PRESS
NORMAL PENTANE	0.0	0.0 PSIA
NORMAL HEXANE	1.00	10.99 PSIA

H2/HYDROCARBON MOLE RATIO	17.82	
HYDROGEN PRESSURE	195.7	PSIA
WEIGHT HOURLY SPACE VELOCITY	6.60	W/HR/W
SUPERFICIAL RESIDENCE TIME	1.39	SEC
MATERIAL BALANCE	99.68	PERCENT

MOLES PRODUCT/100 MOLES FEED

ISO C5	0.0
N C5	1.82
22DMB	0.80
2MP	6.46
3MP	2.51
NC6	88.42

C5 RATE CONSTANT	0.0	CC/GM/SEC
C6 RATE CONSTANT	0.127	CC/GM/SEC

Reproduced with permission of the copyright owner. Further reproduction prohibited without permission.

RUN C61-15

TEMPERATURE	465.	DEG F
PRESSURE	291.	PSIG
CATALYST WEIGHT	2.007	GRAMS
CATALYST TYPE	LJJ 289	

HYDROCARBON FEED COMPOSITION

	MOLE FRACTION	PARTIAL PRESS
NORMAL PENTANE	0.0	0.0 PSIA
NORMAL HEXANE	1.00	19.23 PSIA

H2/HYDROCARBON MOLE RATIO	14.89	
HYDROGEN PRESSURE	286.5	PSIA
WEIGHT HOURLY SPACE VELOCITY	6.58	W/HR/W
SUPERFICIAL RESIDENCE TIME	2.44	SEC
MATERIAL BALANCE	111.95	PERCENT

MOLES PRODUCT/100 MOLES FEED

ISO C5	0.0
N C5	2.81
22DMB	0.30
2MP	11.63
3MP	4.97
NC6	80.28

C5 RATE CONSTANT	0.0	CC/GM/SEC
C6 RATE CONSTANT	0.133	CC/GM/SEC

Reproduced with permission of the copyright owner. Further reproduction prohibited without permission.

RUN C61-16

TEMPERATURE	465.	DEG F
PRESSURE	291.	PSIG
CATALYST WEIGHT	2.013	GRAMS
CATALYST TYPE	HJE 243	

HYDROCARBON FEED COMPOSITION

	MOLE FRACTION	PARTIAL PRESS
NORMAL PENTANE	0.0	0.0 PSIA
NORMAL HEXANE	1.00	19.29 PSIA

H2/HYDROCARBON MOLE RATIO	14.85	
HYDROGEN PRESSURE	286.4	PSIA
WEIGHT HOURLY SPACE VELOCITY	6.56	W/HR/W
SUPERFICIAL RESIDENCE TIME	3.13	SEC
MATERIAL BALANCE	102.03	PERCENT

MOLES PRODUCT/100 MOLES FEED

ISO C5	0.0
N C5	2.13
22DMB	0.23
2MP	7.16
3MP	3.73
NC6	86.75

C5 RATE CONSTANT	0.0	CC/GM/SEC
C6 RATE CONSTANT	0.083	CC/GM/SEC

Reproduced with permission of the copyright owner. Further reproduction prohibited without permission.

RUN C61-17

TEMPERATURE	465.	DEG F
PRESSURE	300.	PSIG
CATALYST WEIGHT	2.013	GRAMS
CATALYST TYPE	HJE 243	

HYDROCARBON FEED COMPOSITION

	MOLE FRACTION	PARTIAL PRESS
NORMAL PENTANE	0.0	0.0 PSIA
NORMAL HEXANE	1.00	28.51 PSIA

H2/HYDROCARBON MOLE RATIO	10.04	
HYDROGEN PRESSURE	286.2	PSIA
WEIGHT HOURLY SPACE VELOCITY	6.56	W/HR/W
SUPERFICIAL RESIDENCE TIME	4.63	SEC
MATERIAL BALANCE	105.30	PERCENT

MOLES PRODUCT/100 MOLES FEED

ISO C5	0.0
N C5	2.59
22DMB	0.21
2MP	6.05
3MP	3.11
NC6	88.05

C5 RATE CONSTANT	0.0	CC/GM/SEC
C6 RATE CONSTANT	0.047	CC/GM/SEC

Reproduced with permission of the copyright owner. Further reproduction prohibited without permission.

RUN C61-19

TEMPERATURE	465.	DEG F
PRESSURE	200.	PSIG
CATALYST WEIGHT	2.007	GRAMS
CATALYST TYPE	HJE 243	

HYDROCARBON FEED COMPOSITION

	MOLE FRACTION	PARTIAL PRESS
NORMAL PENTANE	0.0	0.0 PSIA
NORMAL HEXANE	1.00	19.74 PSIA

H2/HYDROCARBON MOLE RATIO	9.87	
HYDROGEN PRESSURE	195.0	PSIA
WEIGHT HOURLY SPACE VELOCITY	6.58	W/HR/W
SUPERFICIAL RESIDENCE TIME	3.20	SEC
MATERIAL BALANCE	105.84	PERCENT

MOLES PRODUCT/100 MOLES FEED

ISO C5	4.70
N C5	19.36
22DMB	5.43
2MP	5.02
3MP	2.33
NC6	63.15

C5 RATE CONSTANT	0.0	CC/GM/SEC
C6 RATE CONSTANT	0.125	CC/GM/SEC

Reproduced with permission of the copyright owner. Further reproduction prohibited without permission.

RUN C61-18

TEMPERATURE	465.	DEG F
PRESSURE	100.	PSIG
CATALYST WEIGHT	2.003	GRAMS
CATALYST TYPE	HJE 243	

HYDROCARBON FEED COMPOSITION

	MOLE FRACTION	PARTIAL PRESS
NORMAL PENTANE	0.0	0.0 PSIA
NORMAL HEXANE	1.00	10.43 PSIA

H2/HYDROCARBON MOLE RATIO	10.00	
HYDROGEN PRESSURE	104.3	PSIA
WEIGHT HOURLY SPACE VELOCITY	6.59	W/HR/W
SUPERFICIAL RESIDENCE TIME	1.69	SEC
MATERIAL BALANCE	103.03	PERCENT

MOLES PRODUCT/100 MOLES FEED

ISO C5	7.88
N C5	17.77
22DMB	9.37
2MP	10.24
3MP	1.25
NC6	53.48

C5 RATE CONSTANT	0.0	CC/GM/SEC
C6 RATE CONSTANT	0.431	CC/GM/SEC

Reproduced with permission of the copyright owner. Further reproduction prohibited without permission.

RUN C61-20

TEMPERATURE	465.	DEG F
PRESSURE	97.	PSIG
CATALYST WEIGHT	2.001	GRAMS
CATALYST TYPE	HJE 243	

HYDROCARBON FEED COMPOSITION

	MOLE FRACTION	PARTIAL PRESS
NORMAL PENTANE	0.0	0.0 PSIA
NORMAL HEXANE	1.00	7.07 PSIA

H2/HYDROCARBON MOLE RATIO	14.79	
HYDROGEN PRESSURE	104.6	PSIA
WEIGHT HOURLY SPACE VELOCITY	6.60	W/HR/W
SUPERFICIAL RESIDENCE TIME	1.14	SEC
MATERIAL BALANCE	96.14	PERCENT

MOLES PRODUCT/100 MOLES FEED

ISO C5	3.73
N C5	13.41
22DMB	8.26
2MP	9.16
3MP	2.51
NC6	62.93

C5 RATE CONSTANT	0.0	CC/GM/SEC
C6 RATE CONSTANT	0.529	CC/GM/SEC

Reproduced with permission of the copyright owner. Further reproduction prohibited without permission.

RUN C61-22

TEMPERATURE	465.	DEG F
PRESSURE	192.	PSIG
CATALYST WEIGHT	2.002	GRAMS
CATALYST TYPE	HJF 243	

HYDROCARBON FEED COMPOSITION

	MOLE FRACTION	PARTIAL PRESS
NORMAL PENTANE	0.0	0.0 PSIA
NORMAL HEXANE	1.00	10.97 PSIA

H2/HYDROCARBON MOLE RATIO	17.85	
HYDROGEN PRESSURE	195.7	PSIA
WEIGHT HOURLY SPACE VELOCITY	6.60	W/HR/W
SUPERFICIAL RESIDENCE TIME	1.77	SEC
MATERIAL BALANCE	100.60	PERCENT

MOLES PRODUCT/100 MOLES FEED

ISO C5	0.0
N C5	1.04
22DMB	0.13
2MP	12.92
3MP	4.92
NC6	80.99

C5 RATE CONSTANT	0.0	CC/GM/SEC
C6 RATE CONSTANT	0.246	CC/GM/SEC

Reproduced with permission of the copyright owner. Further reproduction prohibited without permission.

RUN MI-4

TEMPERATURE	465.	DEG F
PRESSURE	200.	PSIG
CATALYST WEIGHT	2.000	GRAMS
CATALYST TYPE	LJJ 289	

HYDROCARBON FEED COMPOSITION

	MOLE FRACTION	PARTIAL PRESS
NORMAL PENTANE	0.17	3.16 PSIA
NORMAL HEXANE	0.83	15.80 PSIA

H2/HYDROCARBON MOLE RATIO	10.33	
HYDROGEN PRESSURE	195.7	PSIA
WEIGHT HOURLY SPACE VELOCITY	6.55	W/HR/W
SUPERFICIAL RESIDENCE TIME	2.35	SEC
MATERIAL BALANCE	99.36	PERCENT

MOLES PRODUCT/100 MOLES FEED

ISO C5	1.26
N C5	19.01
22DMB	0.22
2MP	11.09
3MP	5.36
NC6	63.04

C5 RATE CONSTANT	0.046	CC/GM/SEC
C6 RATE CONSTANT	0.171	CC/GM/SEC

Reproduced with permission of the copyright owner. Further reproduction prohibited without permission.

RUN MI-5

TEMPERATURE	465.	DEG F
PRESSURE	200.	PSIG
CATALYST WEIGHT	2.000	GRAMS
CATALYST TYPE	LJJ 289	

HYDROCARBON FEED COMPOSITION

	MOLE FRACTION	PARTIAL PRESS
NORMAL PENTANE	0.38	7.62 PSIA
NORMAL HEXANE	0.62	12.49 PSIA

H2/HYDROCARBON MOLE RATIO	9.68	
HYDROGEN PRESSURE	194.6	PSIA
WEIGHT HOURLY SPACE VELOCITY	6.48	W/HR/W
SUPERFICIAL RESIDENCE TIME	2.43	SEC
MATERIAL BALANCE	99.38	PERCENT

MOLES PRODUCT/100 MOLES FEED

ISO C5	2.55
N C5	36.75
22DMB	0.17
2MP	10.48
3MP	4.35
NC6	45.68

C5 RATE CONSTANT	0.046	CC/GM/SEC
C6 RATE CONSTANT	0.201	CC/GM/SEC

Reproduced with permission of the copyright owner. Further reproduction prohibited without permission.

RUN MI-6

TEMPERATURE	465.	DEG F
PRESSURE	200.	PSIG
CATALYST WEIGHT	2.000	GRAMS
CATALYST TYPE	LJJ 289	

HYDROCARBON FEED COMPOSITION

	MOLE FRACTION	PARTIAL PRESS
NORMAL PENTANE	0.53	10.00 PSIA
NORMAL HEXANE	0.47	8.82 PSIA

H2/HYDROCARBON MOLE RATIO	10.41	
HYDROGEN PRESSURE	195.9	PSIA
WEIGHT HOURLY SPACE VELOCITY	6.43	W/HR/W
SUPERFICIAL RESIDENCE TIME	2.23	SEC
MATERIAL BALANCE	99.62	PERCENT

MOLES PRODUCT/100 MOLES FEED

ISO C5	3.62
N C5	54.37
22DMB	0.19
2MP	6.22
3MP	2.39
NC6	33.37

C5 RATE CONSTANT	0.048	CC/GM/SEC
C6 RATE CONSTANT	0.179	CC/GM/SEC

Reproduced with permission of the copyright owner. Further reproduction prohibited without permission.

RUN MI-10

TEMPERATURE	465.	DEG F
PRESSURE	300.	PSIG
CATALYST WEIGHT	2.000	GRAMS
CATALYST TYPE	LJJ 289	

HYDROCARBON FEED COMPOSITION

	MOLE FRACTION	PARTIAL PRESS
NORMAL PENTANE	0.17	4.68 PSIA
NORMAL HEXANE	0.83	23.40 PSIA

H2/HYDROCARBON MOLE RATIO	10.21	
HYDROGEN PRESSURE	286.6	PSIA
WEIGHT HOURLY SPACE VELOCITY	6.55	W/HR/W
SUPERFICIAL RESIDENCE TIME	3.48	SEC
MATERIAL BALANCE	99.86	PERCENT

MOLES PRODUCT/100 MOLES FEED

ISO C5	1.41
N C5	22.97
22DMB	0.10
2MP	10.91
3MP	4.84
NC6	59.77

C5 RATE CONSTANT	0.029	CC/GM/SEC
C6 RATE CONSTANT	0.115	CC/GM/SEC

Reproduced with permission of the copyright owner. Further reproduction prohibited without permission.

RUN MI-11

TEMPERATURE	465.	DEG F
PRESSURE	300.	PSIG
CATALYST WEIGHT	2.000	GRAMS
CATALYST TYPE	LJJ 289	

HYDROCARBON FEED COMPOSITION

	MOLE FRACTION	PARTIAL PRESS
NORMAL PENTANE	0.53	15.07 PSIA
NORMAL HEXANE	0.47	13.30 PSIA

H2/HYDROCARBON MOLE RATIO	10.09	
HYDROGEN PRESSURE	286.3	PSIA
WEIGHT HOURLY SPACE VELOCITY	6.43	W/HR/W
SUPERFICIAL RESIDENCE TIME	3.36	SEC
MATERIAL BALANCE	100.32	PERCENT

MOLES PRODUCT/100 MOLES FEED

ISO C5	3.22
N C5	48.22
22DMB	0.01
2MP	7.37
3MP	3.21
NC6	37.97

C5 RATE CONSTANT	0.032	CC/GM/SEC
C6 RATE CONSTANT	0.125	CC/GM/SEC

Reproduced with permission of the copyright owner. Further reproduction prohibited without permission.

RUN MI-12

TEMPERATURE	465.	DEG F
PRESSURE	300.	PSIG
CATALYST WEIGHT	2.000	GRAMS
CATALYST TYPE	LJJ 289	

HYDROCARBON FEED COMPOSITION

	MOLE FRACTION	PARTIAL PRESS
NORMAL PENTANE	0.77	21.90 PSIA
NORMAL HEXANE	0.23	6.44 PSIA

H2/HYDROCARBON MOLE RATIO	10.10	
HYDROGEN PRESSURE	286.4	PSIA
WEIGHT HOURLY SPACE VELOCITY	6.35	W/HR/W
SUPERFICIAL RESIDENCE TIME	3.26	SEC
MATERIAL BALANCE	99.64	PERCENT

MOLES PRODUCT/100 MOLES FEED

ISO C5	5.50
N C5	72.31
22DMB	0.0
2MP	4.02
3MP	1.84
NC6	16.34

C5 RATE CONSTANT	0.038	CC/GM/SEC
C6 RATE CONSTANT	0.162	CC/GM/SEC

Reproduced with permission of the copyright owner. Further reproduction prohibited without permission.

RUN MI-13

TEMPERATURE	465.	DEG F
PRESSURE	100.	PSIG
CATALYST WEIGHT	2.000	GRAMS
CATALYST TYPE	LJJ 289	

HYDROCARBON FEED COMPOSITION

	MOLE FRACTION	PARTIAL PRESS
NORMAL PENTANE	0.17	1.77 PSIA
NORMAL HEXANE	0.83	8.84 PSIA

H2/HYDROCARBON MOLE RATIO	9.82	
HYDROGEN PRESSURE	104.1	PSIA
WEIGHT HOURLY SPACE VELOCITY	6.55	W/HR/W
SUPERFICIAL RESIDENCE TIME	1.31	SEC
MATERIAL BALANCE	99.26	PERCENT

MOLES PRODUCT/100 MOLES FEED

ISO C5	1.56
N C5	18.97
22DMB	0.52
2MP	14.32
3MP	4.93
NC6	59.70

C5 RATE CONSTANT	0.101	CC/GM/SEC
C6 RATE CONSTANT	0.374	CC/GM/SEC

Reproduced with permission of the copyright owner. Further reproduction prohibited without permission.

RUN MI-14

TEMPERATURE	465.	DEG F
PRESSURE	100.	PSIG
CATALYST WEIGHT	2.000	GRAMS
CATALYST TYPE	LJJ 289	

HYDROCARBON FEED COMPOSITION

	MOLE FRACTION	PARTIAL PRESS
NORMAL PENTANE	0.53	5.66 PSIA
NORMAL HEXANE	0.47	5.00 PSIA

H2/HYDROCARBON MOLE RATIO	9.76	
HYDROGEN PRESSURE	104.0	PSIA
WEIGHT HOURLY SPACE VELOCITY	6.43	W/HR/W
SUPERFICIAL RESIDENCE TIME	1.26	SEC
MATERIAL BALANCE	99.33	PERCENT

MOLES PRODUCT/100 MOLES FEED

ISO C5	5.75
N C5	53.26
22DMB	0.13
2MP	9.97
3MP	2.79
NC6	28.14

C5 RATE CONSTANT	0.137	CC/GM/SEC
C6 RATE CONSTANT	0.519	CC/GM/SEC

Reproduced with permission of the copyright owner. Further reproduction prohibited without permission.

RUN MI-15

TEMPERATURE	465.	DEG F
PRESSURE	100.	PSIG
CATALYST WEIGHT	2.000	GRAMS
CATALYST TYPE	LJJ 289	

HYDROCARBON FEED COMPOSITION

	MOLE FRACTION	PARTIAL PRESS
NORMAL PENTANE	0.77	8.23 PSIA
NORMAL HEXANE	0.23	2.42 PSIA

H2/HYDROCARBON MOLE RATIO	9.76	
HYDROGEN PRESSURE	104.0	PSIA
WEIGHT HOURLY SPACE VELOCITY	6.35	W/HR/W
SUPERFICIAL RESIDENCE TIME	1.23	SEC
MATERIAL BALANCE	103.22	PERCENT

MOLES PRODUCT/100 MOLES FEED

ISO C5	6.37
N C5	58.95
22DMB	0.05
2MP	8.01
3MP	2.36
NC6	24.26

C5 RATE CONSTANT	0.143	CC/GM/SEC
C6 RATE CONSTANT	0.507	CC/GM/SEC

Reproduced with permission of the copyright owner. Further reproduction prohibited without permission.

RUN MI-19

TEMPERATURE	465.	DEG F
PRESSURE	192.	PSIG
CATALYST WEIGHT	2.002	GRAMS
CATALYST TYPE	LJJ 289	

HYDROCARBON FEED COMPOSITION

	MOLE FRACTION	PARTIAL PRESS
NORMAL PENTANE	0.17	1.81 PSIA
NORMAL HEXANE	0.83	9.05 PSIA

H2/HYDROCARBON MOLE RATIO	18.04	
HYDROGEN PRESSURE	195.8	PSIA
WEIGHT HOURLY SPACE VELOCITY	6.54	W/HR/W
SUPERFICIAL RESIDENCE TIME	1.35	SEC
MATERIAL BALANCE	100.26	PERCENT

MOLES PRODUCT/100 MOLES FEED

ISO C5	0.85
N C5	23.08
22DMB	0.37
2MP	4.87
3MP	1.95
NC6	68.87

C5 RATE CONSTANT	0.045	CC/GM/SEC
C6 RATE CONSTANT	0.124	CC/GM/SEC

Reproduced with permission of the copyright owner. Further reproduction prohibited without permission.

RUN MI-20

TEMPERATURE	465.	DEG F
PRESSURE	192.	PSIG
CATALYST WEIGHT	2.002	GRAMS
CATALYST TYPE	LJJ 289	

HYDROCARBON FEED COMPOSITION

	MOLE FRACTION	PARTIAL PRESS
NORMAL PENTANE	0.53	5.79 PSIA
NORMAL HEXANE	0.47	5.11 PSIA

H2/HYDROCARBON MOLE RATIO	17.97	
HYDROGEN PRESSURE	195.8	PSIA
WEIGHT HOURLY SPACE VELOCITY	6.43	W/HR/W
SUPERFICIAL RESIDENCE TIME	1.29	SEC
MATERIAL BALANCE	99.99	PERCENT

MOLES PRODUCT/100 MOLES FEED

ISO C5	1.99
N C5	50.20
22DMB	0.10
2MP	3.71
3MP	1.46
NC6	42.54

C5 RATE CONSTANT	0.050	CC/GM/SEC
C6 RATE CONSTANT	0.152	CC/GM/SEC

Reproduced with permission of the copyright owner. Further reproduction prohibited without permission.

RUN MI-21

TEMPERATURE	465.	DEG F
PRESSURE	192.	PSIG
CATALYST WEIGHT	2.002	GRAMS
CATALYST TYPE	LJJ 289	

HYDROCARBON FEED COMPOSITION

	MOLE FRACTION	PARTIAL PRESS
NORMAL PENTANE	0.77	8.47 PSIA
NORMAL HEXANE	0.23	2.49 PSIA

H2/HYDROCARBON MOLE RATIO	17.86	
HYDROGEN PRESSURE	195.7	PSIA
WEIGHT HOURLY SPACE VELOCITY	6.34	W/HR/W
SUPERFICIAL RESIDENCE TIME	1.26	SEC
MATERIAL BALANCE	98.65	PERCENT

MOLES PRODUCT/100 MOLES FEED

ISO C5	3.33
N C5	74.39
22DMB	0.0
2MP	1.84
3MP	0.44
NC6	20.01

C5 RATE CONSTANT	0.058	CC/GM/SEC
C6 RATE CONSTANT	0.144	CC/GM/SEC

Reproduced with permission of the copyright owner. Further reproduction prohibited without permission.

RUN MI-22

TEMPERATURE	465.	DEG F
PRESSURE	289.	PSIG
CATALYST WEIGHT	2.007	GRAMS
CATALYST TYPE	LJJ 289	

HYDROCARBON FEED COMPOSITION

	MOLE FRACTION	PARTIAL PRESS
NORMAL PENTANE	0.17	3.19 PSIA
NORMAL HEXANE	0.83	15.95 PSIA

H2/HYDROCARBON MOLE RATIO	14.87	
HYDROGEN PRESSURE	284.6	PSIA
WEIGHT HOURLY SPACE VELOCITY	6.33	W/HR/W
SUPERFICIAL RESIDENCE TIME	2.38	SEC
MATERIAL BALANCE	113.09	PERCENT

MOLES PRODUCT/100 MOLES FEED

ISO C5	1.52
N C5	35.03
22DMB	0.09
2MP	8.27
3MP	3.63
NC6	51.45

C5 RATE CONSTANT	0.030	CC/GM/SEC
C6 RATE CONSTANT	0.150	CC/GM/SEC

Reproduced with permission of the copyright owner. Further reproduction prohibited without permission.

RUN MI-23

TEMPERATURE	465.	DEG F
PRESSURE	291.	PSIG
CATALYST WEIGHT	2.007	GRAMS
CATALYST TYPE	LJJ 289	

HYDROCARBON FEED COMPOSITION

	MOLE FRACTION	PARTIAL PRESS
NORMAL PENTANE	0.53	10.25 PSIA
NORMAL HEXANE	0.47	9.05 PSIA

H2/HYDROCARBON MOLE RATIO	14.84	
HYDROGEN PRESSURE	286.4	PSIA
WEIGHT HOURLY SPACE VELOCITY	6.41	W/HR/W
SUPERFICIAL RESIDENCE TIME	2.30	SEC
MATERIAL BALANCE	109.13	PERCENT

MOLES PRODUCT/100 MOLES FEED

ISO C5	2.32
N C5	50.93
22DMB	0.05
2MP	6.42
3MP	2.84
NC6	37.44

C5 RATE CONSTANT	0.033	CC/GM/SEC
C6 RATE CONSTANT	0.165	CC/GM/SEC

Reproduced with permission of the copyright owner. Further reproduction prohibited without permission.

RUN MI-24

TEMPERATURE	465.	DEG F
PRESSURE	291.	PSIG
CATALYST WEIGHT	2.007	GRAMS
CATALYST TYPE	LJJ 289	

HYDROCARBON FEED COMPOSITION

	MOLE FRACTION	PARTIAL PRESS
NORMAL PENTANE	0.77	14.88 PSIA
NORMAL HEXANE	0.23	4.38 PSIA

H2/HYDROCARBON MOLE RATIO	14.87	
HYDROGEN PRESSURE	286.4	PSIA
WEIGHT HOURLY SPACE VELOCITY	6.33	W/HR/W
SUPERFICIAL RESIDENCE TIME	2.22	SEC
MATERIAL BALANCE	109.37	PERCENT

MOLES PRODUCT/100 MOLES FEED

ISO C5	4.03
N C5	69.55
22DMB	0.0
2MP	4.20
3MP	1.95
NC6	20.27

C5 RATE CONSTANT	0.043	CC/GM/SEC
C6 RATE CONSTANT	0.205	CC/GM/SEC

Reproduced with permission of the copyright owner. Further reproduction prohibited without permission.

RUN MI-25

TEMPERATURE	465.	DEG F
PRESSURE	291.	PSIG
CATALYST WEIGHT	2.013	GRAMS
CATALYST TYPE	HJE 243	

HYDROCARBON FEED COMPOSITION

	MOLE FRACTION	PARTIAL PRESS
NORMAL PENTANE	0.17	3.22 PSIA
NORMAL HEXANE	0.83	16.09 PSIA

H2/HYDROCARBON MOLE RATIO	14.83	
HYDROGEN PRESSURE	286.4	PSIA
WEIGHT HOURLY SPACE VELOCITY	6.51	W/HR/W
SUPERFICIAL RESIDENCE TIME	3.08	SEC
MATERIAL BALANCE	105.53	PERCENT

MOLES PRODUCT/100 MOLES FEED

ISO C5	1.01
N C5	27.39
22DMB	0.04
2MP	3.47
3MP	1.74
NC6	66.35

C5 RATE CONSTANT	0.025	CC/GM/SEC
C6 RATE CONSTANT	0.053	CC/GM/SEC

Reproduced with permission of the copyright owner. Further reproduction prohibited without permission.

RUN MI-26

TEMPERATURE	465.	DEG F
PRESSURE	291.	PSIG
CATALYST WEIGHT	2.013	GRAMS
CATALYST TYPE	HJE 243	

HYDROCARBON FEED COMPOSITION

	MOLE FRACTION	PARTIAL PRESS
NORMAL PENTANE	0.53	10.27 PSIA
NORMAL HEXANE	0.47	9.06 PSIA

H2/HYDROCARBON MOLE RATIO	14.82	
HYDROGEN PRESSURE	286.4	PSIA
WEIGHT HOURLY SPACE VELOCITY	6.39	W/HR/W
SUPERFICIAL RESIDENCE TIME	2.94	SEC
MATERIAL BALANCE	101.72	PERCENT

MOLES PRODUCT/100 MOLES FEED

ISO C5	2.14
N C5	55.50
22DMB	0.0
2MP	1.19
3MP	0.58
NC6	40.59

C5 RATE CONSTANT	0.027	CC/GM/SEC
C6 RATE CONSTANT	0.031	CC/GM/SEC

Reproduced with permission of the copyright owner. Further reproduction prohibited without permission.

RUN MI-27

TEMPERATURE	465.	DEG F
PRESSURE	291.	PSIG
CATALYST WEIGHT	2.013	GRAMS
CATALYST TYPE	HJF 243	

HYDROCARBON FEED COMPOSITION

	MOLE FRACTION	PARTIAL PRESS
NORMAL PENTANE	0.77	15.13 PSIA
NORMAL HEXANE	0.23	4.45 PSIA

H2/HYDROCARBON MOLE RATIO	14.61	
HYDROGEN PRESSURE	286.1	PSIA
WEIGHT HOURLY SPACE VELOCITY	6.31	W/HR/W
SUPERFICIAL RESIDENCE TIME	2.89	SEC
MATERIAL BALANCE	105.42	PERCENT

MOLES PRODUCT/100 MOLES FEED

ISO C5	2.44
N C5	74.12
22DMB	0.0
2MP	0.67
3MP	0.32
NC6	22.45

C5 RATE CONSTANT	0.024	CC/GM/SEC
C6 RATE CONSTANT	0.032	CC/GM/SEC

Reproduced with permission of the copyright owner. Further reproduction prohibited without permission.

RUN MI-28

TEMPERATURE	465.	DEG F
PRESSURE	300.	PSIG
CATALYST WEIGHT	2.013	GRAMS
CATALYST TYPE	HJF 243	

HYDROCARBON FEED COMPOSITION

	MOLE FRACTION	PARTIAL PRESS
NORMAL PENTANE	0.17	4.70 PSIA
NORMAL HEXANE	0.83	23.51 PSIA

H2/HYDROCARBON MOLE RATIO	10.16	
HYDROGEN PRESSURE	286.5	PSIA
WEIGHT HOURLY SPACE VELOCITY	6.51	W/HR/W
SUPERFICIAL RESIDENCE TIME	4.49	SEC
MATERIAL BALANCE	106.59	PERCENT

MOLES PRODUCT/100 MOLES FEED

ISO C5	3.57
N C5	64.13
22DMB	0.04
2MP	1.28
3MP	0.61
NC6	30.41

C5 RATE CONSTANT	0.026	CC/GM/SEC
C6 RATE CONSTANT	0.029	CC/GM/SEC

Reproduced with permission of the copyright owner. Further reproduction prohibited without permission.

RUN MI-29

TEMPERATURE	465.	DEG F
PRESSURE	300.	PSIG
CATALYST WEIGHT	2.013	GRAMS
CATALYST TYPE	HJE 243	

HYDROCARBON FEED COMPOSITION

	MOLE FRACTION	PARTIAL PRESS
NORMAL PENTANE	0.53	15.16 PSIA
NORMAL HEXANE	0.47	13.38 PSIA

H2/HYDROCARBON MOLE RATIO	10.03	
HYDROGEN PRESSURE	286.2	PSIA
WEIGHT HOURLY SPACE VELOCITY	6.39	W/HR/W
SUPERFICIAL RESIDENCE TIME	4.35	SEC
MATERIAL BALANCE	103.71	PERCENT

MOLES PRODUCT/100 MOLES FEED

ISO C5	2.73
N C5	54.79
22DMB	0.01
2MP	0.97
3MP	0.47
NC6	41.03

C5 RATE CONSTANT	0.024	CC/GM/SEC
C6 RATE CONSTANT	0.017	CC/GM/SEC

Reproduced with permission of the copyright owner. Further reproduction prohibited without permission.

RUN MI-30

TEMPERATURE	465.	DEG F
PRESSURE	300.	PSIG
CATALYST WEIGHT	2.013	GRAMS
CATALYST TYPE	HJE 243	

HYDROCARBON FEED COMPOSITION

	MOLE FRACTION	PARTIAL PRESS
NORMAL PENTANE	0.77	22.12 PSIA
NORMAL HEXANE	0.23	6.51 PSIA

H2/HYDROCARBON MOLE RATIO	9.99	
HYDROGEN PRESSURE	286.1	PSIA
WEIGHT HOURLY SPACE VELOCITY	6.31	W/HR/W
SUPERFICIAL RESIDENCE TIME	4.23	SEC
MATERIAL BALANCE	103.72	PERCENT

MOLES PRODUCT/100 MOLES FEED

ISO C5	4.32
N C5	71.88
22DMB	0.0
2MP	0.57
3MP	0.27
NC6	23.53

C5 RATE CONSTANT	0.030	CC/GM/SEC
C6 RATE CONSTANT	0.018	CC/GM/SEC

Reproduced with permission of the copyright owner. Further reproduction prohibited without permission.

RUN MI-31

TEMPERATURE	465.	DEG F
PRESSURE	100.	PSIG
CATALYST WEIGHT	2.003	GRAMS
CATALYST TYPE	HJE 243	

HYDROCARBON FEED COMPOSITION

	MOLE FRACTION	PARTIAL PRESS
NORMAL PENTANE	0.17	1.74 PSIA
NORMAL HEXANE	0.83	8.72 PSIA

H2/HYDROCARBON MOLE RATIO	9.96	
HYDROGEN PRESSURE	104.2	PSIA
WEIGHT HOURLY SPACE VELOCITY	6.54	W/HR/W
SUPERFICIAL RESIDENCE TIME	1.66	SEC
MATERIAL BALANCE	102.10	PERCENT

MOLES PRODUCT/100 MOLES FEED

ISO C5	0.85
N C5	25.48
22DMB	0.43
2MP	13.67
3MP	0.64
NC6	58.93

C5 RATE CONSTANT	0.042	CC/GM/SEC
C6 RATE CONSTANT	0.293	CC/GM/SEC

Reproduced with permission of the copyright owner. Further reproduction prohibited without permission.

RUN MI-32

TEMPERATURE	465.	DEG F
PRESSURE	100.	PSIG
CATALYST WEIGHT	2.003	GRAMS
CATALYST TYPE	HJE 243	

HYDROCARBON FEED COMPOSITION

	MOLE FRACTION	PARTIAL PRESS
NORMAL PENTANE	0.53	5.54 PSIA
NORMAL HEXANE	0.47	4.89 PSIA

H2/HYDROCARBON MOLE RATIO	10.00	
HYDROGEN PRESSURE	104.3	PSIA
WEIGHT HOURLY SPACE VELOCITY	6.42	W/HR/W
SUPERFICIAL RESIDENCE TIME	1.58	SEC
MATERIAL BALANCE	103.52	PERCENT

MOLES PRODUCT/100 MOLES FEED

ISO C5	3.45
N C5	47.52
22DMB	0.32
2MP	6.60
3MP	0.0
NC6	42.11

C5 RATE CONSTANT	0.095	CC/GM/SEC
C6 RATE CONSTANT	0.208	CC/GM/SEC

Reproduced with permission of the copyright owner. Further reproduction prohibited without permission.

RUN MI-33

TEMPERATURE	465.	DEG F
PRESSURE	100.	PSIG
CATALYST WEIGHT	2.003	GRAMS
CATALYST TYPE	HJE 243	

HYDROCARBON FEED COMPOSITION

	MOLE FRACTION	PARTIAL PRESS
NORMAL PENTANE	0.77	8.16 PSIA
NORMAL HEXANE	0.23	2.40 PSIA

H2/HYDROCARBON MOLE RATIO	9.86	
HYDROGEN PRESSURE	104.1	PSIA
WEIGHT HOURLY SPACE VELOCITY	6.34	W/HR/W
SUPERFICIAL RESIDENCE TIME	1.55	SEC
MATERIAL BALANCE	103.78	PERCENT

MOLES PRODUCT/100 MOLES FEED

ISO C5	4.36
N C5	72.28
22DMB	0.10
2MP	2.78
3MP	0.0
NC6	20.49

C5 RATE CONSTANT	0.081	CC/GM/SEC
C6 RATE CONSTANT	0.183	CC/GM/SEC

Reproduced with permission of the copyright owner. Further reproduction prohibited without permission.

RUN MI-34

TEMPERATURE	465.	DEG F
PRESSURE	200.	PSIG
CATALYST WEIGHT	2.007	*GRAMS
CATALYST TYPE	HJE 243	

HYDROCARBON FEED COMPOSITION

	MOLE FRACTION	PARTIAL PRESS
NORMAL PENTANE	0.17	3.26 PSIA
NORMAL HEXANE	0.83	16.29 PSIA

H2/HYDROCARBON MOLE RATIO	9.98	
HYDROGEN PRESSURE	195.2	PSIA
WEIGHT HOURLY SPACE VELOCITY	6.53	W/HR/W
SUPERFICIAL RESIDENCE TIME	3.10	SEC
MATERIAL BALANCE	109.41	PERCENT

MOLES PRODUCT/100 MOLES FEED

ISO C5	1.47
N C5	49.91
22DMB	0.0
2MP	3.53
3MP	1.64
NC6	43.45

C5 RATE CONSTANT	0.020	CC/GM/SEC
C6 RATE CONSTANT	0.078	CC/GM/SEC

Reproduced with permission of the copyright owner. Further reproduction prohibited without permission.

RUN MI-35

TEMPERATURE	465.	DEG F
PRESSURE	200.	PSIG
CATALYST WEIGHT	2.007	GRAMS
CATALYST TYPE	HJE 243	

HYDROCARBON FEED COMPOSITION

	MOLE FRACTION	PARTIAL PRESS
NORMAL PENTANE	0.53	10.47 PSIA
NORMAL HEXANE	0.47	9.24 PSIA

H2/HYDROCARBON MOLE RATIO	9.90	
HYDROGEN PRESSURE	195.0	PSIA
WEIGHT HOURLY SPACE VELOCITY	6.41	W/HR/W
SUPERFICIAL RESIDENCE TIME	2.99	SEC
MATERIAL BALANCE	104.76	PERCENT

MOLES PRODUCT/100 MOLES FEED

ISO C5	1.84
N C5	61.82
22DMB	0.03
2MP	1.68
3MP	0.40
NC6	34.23

C5 RATE CONSTANT	0.021	CC/GM/SEC
C6 RATE CONSTANT	0.043	CC/GM/SEC

Reproduced with permission of the copyright owner. Further reproduction prohibited without permission.

RUN MI-36

TEMPERATURE	465.	DEG F
PRESSURE	200.	PSIG
CATALYST WEIGHT	2.007	GRAMS
CATALYST TYPE	HJE 243	

HYDROCARBON FEED COMPOSITION

	MOLE FRACTION	PARTIAL PRESS
NORMAL PENTANE	0.77	15.15 PSIA
NORMAL HEXANE	0.23	4.46 PSIA

H2/HYDROCARBON MOLE RATIO	9.95	
HYDROGEN PRESSURE	195.1	PSIA
WEIGHT HOURLY SPACE VELOCITY	6.33	W/HR/W
SUPERFICIAL RESIDENCE TIME	2.89	SEC
MATERIAL BALANCE	102.00	PERCENT

MOLES PRODUCT/100 MOLES FEED

ISO C5	2.56
N C5	78.59
22DMB	0.0
2MP	0.83
3MP	0.12
NC6	17.90

C5 RATE CONSTANT	0.024	CC/GM/SEC
C6 RATE CONSTANT	0.038	CC/GM/SEC

Reproduced with permission of the copyright owner. Further reproduction prohibited without permission.

RUN MI-37

TEMPERATURE	465.	DEG F
PRESSURE	97.	PSIG
CATALYST WEIGHT	2.001	GRAMS
CATALYST TYPE	HJE 243	

HYDROCARBON FEED COMPOSITION

	MOLE FRACTION	PARTIAL PRESS
NORMAL PENTANE	0.17	1.17 PSIA
NORMAL HEXANE	0.83	5.86 PSIA

H2/HYDROCARBON MOLE RATIO	14.89	
HYDROGEN PRESSURE	104.7	PSIA
WEIGHT HOURLY SPACE VELOCITY	6.55	W/HR/W
SUPERFICIAL RESIDENCE TIME	1.11	SEC
MATERIAL BALANCE	99.88	PERCENT

MOLES PRODUCT/100 MOLES FEED

ISO C5	2.09
N C5	39.69
22DMB	0.0
2MP	10.24
3MP	2.30
NC6	45.68

C5 RATE CONSTANT	0.099	CC/GM/SEC
C6 RATE CONSTANT	0.476	CC/GM/SEC

Reproduced with permission of the copyright owner. Further reproduction prohibited without permission.

RUN MI-38

TEMPERATURE	465.	DEG F
PRESSURE	97.	PSIG
CATALYST WEIGHT	2.001	GRAMS
CATALYST TYPE	HJE 243	

HYDROCARBON FEED COMPOSITION

	MOLE FRACTION	PARTIAL PRESS
NORMAL PENTANE	0.53	3.74 PSIA
NORMAL HEXANE	0.47	3.30 PSIA

H2/HYDROCARBON MOLE RATIO	14.85	
HYDROGEN PRESSURE	104.7	PSIA
WEIGHT HOURLY SPACE VELOCITY	6.43	W/HR/W
SUPERFICIAL RESIDENCE TIME	1.07	SEC
MATERIAL BALANCE	97.90	PERCENT

MOLES PRODUCT/100 MOLES FEED

ISO C5	3.00
N C5	44.84
22DMB	0.0
2MP	6.31
3MP	1.78
NC6	44.07

C5 RATE CONSTANT	0.130	CC/GM/SEC
C6 RATE CONSTANT	0.342	CC/GM/SEC

Reproduced with permission of the copyright owner. Further reproduction prohibited without permission.

RUN MI-39

TEMPERATURE	465.	DEG F
PRESSURE	97.	PSIG
CATALYST WEIGHT	2.001	GRAMS
CATALYST TYPE	HJE 243	

HYDROCARBON FEED COMPOSITION

	MOLE FRACTION	PARTIAL PRESS
NORMAL PENTANE	0.77	5.44 PSIA
NORMAL HEXANE	0.23	1.60 PSIA

H2/HYDROCARBON MOLE RATIO	14.87	
HYDROGEN PRESSURE	104.7	PSIA
WEIGHT HOURLY SPACE VELOCITY	6.34	W/HR/W
SUPERFICIAL RESIDENCE TIME	1.03	SEC
MATERIAL BALANCE	96.44	PERCENT

MOLES PRODUCT/100 MOLES FEED

ISO C5	4.07
N C5	63.64
22DMB	0.0
2MP	3.70
3MP	0.90
NC6	27.70

C5 RATE CONSTANT	0.129	CC/GM/SEC
C6 RATE CONSTANT	0.321	CC/GM/SEC

Reproduced with permission of the copyright owner. Further reproduction prohibited without permission.

RUN MI-43

TEMPERATURE	465.	DEG F
PRESSURE	192.	PSIG
CATALYST WEIGHT	2.002	GRAMS
CATALYST TYPE	HJE 243	

HYDROCARBON FEED COMPOSITION

	MOLE FRACTION	PARTIAL PRESS
NORMAL PENTANE	0.17	1.81 PSIA
NORMAL HEXANE	0.83	9.05 PSIA

H2/HYDROCARBON MOLE RATIO	18.02	
HYDROGEN PRESSURE	195.8	PSIA
WEIGHT HOURLY SPACE VELOCITY	6.54	W/HR/W
SUPERFICIAL RESIDENCE TIME	1.72	SEC
MATERIAL BALANCE	120.87	PERCENT

MOLES PRODUCT/100 MOLES FEED

ISO C5	0.86
N C5	25.16
22DMB	0.90
2MP	5.68
3MP	2.19
NC6	65.32

C5 RATE CONSTANT	0.042	CC/GM/SEC
C6 RATE CONSTANT	0.156	CC/GM/SEC

Reproduced with permission of the copyright owner. Further reproduction prohibited without permission.

RUN MI-44

TEMPERATURE	465.	DEG F
PRESSURE	192.	PSIG
CATALYST WEIGHT	2.002	GRAMS
CATALYST TYPE	HJE 243	

HYDROCARBON FEED COMPOSITION

	MOLE FRACTION	PARTIAL PRESS
NORMAL PENTANE	0.53	5.85 PSIA
NORMAL HEXANE	0.47	5.16 PSIA

H2/HYDROCARBON MOLE RATIO	17.78	
HYDROGEN PRESSURE	195.7	PSIA
WEIGHT HOURLY SPACE VELOCITY	6.43	W/HR/W
SUPERFICIAL RESIDENCE TIME	1.67	SEC
MATERIAL BALANCE	101.70	PERCENT

MOLES PRODUCT/100 MOLES FEED

ISO C5	1.89
N C5	52.70
22DMB	0.0
2MP	3.78
3MP	0.20
NC6	41.43

C5 RATE CONSTANT	0.045	CC/GM/SEC
C6 RATE CONSTANT	0.118	CC/GM/SEC

Reproduced with permission of the copyright owner. Further reproduction prohibited without permission.

RUN MI-45

TEMPERATURE	465.	DEG F
PRESSURE	192.	PSIG
CATALYST WEIGHT	2.002	GRAMS
CATALYST TYPE	HJE 243	

HYDROCARBON FEED COMPOSITION

	MOLE FRACTION	PARTIAL PRESS
NORMAL PENTANE	0.77	8.42 PSIA
NORMAL HEXANE	0.23	2.48 PSIA

H2/HYDROCARBON MOLE RATIO	17.96	
HYDROGEN PRESSURE	195.8	PSIA
WEIGHT HOURLY SPACE VELOCITY	6.34	W/HR/W
SUPERFICIAL RESIDENCE TIME	1.60	SEC
MATERIAL BALANCE	99.82	PERCENT

MOLES PRODUCT/100 MOLES FEED

ISO C5	2.76
N C5	65.12
22DMB	0.0
2MP	1.68
3MP	0.14
NC6	29.59

C5 RATE CONSTANT	0.055	CC/GM/SEC
C6 RATE CONSTANT	0.080	CC/GM/SEC

Reproduced with permission of the copyright owner. Further reproduction prohibited without permission.

RUN C51-6

TEMPERATURE	465.	DEG F
PRESSURE	200.	PSIG
CATALYST WEIGHT	2.012	GRAMS
CATALYST TYPE	LJJ 289	

HYDROCARBON FEED COMPOSITION

	MOLE FRACTION	PARTIAL PRESS
NORMAL PENTANE	1.00	19.34 PSIA
NORMAL HEXANE	0.0	0.0 PSIA

H2/HYDROCARBON MOLE RATIO	10.10	
HYDROGEN PRESSURE	195.4	PSIA
WEIGHT HOURLY SPACE VELOCITY	6.22	W/HR/W
SUPERFICIAL RESIDENCE TIME	2.17	SEC
MATERIAL BALANCE	92.92	PERCENT

MOLES PRODUCT/100 MOLES FEED

ISO C5	7.60
+ C5	92.40

C5 RATE CONSTANT 0.061 CC/GM/SEC

Reproduced with permission of the copyright owner. Further reproduction prohibited without permission.

RUN C51-10

TEMPERATURE	465.	DEG F
PRESSURE	300.	PSIG
CATALYST WEIGHT	2.000	GRAMS
CATALYST TYPE	LJJ 289	

HYDROCARBON FEED COMPOSITION

	MOLE FRACTION	PARTIAL PRESS
NORMAL PENTANE	1.00	28.44 PSIA
NORMAL HEXANE	0.0	0.0 PSIA

H2/HYDROCARBON MOLE RATIO	10.07	
HYDROGEN PRESSURE	286.3	PSIA
WEIGHT HOURLY SPACE VELOCITY	6.26	W/HR/W
SUPERFICIAL RESIDENCE TIME	3.17	SEC
MATERIAL BALANCE	98.79	PERCENT

MOLES PRODUCT/100 MOLES FEED

ISO C5	12.42
N C5	87.58

C5 RATE CONSTANT 0.071 CC/GM/SEC

Reproduced with permission of the copyright owner. Further reproduction prohibited without permission.

RUN C51-12

TEMPERATURE	465.	DEG F
PRESSURE	100.	PSIG
CATALYST WEIGHT	2.000	GRAMS
CATALYST TYPE	LJJ 289	

HYDROCARBON FEED COMPOSITION

	MOLE FRACTION	PARTIAL PRESS
NORMAL PENTANE	1.00	10.43 PSIA
NORMAL HEXANE	0.0	0.0 PSIA

H2/HYDROCARBON MOLE RATIO	10.00	
HYDROGEN PRESSURE	104.3	PSIA
WEIGHT HOURLY SPACE VELOCITY	6.26	W/HR/W
SUPERFICIAL RESIDENCE TIME	1.16	SEC
MATERIAL BALANCE	97.66	PERCENT

MOLES PRODUCT/100 MOLES FEED

ISO C5	15.19
N C5	84.91

C5 RATE CONSTANT 0.241 CC/GM/SEC

Reproduced with permission of the copyright owner. Further reproduction prohibited without permission.

RUN C51-15

TEMPERATURE	465.	DEG F
PRESSURE	192.	PSIG
CATALYST WEIGHT	2.002	GRAMS
CATALYST TYPE	LJJ 289	

HYDROCARBON FEED COMPOSITION

	MOLE FRACTION	PARTIAL PRESS
NORMAL PENTANE	1.00	10.97 PSIA
NORMAL HEXANE	0.0	0.0 PSIA

H2/HYDROCARBON MOLE RATIO	17.85	
HYDROGEN PRESSURE	195.7	PSIA
WEIGHT HOURLY SPACE VELOCITY	6.26	W/HR/W
SUPERFICIAL RESIDENCE TIME	1.22	SEC
MATERIAL BALANCE	101.12	PERCENT

MOLES PRODUCT/100 MOLES FEED

ISO C5	5.20
N C5	94.80

C5 RATE CONSTANT 0.073 CC/GM/SEC

Reproduced with permission of the copyright owner. Further reproduction prohibited without permission.

RUN C51-16

TEMPERATURE	465.	DEG F
PRESSURE	290.	PSIG
CATALYST WEIGHT	2.007	GRAMS
CATALYST TYPE	LJJ 289	

HYDROCARBON FEED COMPOSITION

	MOLE FRACTION	PARTIAL PRESS
NORMAL PENTANE	1.00	19.18 PSIA
NORMAL HEXANE	0.0	0.0 PSIA

H2/HYDROCARBON MOLE RATIO	14.89	
HYDROGEN PRESSURE	285.5	PSIA
WEIGHT HOURLY SPACE VELOCITY	6.24	W/HR/W
SUPERFICIAL RESIDENCE TIME	2.15	SEC
MATERIAL BALANCE	103.68	PERCENT

MOLES PRODUCT/100 MOLES FEED

ISO C5	7.11
N C5	92.89

C5 RATE CONSTANT 0.058 CC/GM/SEC

Reproduced with permission of the copyright owner. Further reproduction prohibited without permission.

RUN C51-17

TEMPERATURE	465.	DEG F
PRESSURE	291.	PSIG
CATALYST WEIGHT	2.013	GRAMS
CATALYST TYPE	HJE 243	

HYDROCARBON FEED COMPOSITION

	MOLE FRACTION	PARTIAL PRESS
NORMAL PENTANE	1.00	19.52 PSIA
NORMAL HEXANE	0.0	0.0 PSIA

H2/HYDROCARBON MOLE RATIO	14.66	
HYDROGEN PRESSURE	286.2	PSIA
WEIGHT HOURLY SPACE VELOCITY	6.22	W/HR/W
SUPERFICIAL RESIDENCE TIME	2.80	SEC
MATERIAL BALANCE	103.51	PERCENT

MOLES PRODUCT/100 MOLES FEED

ISO C5	6.68
N C5	93.32

C5 RATE CONSTANT 0.063 CC/GM/SEC

Reproduced with permission of the copyright owner. Further reproduction prohibited without permission.

RUN C51-18

TEMPERATURE	465.	DEG F
PRESSURE	300.	PSIG
CATALYST WEIGHT	2.013	GRAMS
CATALYST TYPE	HJE 243	

HYDROCARBON FEED COMPOSITION

	MOLE FRACTION	PARTIAL PRESS
NORMAL PENTANE	1.00	23.46 PSIA
NORMAL HEXANE	0.0	0.0 PSIA

H2/HYDROCARBON MOLE RATIO	10.06	
HYDROGEN PRESSURE	286.2	PSIA
WEIGHT HOURLY SPACE VELOCITY	6.22	W/HR/W
SUPERFICIAL RESIDENCE TIME	4.03	SEC
MATERIAL BALANCE	100.86	PERCENT

MOLES PRODUCT/100 MOLES FEED

ISO C5	8.36
N C5	91.64

C5 RATE CONSTANT 0.046 CC/GM/SEC

Reproduced with permission of the copyright owner. Further reproduction prohibited without permission.

Run C51-19

TEMPERATURE	465.	DEG F
PRESSURE	100.	PSIG
CATALYST WEIGHT	2.003	GRAMS
CATALYST TYPE	HJE 243	

HYDROCARBON FEED COMPOSITION

	MOLE FRACTION	PARTIAL PRESS
NORMAL PENTANE	1.00	10.54 PSIA
NORMAL HEXANE	0.0	0.0 PSIA

H2/HYDROCARBON MOLE RATIO	9.88	
HYDROGEN PRESSURE	104.2	PSIA
WEIGHT HOURLY SPACE VELOCITY	6.25	W/HR/W
SUPERFICIAL RESIDENCE TIME	1.60	SEC
MATERIAL BALANCE	119.79	PERCENT

MOLES PRODUCT/100 MOLES FEED

ISO C5	12.16
N C5	87.94

C5 RATE CONSTANT 3.187 CC/GM/SEC

Reproduced with permission of the copyright owner. Further reproduction prohibited without permission.

RUN C51-20

TEMPERATURE	465.	DEG F
PRESSURE	200.	PSIG
CATALYST WEIGHT	2.007	GRAMS
CATALYST TYPE	HJE 243	

HYDROCARBON FEED COMPOSITION

	MOLE FRACTION	PARTIAL PRESS
NORMAL PENTANE	1.00	19.61 PSIA
NORMAL HEXANE	0.0	0.0 PSIA

H2/HYDROCARBON MOLE RATIO	9.95	
HYDROGEN PRESSURE	195.1	PSIA
WEIGHT HOURLY SPACE VELOCITY	6.24	W/HR/W
SUPERFICIAL RESIDENCE TIME	2.80	SEC
MATERIAL BALANCE	99.71	PERCENT

MOLES PRODUCT/100 MOLES FEED

ISO C5	11.13
N C5	88.87

C5 RATE CONSTANT 3.091 CC/GM/SEC

Reproduced with permission of the copyright owner. Further reproduction prohibited without permission.

RUN C51-21

TEMPERATURE	465.	DEG F
PRESSURE	97.	PSIG
CATALYST WEIGHT	2.001	GRAMS
CATALYST TYPE	HJE 243	

HYDROCARBON FEED COMPOSITION

	MOLE FRACTION	PARTIAL PRESS
NORMAL PENTANE	1.00	7.04 PSIA
NORMAL HEXANE	0.0	0.0 PSIA

H2/HYDROCARBON MOLE RATIO	14.87	
HYDROGEN PRESSURE	104.7	PSIA
WEIGHT HOURLY SPACE VELOCITY	6.26	W/HR/W
SUPERFICIAL RESIDENCE TIME	1.00	SEC
MATERIAL BALANCE	99.13	PERCENT

MOLES PRODUCT/100 MOLES FEED

ISO C5	10.17
N C5	89.83

C5 RATE CONSTANT 0.231 CC/GM/SEC

Reproduced with permission of the copyright owner. Further reproduction prohibited without permission.

RUN C51-22

TEMPERATURE	465.	DEG F
PRESSURE	192.	PSIG
CATALYST WEIGHT	2.001	GRAMS
CATALYST TYPE	HJE 243	

HYDROCARBON FEED COMPOSITION

	MOLE FRACTION	PARTIAL PRESS
NORMAL PENTANE	1.00	11.12 PSIA
NORMAL HEXANE	0.0	0.0 PSIA

H2/HYDROCARBON MOLE RATIO	17.58	
HYDROGEN PRESSURE	195.6	PSIA
WEIGHT HOURLY SPACE VELOCITY	6.26	W/HR/W
SUPERFICIAL RESIDENCE TIME	1.59	SEC
MATERIAL BALANCE	106.96	PERCENT

MOLES PRODUCT/100 MOLES FEED

ISO C5	5.69
N C5	94.31

C5 RATE CONSTANT 0.079 CC/GM/SEC

Reproduced with permission of the copyright owner. Further reproduction prohibited without permission.

APPENDIX 5

Nomenclature

Reproduced with permission of the copyright owner. Further reproduction prohibited without permission.

Nomenclature

A	Cross Sectional Area
A_j	Deactivation Time Constant
a	Redlich Kwong Constant
B_j	Adsorption Parameter of Component j
b	Redlich Kwong Constant
C_i	Concentration of Component i
d_p	Catalyst Particle Diameter
D	Total Diffusivity
D_c	Configurational Diffusity
D_e	Effective Diffusivity
D_k	Knudsen Diffusivity
D_m	Molecular Diffusivity
D_s	"Slip" Region Diffusivity
E'	True Reaction Activation Energy
E_{app}	Apparent Reaction Activation Energy
ΔH_m	Heat of Adsorption of Component m
h	Redlich Kwong Constant
h_s	Thiele Modulus for Spherical Catalyst Particles
k	General Reaction Rate Constant
$\bar{k}$	General Surface Reaction Rate Constant
k_i	Boltzman's Constant Reaction Rate Constant for Reactant i
k_o	Surface Reaction Rate Constant Pre-exponential Term
K	General Equilibrium Constant
K_i	Adsorption Constant for Species i

Reproduced with permission of the copyright owner. Further reproduction prohibited without permission.

Nomenclature (Cont'd.)

M	Mixing Intensity
MD	Molecular Diameter
N_i	Molar Flow Rate of Component i
n	Number of Catalyst Active Sites
n_i	Moles of Component i
PD	Catalyst Pore Diameter
Pe	Peclet Number
P_i	Partial Pressure of Species i
P_{tot}	Total Pressure
R	Overall Reaction Rate, Catalyst Pore Radius
$\tilde{R}$	Hydrogen/Hydrocarbon Mole Ratio
R	Ideal Gas Constant
Re_p	Particle Reynolds Number
S	Specific Surface Area of the Catalyst
T	Absolute Temperature
t_H	Holding Time
V	Molar Volume
V_T	Total Volumetric Molar Flow Rate
w	Relative number of Water Molecules in the General Zeolite Structure
W	Mass Flow Rate Weight of Catalyst
X	Relative Number of Alumina Molecules in the General Zeolite Structure
y	Relative Number of Silica Molecules in the General Zeolite Structure
Y_i^*	Hydrogen-free Mole Fraction of Species i at Equilibrium
Z	Compressibility

Reproduced with permission of the copyright owner. Further reproduction prohibited without permission.

Greek Symbols

ε	Porosity of Catalyst Particle
λ_i	Mean Free Path of Molecule i
$\hat{\phi}_i$	Fugacity of Component i in a Mixture
ρ_i	Density of Species i
ρ_B	Bulk Density of the Catalyst
ρ_G	Molar Gas Density
ρ_P	True Catalyst Particle Density
σ	Molecular Diameter, equation (3)
	Standard Deviation
	Constriction Factor, equation (6)
τ	Tortuosity Factor
τ_w	Weight Hourly Space Velocity
μ	Fluid Viscosity

Reproduced with permission of the copyright owner. Further reproduction prohibited without permission.

VITA

James Jerome Spivey was born July 26, 1950 in Gastonia, North Carolina. He attended Grimsley Senior High School in Greensboro, North Carolina and graduated in 1968.

He attended North Carolina State University in Raleigh, North Carolina on an athletic scholarship in track and was co-captain of the track team in 1971 and 1972. He received his B.S. degree in Chemical Engineering in May, 1972. Work toward an M.S. degree in the same field was begun after graduation and completed in February, 1974. He accepted employment at Ethyl Corporation in Baton Rouge, Louisiana in February 1974. Part-time class and experimental work was begun toward a Ph.D. degree in 1975. He spent a year in residence at LSU in 1978 with a leave of absence from Ethyl Corporation. Work toward the Ph.D. degree was completed in 1980. He is currently employed as a Process Design Engineer at Ethyl Corporation.

Reproduced with permission of the copyright owner. Further reproduction prohibited without permission.

EXAMINATION AND THESIS REPORT

Candidate: James Jerome Spivey

Major Field: Chemical Engineering

Title of Thesis: Hydroisomerization of Pentane and Hexane Mixtures on Zeolite Catalysts

Approved:

Philip A Bryant
Major Professor and Chairman

James D. Traynham
Dean of the Graduate School

EXAMINING COMMITTEE:

Edward von Lavgelin

Alexis Voorhies, Jr.

Armando B. Corripio

Jerry A. Wallin

Date of Examination:

July 14, 1980

Reproduced with permission of the copyright owner. Further reproduction prohibited without permission.